CHALMERS

Energy Storage Equipped STATCOM for Power Quality Improvements in Distribution Grids

Impact of Load Dynamics on System Performance

Master's thesis in Electric Power Engineering

VIKTOR WEIDENMO

Division of Electric Power Engineering
Department of Energy and Environment
CHALMERS UNIVERSITY OF TECHNOLOGY
Gothenburg, Sweden 2012
Master's thesis

Energy Storage Equipped STATCOM for Power Quality Improvements in Distribution Grids

Impact of Load Dynamics on System Performance

VIKTOR WEIDENMO

Division of Electric Power Engineering
Department of Energy and Environment
CHALMERS UNIVERSITY OF TECHNOLOGY

Gothenburg, Sweden 2012

Energy Storage Equipped STATCOM for Power Quality Improvements in Distribution Grids
Impact of Load Dynamics on System Performance
VIKTOR WEIDENMO

Master's thesis
ISSN 1652-8557
Department of Energy and Environment
Division of Electric Power Engineering
Chalmers University of Technology
SE-412 96 Gothenburg
Sweden
Telephone: +46 (0)31-772 1000

Chalmers Reproservice
Gothenburg, Sweden 2012

Energy Storage Equipped STATCOM for Power Quality Improvements in Distribution Grids
Master's thesis in Electric Power Engineering
VIKTOR WEIDENMO
Department of Energy and Environment
Division of Electric Power Engineering
Chalmers University of Technology

Abstract

Increasing awareness and concerns regarding unacceptable power quality are causing a growing interest in custom power devices, used to improve power quality on distribution level. One of the most interesting types of custom power devices, due to its flexibility and fast control, is the shunt-connected voltage source converter (VSC), also known as the static synchronous compensator (STATCOM). This thesis deals with the control, performance and applications of STATCOMs equipped with energy storage for power quality improvements.

The additional power quality applications, made possible by the energy storage, include a more complete mitigation of voltage dips. Furthermore, the energy storage also enables a STATCOM to support an entry into islanding operation, by rapid balancing of loads, after tripping of a single feeder.

The final part in the thesis treats dynamic loads and their impact on system performance. Dynamic loads of this type are not common in the power system today, but might be in the future. Using state space analysis and simulations, it is shown that dynamic loads can cause serious stability problems in power systems and that STATCOMs without energy storages might even worsen this effect. It is further shown that STATCOMs equipped with energy storages, due to the ability of controlling both active and reactive power, can keep the system performance practically unaffected during the same conditions.

Keywords: Power Electronics, Voltage Soruce Converter (VSC), Static Synchronous Compensator (STATCOM), Energy Storage, Power Quality, Dynamic Loads

Acknowledgements

This work has been carried out at the Department of Energy and Environment at Chalmers University of Technology in cooperation with Falbygdens Energi AB.

My deepest thanks to my examiner and supervisor, Assoc. Prof. Massimo Bongiorno for his help and support during this work.

I would like to thank my supervisor at Falbygdens Energi, CEO Lars Ohlsson, for his help and inspiration during this work. I would also like to thank Pia Borg, Falbygdens Energi, for her help, friendliness and for giving me the opportunity to work with energy storage systems in practice.

I would further like to thank my fellow M.Sc. students for creating a friendly atmosphere.

Last, but surely not least, I would like to thank Karin for her love and support.

Viktor Weidenmo
Gothenburg, Sweden, 2012

List of acronyms

CPL	Constant active power load
CQL	Constant reactive power load
CSC	Current source converter
CZL	Constant impedance load
D-STATCOM	Distribution static synchronous compensator
DVR	Dynamic voltage restorer
E-STATCOM	Energy storage static synchronous compensator
FACTS	Flexible AC transmission systems
HVDC	High voltage direct current
IGBT	Insulated-gate bipolar transistor
KCL	Kirchhoff's current law
KVL	Kirchhoff's voltage law
PCC	Point of common coupling
PLL	Phase-locked-loop
pu	Per unit
PWM	Pulse width modulation
RPC	Reactive power controller
SCR	Short circuit ratio
SSSC	Static synchronous series compensator
STATCOM	Static synchronous compensator
STS	Static transfer switch
SVC	Static Var compensator
TCSC	Thyristor controlled series capacitor
UPS	Uninterruptible power supply
VC	Voltage controller
VCC	Vector current controller
VSC	Voltage source converter

Contents

Abstract i

Acknowledgements ii

List of Acronyms iii

Contents v

1 Introduction 1
1.1 Background . . . 1
1.2 Project Objectives . . . 2
1.3 Main Contributions . . . 2
1.4 Outline of the Thesis . . . 2

2 Power Electronics in Power Systems 5
2.1 Introduction . . . 5
2.2 Transmission Level . . . 5
2.3 Distribution Level . . . 7
2.4 Conclusion . . . 10

3 Energy Storage at Distribution Level 11
3.1 Introduction . . . 11
3.2 Classification of Energy Storage Applications . . . 11
3.2.1 Energy Time-Shifting and Auxiliary Services . . . 12
3.2.2 Power Quality Improvements . . . 12
3.3 Storage Types for Power Quality Applications . . . 12
3.3.1 Batteries . . . 13
3.3.2 Flywheels . . . 13
3.3.3 Capacitors . . . 13
3.3.4 Superconducting Magnetic Energy Storage . . . 14
3.4 Conclusion . . . 14

4 Control of Shunt-Connected VSC for Power Quality Applications 15
4.1 Introduction . . . 15
4.2 Vector Current Controller . . . 16
4.2.1 Electric System . . . 16
4.2.2 Controller Design . . . 18
4.3 Reactive Power Controller - VSC without significant Energy Storage . . . 21
4.3.1 Electric System . . . 22
4.3.2 Controller Design . . . 22
4.4 Voltage Controller - VSC with Energy Storage . . . 25
4.4.1 Electric System . . . 25
4.4.2 Controller Design . . . 26
4.5 Synchronization System - PLL . . . 28
4.6 Simplifications in the Used System . . . 28
4.6.1 Continuous System . . . 28
4.6.2 Balanced System and Faults . . . 29
4.6.3 Unlimited Converter Rating . . . 29
4.6.4 Sinusoidal Three-Phase VSC . . . 29
4.6.5 Fixed DC-voltage . . . 29
4.7 System Performance During Voltage Dips . . . 30

4.7.1 D-STATCOM . . . 31
4.7.2 E-STATCOM . . . 33
4.8 Conclusion . . . 34

5 Energy Storage Applications for Power Quality Improvements 35
5.1 Introduction . . . 35
5.2 Voltage Dips and Phase Jumps . . . 35
5.2.1 Problems Related to Phase Jumps . . . 37
5.2.2 Phase Jump Mitigation . . . 37
5.2.3 Understanding the Phase Jump Mitigation . . . 38
5.3 Rapid Balancing of Loads . . . 40
5.4 Conclusion . . . 41

6 Impact of Load Dynamics on System Performance 43
6.1 Introduction . . . 43
6.2 Dynamic Loads . . . 44
6.2.1 Understanding Constant Power Loads . . . 44
6.2.2 Modelling of Constant Power Loads . . . 45
6.3 State Space Models . . . 46
6.3.1 State Space Systems . . . 47
6.3.2 Without Compensator . . . 48
6.3.3 With D-STATCOM . . . 50
6.3.4 With E-STATCOM . . . 54
6.3.5 Linearization Method . . . 55
6.3.6 Operation Points and System Parameters . . . 55
6.4 Damping and Stability . . . 56
6.4.1 Without Compensator . . . 58
6.4.2 With D-STATCOM . . . 60
6.4.3 With E-STATCOM . . . 62
6.5 Mixed Load Characteristic . . . 64
6.5.1 Constant Active and Reactive Power Load . . . 65
6.5.2 Mixed Constant Impedance and Constant Power Loads . . . 65
6.6 Conclusion . . . 68

7 Conclusions and Future Work 69
7.1 Conclusions . . . 69
7.2 Future Work . . . 70

References 71

A Transformations for Three-Phase Systems 73
A.1 Transformation of Three-Phase Quantities into Vectors . . . 73
A.2 Transformation between fixed and rotating coordinate systems . . . 73

Chapter 1

Introduction

This section explains the background of the studied topic, the project objectives, the main contributions of this work and the outline of this thesis.

1.1 Background

In power systems, and especially distribution systems, power electronic devices are getting more common. They are utilized both as interfaces in customer loads, and as a solution in the grid itself. One reason behind the later, is the increased interest in power quality, a term which targets the quality of the voltages and currents, focused on distortions from ideal power supplies. With respect to power quality, power electronic based loads are, on one hand, more demanding than conventional loads. At the same time, these loads tend to pollute the power system with more power quality related issues.

One solution, for improving the power quality, is to use power electronic controllers. One of the most popular controllers are the static synchronous compensator (STATCOM) which can be applied for many uses. However, by equipping STATCOMs with energy storages, additional applications can be obtained. Hence, there is a need for a study to determine the power quality applications and extra benefits that are gained by equipping STATCOMs with energy storages.

Furthermore, many studies so far have investigated isolated objects of the power system, with the aim to optimize the performance of that specific component. However, this approach does not always give a complete picture since an isolated model cannot show how different objects interact with each other in a combined system. This is particularly true when considering dynamics and transients, where almost no studies of system interaction exists. Due to this, dynamic interaction between parts in a power system is a fairly unknown phenomena, although it can cause serious stability problems.

To examine the performance of a complete system, all parts in a real system should ideally be included. However, to identify a phenomena and analyse why it appears, the model has to be simplified in order to suppress all other effects than the ones investigated. Hence, a model is needed which includes all vital parts of a power system, but with each part simplified to an adequate level. Following the current trend with more power electronic based loads, which possess other dynamic properties than conventional loads, and with more frequent use of compensators like the STATCOM, it creates a need of a study that investigates the interaction between these objects and the impact this has on the performance of power systems.

1.2 Project Objectives

The aim of this work is to investigate the applications that are enabled by equipping STATCOMs with energy storage. With energy storage, the devices are able to exchange both active and reactive power, compared to only reactive power without storage. This gives an increased controllability and some additional uses. Furthermore, the studied applications concern power quality improvements which demand fast response times. Hence, uses which utilize slower response times, for example energy trading or deferring of grid reinforcements, are not treated.

Additionally, this work examines the impact from dynamic loads on power system performance when compensators with and without energy storage, respectively, are used. In particular, system damping and stability are investigated when the dynamic properties of the loads vary.

1.3 Main Contributions

In this thesis, Chapter 6 contains studies which, according to the author, have not previously been done. The list below summarizes what, in the opinion of the author, are the main contributions of this thesis:

- A simplified dynamic model of a combined system of a dynamic load, a STATCOM (with or without energy storage) and a grid source is investigated. This model shows that dynamic properties of loads can have a large impact on the performance of power systems.
- It is shown that a dynamic load, modelled as a constant power load, itself can make a system unstable when no compensator is connected to the system.
- A system compensated by a STATCOM without energy storage, hence only capable of exchanging reactive power, is shown to turn unstable at less demanding dynamic loads than a system without a STATCOM. This could be due to interactions between the internal controllers in the STATCOM and the dynamic load.
- It is shown that a STATCOM with energy storage is able to maintain the stability of the system under the same dynamic loads, due to its ability to control both active and reactive power. In fact, the system performance gets practically independent of the load properties.
- Furthermore, it is shown that the bandwidth of the controller in a STATCOM, without energy storage, has a large impact on the stability of the system when connected to a dynamic load. The controller bandwidth has a much smaller impact on the system performance if the STATCOM is equipped with an energy storage.

1.4 Outline of the Thesis

Chapter 2 provides a short background of the use of power electronics in modern power systems. The systems and devices used on transmission and distribution level, respectively, are described together with their most common applications.

In chapter 3 are applications for energy storage systems classified depending on their required response times. Furthermore, different types of storage mediums used for power quality applications are treated.

The control structure and the derivation of the controller parameters in the compensators are presented in Chapter 4. This is done for a STATCOM which is equipped with an energy storage and one which is not. The impact of the controller parameters on the system performance is also treated and showed by simulations.

Power quality applications enabled by the use of compensators equipped with energy storages are described in Chapter 5. It is explained why compensation with both active and reactive

power enables a more complete mitigation of voltage dips compared to a compensator with only reactive power capabilities.

The impact of load dynamics on system performances is studied in Chapter 6. A dynamic load model with constant power load characteristics is presented and compared to a generic load model. Using the dynamic load model, state space systems are derived for grids with and without STATCOMs, with and without energy storage, respectively. The damping and stability of the investigated systems are studied by the placement of the system poles while varying the properties of the dynamic load. Finally, the results are validated by simulations.

Chapter 2

Power Electronics in Power Systems

This chapter provides a background of where and how power electronics is used in modern power systems. Uses in both transmission and distribution level are covered.

2.1 Introduction

The use of power electronics has grown significantly in the last decades, both on consumer side and grid side. On transmission level, there are two main groups of power electronic contorllers, high voltage direct current (HVDC) links and flexible AC transmission systems (FACTS). While HVDC links are used as an alternative way of power transmission, FACTS is used to improve the transmission of conventional AC systems.

Devices on distribution level, often called custom power devices, are mostly used for improving the power quality. On the contrary to power electronic controllers on transmission level, where minimizing the losses is the key to success, custom power devices are more off-the-shelf products which are not optimized for each use.

This thesis is focused on power quality applications, i.e. mostly on devices on distribution level. Hence, this chapter first describes power electronic controllers on transmission level before moving to custom power devices on distribution level.

2.2 Transmission Level

The first uses of power electronics on transmission level were HVDC transmission systems [14]. HVDC links are used to transport power and possess an alternative to normal AC lines. Especially in submarine cables, long distance overhead transmission, underground transmission and for connecting ac systems of different frequencies [23].

FACTS on the other hand, is used to improve existing AC transmission systems where growing power demand creates a need of increased power transmission. While it has been proven to be difficult, expensive and time-consuming to authorizing, locate and construct new transmission lines, especially for overhead lines where it is close to impossible, FACTS provides usable alternatives [14]. There are a number of power electronic controllers in the FACTS family which can be connected in shunt, series or in a combination. The controllers can be used individually or in coordination to control the interrelated system parameters such as series impedance, shunt impedance, voltages, phase angles or currents [23]. This offers a greater control of the power flow in the transmission system and the possibility to provide damping of subsynchronous oscillations [7].

In the following part is a few of the most important FACTS controllers described.

STATCOM

The STATCOM is a shunt-connected VSC, showed in Figure 2.1. It is one of the key FACTS controllers with the ability to control the output reactive current, and hence the reactive power, independently of the AC voltage [23]. It is mainly used for voltage control but can also be used for increasing of transmission capacity in power lines, improving the voltage/angle stability, damping of oscillations and as an active filter [33]. Furthermore, the STATCOM can be used for grid connection of renewable energy sources to fulfill the grid codes.

In its basic structure, the STATCOM can only exchange reactive power with the grid, but if equipped with an energy storage, the STATCOM can also exchange active power. The performance and applications of STATCOMs are analysed in this work, however, the thesis is focused on STATCOMs used on distribution level.

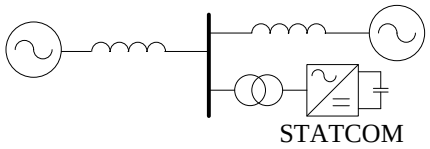

Figure 2.1: Transmission line with a STATCOM.

SVC

The static Var compensator (SVC) is another shunt-connected power electronic controller which can exchange reactive power with the grid. The SVC is thyristor based and uses passive components, like capacitors or inductors, to produce or consume reactive power, see Figure 2.2 for one example of a structure. The reactive power can either be controlled by varying the fire-angle of the thyristors, or by switching a number of passive components on or off (which is the chosen strategy for capacitors) [23]. The SVC is, compared to the STATCOM, a cheaper alternative but without the fast dynamic properties to mitigate transients [23]. For applications which need very high reactive power compensation, the SVC is always preferred before the STATCOM due to its lower losses.

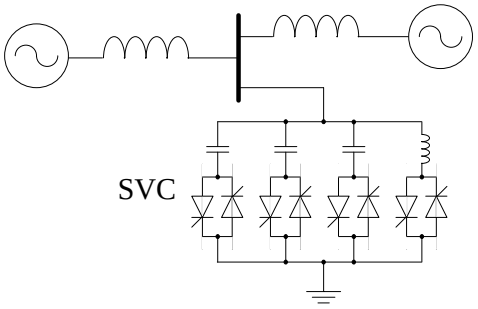

Figure 2.2: Transmission line with a SVC.

SSSC

A static synchronous series compensator (SSSC) is a converter connected in series with a transmission line, showed in Figure 2.3. The SSSC controls the voltage drop over a transmission line by injecting a voltage in quadrature to the line current. Hence, it controls the amount of

transmitted power [14]. Just as the STATCOM and the SVC, it can only exchange reactive power with the grid (unless an energy storage is provided).

It is of importance to mention that the SSSC has a pure academic interest and today it does not find a commercial application.

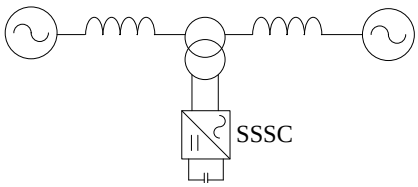

Figure 2.3: Transmission line with a SSSC.

TCSC

The thyristor controlled series capacitor (TCSC), shown in Figure 2.4, is the series connected-system corresponding to the shunt-connected SVC. The TCSC consists of a series capacitor bank shunted by a reactor controlled by thyristor switches. This provides a variable series capacitance which can be varied smoothly [23]. Hence, the total line inductance can be reduced which increases the power capacity and improves the stability. As the previous controllers, the TCSC can only produce or consume reactive power.

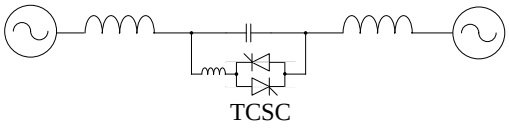

Figure 2.4: Transmission line with a TCSC.

2.3 Distribution Level

While power electronic controllers on transmission level are used to control the power flow and to increase the stability, custom power devices on distribution level are mostly used for power quality improvements. Problems with harmonic pollution, damages related to transient overvoltages or tripping of equipment caused by voltage dips have attracted attention to dynamic and adjustable devices to mitigate such problems [14]. The devices could be either current source converters (CSC) or VSC, however, almost all custom power devices installed in practical applications uses VSCs. The reasons include lower initial cost, higher efficiency, lower weight and the possibility to use multilevel or multi-step versions [14].

Similar to FACTS, custom power devices can be connected in shunt, series or in a combination of both. The following part describes some of the most important custom power devices.

D-STATCOM

The version of the STATCOM used on distribution level is often called distribution STATCOM (D-STATCOM) and it is shown in Figure 2.5. Just as the transmission level STATCOM, the D-STATCOM is a shunt-connected VSC which can only exchange reactive power with the grid. Its main application is to provide voltage control but it can also be used for active filtering to

reduce the level of current harmonics in the system, reactive power support and load balancing [14].

If reconfigurated for faster dynamic applications, the D-STATCOM can also be used to control the voltage during very fast transients and voltage dips. Thanks to its flexibility and wide range of applications it is the basic device that will be studied in this thesis.

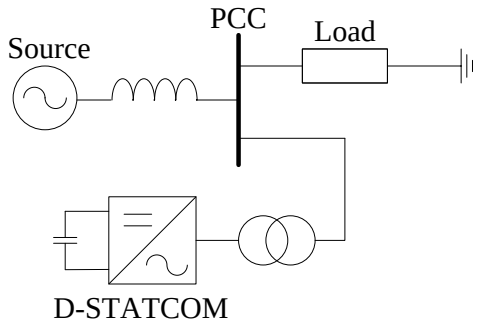

Figure 2.5: Distribution grid with a D-STATCOM.

E-STATCOM

The energy storage static synchronous compensator (E-STATCOM), showed in Figure 2.6, has the same structure as the D-STATCOM. It can be used for the same applications but, thanks to the energy storage, also exchange active power with the grid. Thus, this device has some additional applications and benefits which will be studied in this thesis and compared to the D-STATCOM. Some of the most common storage mediums for the E-STATCOM will be described in Chapter *3 Energy Storage at Distribution Level*.

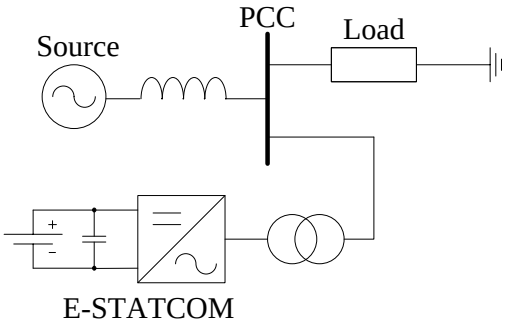

Figure 2.6: Distribution grid with an E-STATCOM.

DVR

A VSC connected in series is often called a dynamic voltage restorer (DVR), shown in Figure 2.7. The series connection enables an intuitive way of mitigating voltage dips since the DVR directly can inject the missing voltage when the source voltage drops. This, together with a dynamic performance which is independent of the source impedance, is the main advantage of the DVR and it makes the DVR the preferred choice for voltage dip mitigation [6]. It can also be used to filter voltage harmonics and to compensate for unbalanced voltages [14].

If the source to the voltage dip, e.g. a short-circuit fault, is downstream of the device, the

DVR has to take the full short-circuit current which requires an advanced protection system. This increases the costs of the device and stands as the main disadvantage of the DVR.

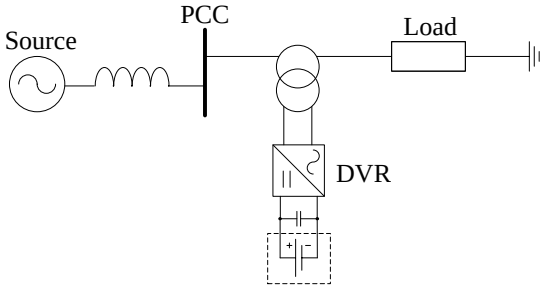

Figure 2.7: Distribution grid with a DVR.

UPS

For very sensitive low power equipment such as computers and servers, up to 4000 kVA, static uninterruptible power supplies (UPSs) can be used [22]. There are different structures of UPSs, however, common to all structures are that active power can be supplied from an energy storage. Hence, complete mitigation of voltage dips and other power quality problems can be obtained. Depending on the size of the storage, even interruptions can be mitigated. One structure of an UPS is shown in Figure 2.8.

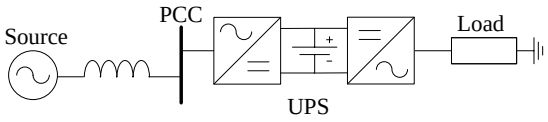

Figure 2.8: Distribution grid with an UPS.

STS

An alternative way to protect a sensitive load from voltage dips is to use a static transfer switch (STS), showed in Figure 2.9. With an STS, the load is feed from either a primary feeder or a secondary feeder. If a voltage dip is detected on the primary feeder, thyristor switches are used to change the supply to the secondary feeder [22]. It should be noticed that voltage dips on transmission level will affect both feeders, hence, the STS does not provide any protection for these types of voltage dips.

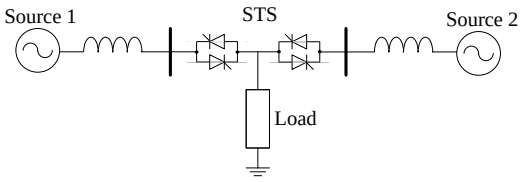

Figure 2.9: Distribution grid with an STS.

2.4 Conclusion

In this chapter has the most important FACTS controllers used on transmission level been described. Furthermore, the most common custom power devices used for power quality improvements on distribution level have been described.

Chapter 3

Energy Storage at Distribution Level

This chapter treats the classification of applications for energy storage systems and describes some of the most common storage mediums for power quality applications.

3.1 Introduction

It is not the lack of applications, but rather the shortage of suitable storage mediums, that so far has limited the use of energy storages in the power system. However, decreasing prices and rapid development in especially battery performance, have caused an increased interest in energy storages for power systems. Hence, when describing the future power system, the smart grid, energy storage systems are usually described as one of solutions [4].

This chapter classifies energy storage applications depending on the required speed of response and presents an overview of the applications which demand slower responses. Furthermore, the types of storage mediums possible to use in faster applications are described.

3.2 Classification of Energy Storage Applications

Different energy storage systems have been developed for the wide range of needs that exist in the power system, driven by requirements of lower costs and better performance. Basically, a storage system consists of two parts, a storage medium for storing the energy and an interface between the storage and the grid. Each individual application provides specific characteristics on the storage and the interface, the most common criteria include power and energy rating, cost and response time. A common method to classify applications is to split them into power applications and energy applications as in [12]. The power applications require a storage medium with a high power to energy ratio while the energy applications need the opposite.

Another classification is obtained by dividing the applications into those which demand fast responses, and those which can be fulfilled with slower responses. A “fast” response does, in this thesis, correspond to a power exchange which can be controlled in the range of milliseconds. To meet these demands, both the storage medium and the interface need to react with this speed. This requires power electronic based interfaces, like the E-STATCOM, which is used as the interface for the storage systems in this thesis. Fast applications can also be denoted power quality applications since these applications regard time scales within one fundamental cycle, hence in the range which concerns power quality. The maximum amount of energy that needs to be stored in these “fast” applications are normally less than one hour of maximum output power,

and most often not more than fifteen minutes. In some applications, the amount of energy equals the maximum output power during a few seconds [8].

A few of the most common slower applications, e.g. energy shifting, and the corresponding storage systems, will be described in the next part. It is followed by a short overview of power quality applications.

3.2.1 Energy Time-Shifting and Auxiliary Services

Energy storage systems for slower applications can range from utility-scale systems down to small consumer products. The largest systems on hundreds of MW are used for energy time-shifting [28], i.e. electricity is bought and stored when the price is low, and later sold and extracted into the system when the price is higher. This can be done on a daily bases to counteract daily consumption profiles, or to store excess renewable power and save it until the demand is higher. Energy storage systems used for these applications are often pumped hydro power or compressed air energy storage [12]. These systems operate by pumping water to a higher reservoir, or by compressing air in a chamber, respectively, to store energy. Later, the energy is extracted by letting the water or air, respectively, flow though a turbine.

Midrange applications, likely to be installed on distribution level, include integration of renewables (mostly wind power) and auxiliary services like black start capability and ramping services, and possibly frequency regulation (where response times can be in the range of seconds) [12]. Stationary or transportable energy storage systems can be used for congestion relief or upgrade deferral, i.e. to supply power during peak hours when the grid is fully loaded. The storage systems commonly used for these applications are different types of batteries with a capacity which range from a few MW up to a hundred MW for one to a few hours [28].

The smallest systems are those used for consumer applications, e.g. providing increased reliability and reduction of overall costs of electricity [12]. This can be done by shifting the consumption from hours with high prices, to hours with lower prices (this require variable customers' tariffs). Storage systems on this level are not common yet, but are believed to be battery based with capacities in the range of kW for a few hours [12].

More extensive information concerning the status, future predictions and economic potential for different types of energy storage systems can be found in [28] and [12].

3.2.2 Power Quality Improvements

This thesis has focused on applications which require fast power exchange, i.e. applications which concern power quality, installed on distribution level. By the use of an E-STATCOM, the active and reactive power can be precisely controlled to improve the power quality of a system. Since this is the main part of this work, it will be further explained in later chapters. A derivation of how the technical system is designed is given in Chapter 4, and in Chapter 3 is the power quality applications, made possible by the usage of energy storage, treated. Further improvements in power quality, enabled by energy storage systems, are investigated in Chapter 6.

In short, the found applications concern complete mitigation of voltage dips and balancing of loads when entering islanding operation.

3.3 Storage Types for Power Quality Applications

In this thesis, no particular storage type has been considered to be used together with the E-STATCOM. Instead, the system performance and the interaction with the grid have been in focus. Also, no single storage medium is the obvious choose in practice, and a medium that is suggested today is likely to be outdated in a few years. Due to an intensive research, the development of new and better storage types is, especially for batteries, rapid, which results in improved performance and reduced costs.

Nevertheless, this section gives an overview of the most common storage types for applications which require fast response.

3.3.1 Batteries

In batteries, bidirectional electrochemical reactions are used to convert electric energy into chemical energy for charging, and the opposite for discharging [8]. There are various types of chemical substance used in batteries, providing different characteristics such as energy density, power density, number of cycles and cost.

Lead-acid, NiCd and sodium-sulfur batteries are today described as commercial while NiMH, vanadium redox, advanced lead-acid and some Li-ion types are on demonstration level [28]. The characteristics depend on the application but for grid support applications on transmission and distribution level, [28] gives the following numbers; the price for these types of batteries are in the range from 1200-4600 $/kW and 300-1700 $/kWh , the efficiency range from 60 % to about 94 % with a number of life cycles from 4500 to over 10 000. However, these numbers are hugely dependent on the exact application. Substantial funding is today put on research concerning various lithium batteries, often driven by interest from industries in the area of electric vehicles or mobile consumer products [8].

Compared to flywheels and capacitors, some types of batteries can store more energy and at the same time be used in power quality applications [28].

Batteries are connected to the DC-side of an E-STATCOM with a DC/DC converter to control the power exchange between the storage and the interface.

3.3.2 Flywheels

A flywheels system consists of a rotating mass which stores energy as kinetic energy. By increasing the rotational speed, energy can be stored in the flywheel and by reducing the speed, energy can be extracted. This can be expressed as

$$W = \frac{1}{2} m \left(\omega_2^2 - \omega_1^2 \right) \tag{3.1}$$

The speed of the flywheel is controlled by an AC generator connected though an AC/DC converter to the DC-side of the grid interface.

Flywheels are characterised by a high power vs. energy ratio, i.e. they can provide high powers for short moments [8]. Two examples are smoothing of a pulsating power demand and as storage in UPS.

According to [28]; flywheels used in demo projects for fast frequency regulation have an efficiency around 85-87 % with a lifetime of more than 100 00 cycles and a price of 1950-2200 $/kW and 7800-8800 $/kWh. Furthermore, flywheels have response times of 4 ms or less [28].

Currently, most research is directed towards improving the material of the rotational mass [8], i.e. making it more durable. Hence, the amount of energy that can be stored in a flywheel could be increased.

3.3.3 Capacitors

In a capacitor, energy is stored as electric charges between two metallic plates separated by a dielectric. Energy can be stored by increasing the voltage across the capacitor and extracted by decreasing the voltage, as expressed by

$$W = \frac{1}{2} C \left(V_2^2 - V_1^2 \right) \tag{3.2}$$

where C is the capacitance of the capacitor which depends on the physical properties of the capacitor.

There is a big variety of chemical and physical solutions for capacitor storages. Some types significantly differ from ordinary capacitors and are given specific names, for example supercapacitors. A supercapacitor obtains a much higher charge density compared to conventional capacitors by utilizing electrochemical double layers and, during the last two decades, it has been commercialized and is now used when a high capacitance is needed [8].

Similarly to flywheels, capacitors are mostly used in high power applications with relatively small amounts of stored energy. According to [4] do capacitors offer a higher efficiency than flywheels, up to 97 % and 50 % longer lifetime. Also, the price is less than one tenth compared to flywheels.

3.3.4 Superconducting Magnetic Energy Storage

The lack of electric resistance in a superconductor enables it to store magnetic energy by conducting a current in a closed loop which, under ideal conditions, can persist indefinitely [8]. Superconducting magnets control the amount of current flowing through the loop and hence, energy can be stored or extracted from the system.

Just as with flywheels and capacitors, the technique is used in high power applications with limited demands on the amount of energy. The technique is commercialized but only used in a few special applications [8].

3.4 Conclusion

In this chapter has energy storage applications been classified with respect to their required response times. A few applications which do not demand a particularly fast response have been described. Some storage mediums which potentially could be used in power quality application on distribution level have been covered.

It should be stressed again that no specific storage type is considered in the rest of the thesis. Instead, a general energy storage will be used which is modelled as a constant DC-source.

Chapter 4

Control of Shunt-Connected VSC for Power Quality Applications

This chapter treats the derivation of the control system used in a shunt-connected VSC, both with and without energy storage. Furthermore, the influence of the control system on the system performance during a voltage dip is analysed.

4.1 Introduction

Grid-connected VSCs with self-commutated valves, like the insulated-gate bipolar transistor (IGBT), are getting more and more common on distribution level for many types of applications. As mentioned in Chapter *2 Power Electronics in Power Systems*, a shunt-connected VSC can be used to provide an increased control of the voltage and improve the power quality in distribution grids.

The control of a VSC is often realized by a cascade controller as shown in Figure 4.1, i.e. two closed loop controllers where the outer loop provides a reference for the inner loop. The inner controller is often called the vector current controller (VCC) with the objective to control the current through the filter reactor by adjusting the terminal voltage. The outer controller is used to control the bus voltage at the PCC by sending a current reference to the inner current loop. Depending on how the outer controller is realized, it is denoted reactive power controller (RPC), when no energy storage is attached, or voltage controller (VC), when there is an energy storage on the DC-side of the VSC.

In this chapter is first the derivation of the VCC treated, followed by the derivation of the VC and the RPC. Furthermore, the used synchronization system is explained. Then, a list of the simplifications in the derived control system, compared to a real system, is given and finally the system performance is investigated during a voltage dip.

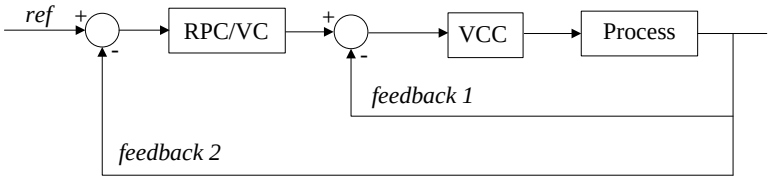

Figure 4.1: Structure of the cascade controller.

4.2 Vector Current Controller

The key element in the investigated systems is the VSC and its main circuit scheme is shown in Figure 4.2. Pulse width modulation (PWM) technique is used to set the switching signals $sw_a(t)$, $sw_b(t)$ and $sw_c(t)$ to ± 1. If the switching signal for one phase is set to 1, the upper valve in that phase is turned on and the terminal voltage in that phase will be equal to $u_{dc}(t)/2$. Opposite, if the switching signal is set to -1, the lower valve is turned on and the terminal voltage of that phase will be equal to $-u_{dc}(t)/2$. A blanking time is needed to avoid short-circuit of the VSC phase-legs [33]. If the switching frequency is assumed to be very high, the VSC can be modelled as an ideal sinusoidal three-phase voltage source, thus, neglecting all switching harmonics. This is a useful approximation when the performance of the device is of interest and not its exact behaviour.

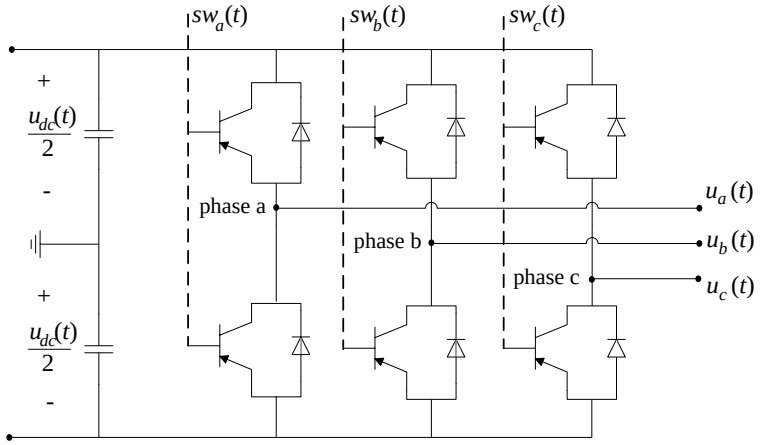

Figure 4.2: Three-phase VSC.

The VSC is connected to the point of common coupling (PCC) through a LCL-filter as shown in Figure 4.3. The inductance of the converter-side filter reactor is denoted L_f, the resistance of the filter reactor R_f, the filter capacitance C_f and the grid-side filter inductance, constituted by the leakage inductance of the injection transformer, is denoted L_{tr}. The terminal voltages are denoted $u_a(t)$, $u_b(t)$ and $u_c(t)$, the current through the filter reactor $i_{f,a}(t)$, $i_{f,b}(t)$ and $i_{f,c}(t)$ and the capacitor voltage $e_{c,a}(t)$, $e_{c,b}(t)$ and $e_{c,c}(t)$. All loads that will be connected to the PCC are assumed to be balanced.

4.2.1 Electric System

Using Kirchhoff's voltage law (KVL) between the VSC terminals and the capacitors in Figure 4.3, the following differential equations can be obtained

$$u_a(t) = e_{c,a}(t) + R_f i_{f,a}(t) + L_f \frac{di_{f,a}(t)}{dt} \tag{4.1}$$

$$u_b(t) = e_{c,b}(t) + R_f i_{f,b}(t) + L_f \frac{di_{f,b}(t)}{dt} \tag{4.2}$$

$$u_c(t) = e_{c,c}(t) + R_f i_{f,c}(t) + L_f \frac{di_{f,c}(t)}{dt} \tag{4.3}$$

The three-phase equations of (4.1)-(4.3) can be transformed into a two phase stationary system using Clark's transformation. This fixed coordinate system is denoted the $\alpha\beta$-system and a three-

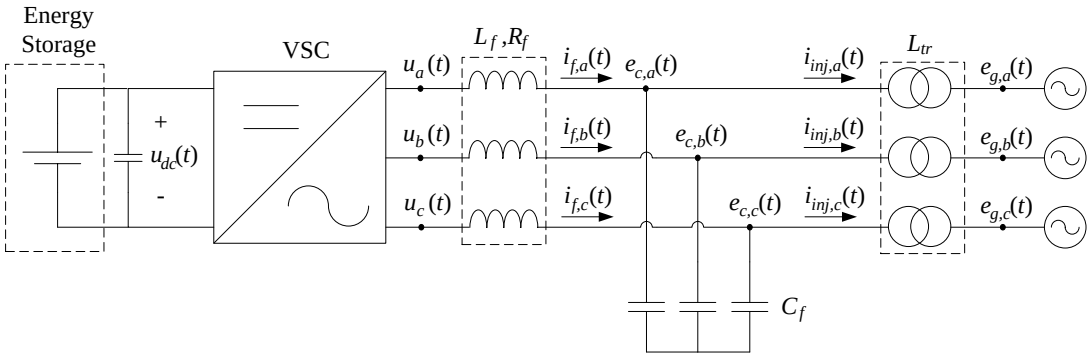

Figure 4.3: Three-phase VSC connected to the PCC through a LCL-filter.

phase system can, assuming no zero sequence components, be transformed into the $\alpha\beta$-system using the following (power invariant) transformation matrix

$$\begin{bmatrix} x^\alpha \\ x^\beta \end{bmatrix} = \sqrt{\frac{2}{3}} \begin{bmatrix} 1 & -\frac{1}{2} & -\frac{1}{2} \\ 0 & \frac{\sqrt{3}}{2} & -\frac{\sqrt{3}}{2} \end{bmatrix} \begin{bmatrix} x_a \\ x_b \\ x_c \end{bmatrix} \tag{4.4}$$

where the transformation is explained in Appendix *A Transformations for Three-Phase Systems*. Applying (4.4) to the three-phase equations in (4.1)-(4.3), the differential equations can be rewritten as

$$u^\alpha(t) = e_c^\alpha(t) + R_f i_f^\alpha(t) + L_f \frac{di_f^\alpha(t)}{dt} \tag{4.5}$$

$$u^\beta(t) = e_c^\beta(t) + R_f i_f^\beta(t) + L_f \frac{di_f^\beta(t)}{dt} \tag{4.6}$$

Equations (4.5) and (4.6) can be combined and written in space vector form as

$$\underline{u}^{\alpha\beta}(t) = \underline{e}_c^{\alpha\beta}(t) + R_f \underline{i}_f^{\alpha\beta}(t) + L_f \frac{d\underline{i}_f^{\alpha\beta}(t)}{dt} \tag{4.7}$$

where an underline denotes a complex space vector, e.g. $\underline{e}^{\alpha\beta} = e^\alpha + je^\beta$. The same notation is used for voltages, currents and other quantities.

Since the $\alpha\beta$-frame is fixed, the vectors are AC quantities rotating with a frequency ω in the $\alpha\beta$-frame. Moving into the dq-synchronous reference frame transform the vectors into DC quantities, hence, making it more simple to use PI-regulators [19]. Figure 4.4 shows how the $\alpha\beta$- and dq-frames are coupled. The transformation from the $\alpha\beta$-frame to the dq-frame is given by

$$\begin{bmatrix} x^d \\ x^q \end{bmatrix} = \begin{bmatrix} \cos(\theta(t)) & -\sin(\theta(t)) \\ \sin(\theta(t)) & \cos(\theta(t)) \end{bmatrix} \begin{bmatrix} x^\alpha \\ x^\beta \end{bmatrix} \tag{4.8}$$

where $\theta(t)$ is the transformation angle given by the phase-locked-loop (PLL). The PLL is synchronized with the PCC such that, in steady state, the d-axis in the dq-frame is aligned with the voltage vector as showed in Figure 4.4. See Section *4.5 Synchronization System - PLL* for an explanation of the structure of the PLL. Using (4.8), the system in (4.7) can be expressed in dq-quantities as

$$\underline{u}^{dq}(t) = \underline{e}_c^{dq}(t) + R_f \underline{i}_f^{dq}(t) + L_f \frac{d\underline{i}_f^{dq}(t)}{dt} + j\omega L_f \underline{i}_f^{dq}(t) \tag{4.9}$$

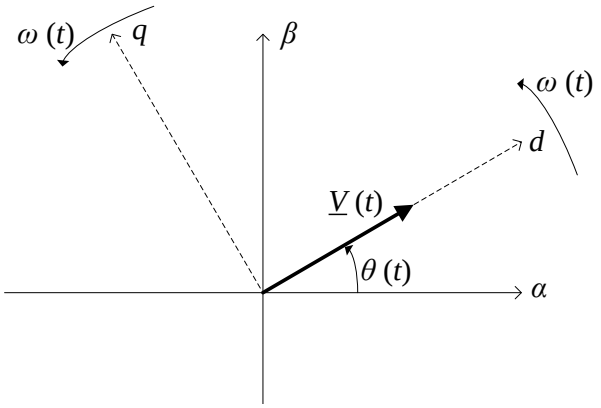

Figure 4.4: $\alpha\beta$- and dq-frames.

Since the d-axis, in steady state, is aligned with the voltage vector, the q-component of the voltage is equal to zero. This also means that the current vector easily can be split into an active and a reactive component. The d-component of the current vector, which in steady state is parallel to the voltage vector, therefore corresponds to the active component of the current (power). Also, the q-component of the current vector, which in steady state is perpendicular to the voltage vector, corresponds to the reactive component of the current (power). It should be noticed that, in agreement with Figure 4.3, a positive current (power) is injected into the grid by the VSC.

4.2.2 Controller Design

Transforming (4.9) into the Laplace domain and reorganizing gives

$$\underline{i}_f^{dq}(s) = \frac{1}{R_f + j\omega L_f + sL_f}\left(\underline{u}^{dq}(s) - \underline{e}_c^{dq}(s)\right) \tag{4.10}$$

which describes how the filter current is related to the voltages, and in particular to the controllable parameter $\underline{u}^{dq}(s)$.

Measuring the filter current and comparing it to the reference value (obtained from the outer control loop), gives an error which acts as an input to the PI-regulator in the VCC. There are two parallel control systems, one for the real current (active power), and one for the imaginary current (reactive power) of the current vector. The output from the VCC is the terminal voltage vector reference $\underline{u}_{ref}^{dq}(s)$ which is transformed to a three-phase value and sent to the PWM to obtain the switching signals. This process is assumed to be very fast, such that, from the VCC's view, the reference vector $\underline{u}_{ref}^{dq}(s)$ is instantaneously transformed into the actual terminal voltage vector $\underline{u}^{dq}(s)$.

Hence, using (4.10), the process of the system, from the controllable terminal voltage $\underline{u}^{dq}(s)$ to the filter current, $\underline{i}_f^{dq}$, can be written as

$$G_{c1} = \frac{\underline{i}_f^{dq}(s)}{\underline{u}^{dq}(s)} = \frac{1}{sL_f + R_f + j\omega L_f} \tag{4.11}$$

However, the objective of the VCC is to control the active and the reactive current components separately. By looking at (4.11) it can be noticed that there is a cross-coupling term $j\omega L_f$ which originates from the rotation of the dq-frame. The cross-coupling term would map a component on the d-axis onto the q-axis and vice verse. When designing the controller, the cross-coupling term can be feed-forwarded to cancel out its effects. Hence, G_{c1} can be simplified to an equivalent process

$$G_{c2} = \frac{G_{c1}}{1 - G_{c1} j\omega L_f} = \frac{\dfrac{1}{sL_f + R_f + j\omega L_f}}{1 - \dfrac{1}{sL_f + R_f + j\omega L_f} j\omega L_f}$$
$$= \frac{\dfrac{1}{sL_f + R_f + j\omega L_f}}{\dfrac{sL_f + R_f + j\omega L_f - j\omega L_f}{sL_f + R_f + j\omega L_f}} = \frac{1}{sL_f + R_f} \tag{4.12}$$

which also shows that the cross-coupling can be eliminated by feed-forwarding. Note that this only holds when the feed-forward parameter can be measured and feed-forward instantaneously, like in a continuous system. If there are delays, the feed-forwarded value would no longer equal the measured value, since the parameter value would have changed after the sampling. Feed-forwarding can still be used in discrete system, but it can not completely eliminate the effects from the disturbances caused by the parameter.

From (4.10) it can be noticed that also $\underline{e}_c^{dq}$ have an impact on the filter current. This could be seen as a disturbance to the system and the capacitor voltage is thus also feed-forwarded into the VCC to cancel out its effects. Figure 4.5 shows the block diagram of the VCC with the feed-forward terms, the PMW and the process included.

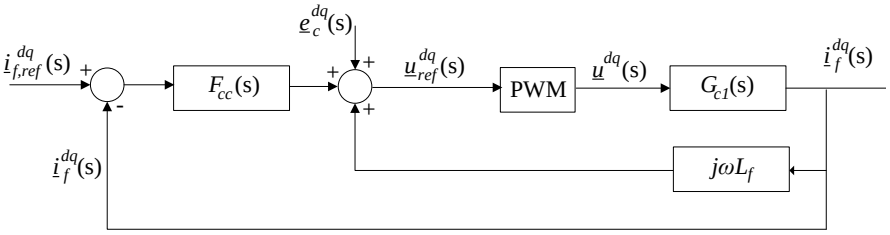

Figure 4.5: Block diagram of the VCC with feed-forward of the cross coupling term $j\omega L_f$ and the disturbance $\underline{e}_c^{dq}$.

In Figure 4.5, the block $F_{cc}(s)$ denotes the PI-regulator of the VCC, described by

$$F_{cc}(s) = k_{p,cc} + \frac{k_{i,cc}}{s} = \frac{k_{p,cc}s + k_{i,cc}}{s} \tag{4.13}$$

where $k_{p,cc}$ is the proportional gain and $k_{i,cc}$ is the integral gain which can be determined by using the closed-loop transfer function from $\underline{i}_{f,ref}^{dq}$ to $\underline{i}_f^{dq}$ in Figure 4.5.

The closed-loop transfer function, i.e. the current control loop, can thus be written as

$$G'_{cc} = \frac{F_{cc}G_{c2}}{1 + F_{cc}G_{c2}} = \frac{\dfrac{k_{p,cc}s + k_{i,cc}}{s}\dfrac{1}{sL_f + R_f}}{1 + \dfrac{k_{p,cc}s + k_{i,cc}}{s}\dfrac{1}{sL_f + R_f}}$$
$$= \frac{k_{p,cc}s + k_{i,cc}}{s^2 L_f + (R_f + k_{p,cc})\, s + k_{i,cc}} \tag{4.14}$$

The objective of the design of the controller is to obtain a good performance, basically a fast response and a good damping. Since the resistance in the filter is included in the used model, the damping of the controller gets dependent on R_f as seen in (4.14). Increasing the value of R_f improves the damping of the system but it also increases the losses in the filter, which is not

desired. Furthermore, the exact value of R_f is needed in order to obtain an accurate controller, and this can be difficult since the resistance in the filter depends not only on the power flow through the filter, but also outer effects like the ambient temperature.

Instead, as proposed in [13], a fictitious damping resistance R_{acc} can be introduced in the controller and the filter resistance can be kept low while still obtaining a proper damping. As it will later be shown, the controller performance can this way be made less dependent on the filter resistance. Similar to the cross-coupling term, R_{acc} is also feed-forwarded and the updated block diagram is shown in Figure 4.6.

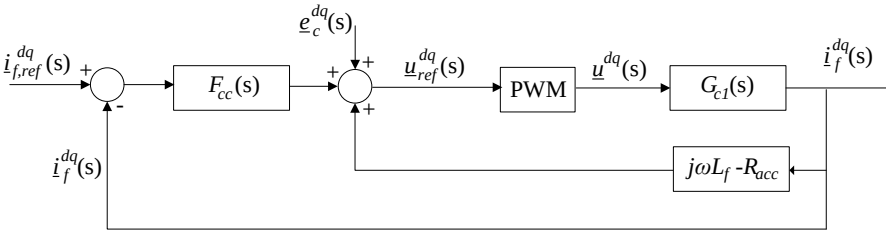

Figure 4.6: Block diagram of the vector current controller with feed-forward of $j\omega L_f$ and the active damping.

Hence, with the damping term included, the process G_{c2} can be rewritten (with the same method as for the cross-coupling term) as the equivalent process

$$G_{c3} = \frac{1}{sL_f + R_f + R_{acc}} \tag{4.15}$$

giving the updated closed-loop transfer function

$$\begin{aligned} G_{cc} &= \frac{F_{cc}G_{c3}}{1 + F_{cc}G_{c3}} \\ &= \frac{k_{p,cc}s + k_{i,cc}}{s^2L_f + (R_f + R_{acc} + k_{p,cc})\,s + k_{i,cc}} \end{aligned} \tag{4.16}$$

It is desired that the response of the VCC should be equal to a low-pass filter. Denoting the bandwidth of the VCC ω_{cc}, the ideal performance can be expressed as

$$\begin{aligned} G_{cc} &= \frac{\omega_{cc}}{s + \omega_{cc}} = \frac{\omega_{cc}\,(s + \omega_{cc})}{(s + \omega_{cc})\,(s + \omega_{cc})} \\ &= \frac{\omega_{cc}\,(s + \omega_{cc})}{s^2 + 2\omega_{cc}s + \omega_{cc}^2} \end{aligned} \tag{4.17}$$

which is written in the same form as (4.16) and, by solving the equations, the controller gains and the active damping can be selected as

$$R_{acc} = \omega_{cc}L_f - R_f \tag{4.18}$$

$$k_{p,cc} = \omega_{cc}L_f \tag{4.19}$$

$$k_{i,cc} = \omega_{cc}\,(R_{acc} + R_f) \tag{4.20}$$

It can be noticed that neither the proportional gain nor the integral gain is dependent on R_f. R_{acc} on the other hand, is depending on the filter resistance. However, R_f is, compared to $\omega_{cc}L_f$, small and it can thus be said that the controller in total has a small dependency of R_f.

In all, according to Figure 4.6 and with the parameters selected according to (4.18)-(4.20), the control law can in the time domain be written as

$$\begin{aligned}\underline{u}_{ref}^{dq}(t) = \underline{e}_c^{dq}(t) + (-R_{acc} + j\omega L_f)\,\underline{i}_f^{dq}(t) \\ + k_{p,cc}\left(\underline{i}_{f,ref}^{dq}(t) - \underline{i}_f^{dq}(t)\right) + \int_0^t k_{i,cc}\left(\underline{i}_{f,ref}^{dq}(\tau) - \underline{i}_f^{dq}(\tau)\right) d\tau\end{aligned} \tag{4.21}$$

4.3 Reactive Power Controller - VSC without significant Energy Storage

As mentioned before, a cascade control structure is used which means that an outer control loop sends a reference value to the inner controller, i.e. the VCC. The structure of the whole control system is shown in Figure 4.7 where the RPC is the controller in the outer loop.

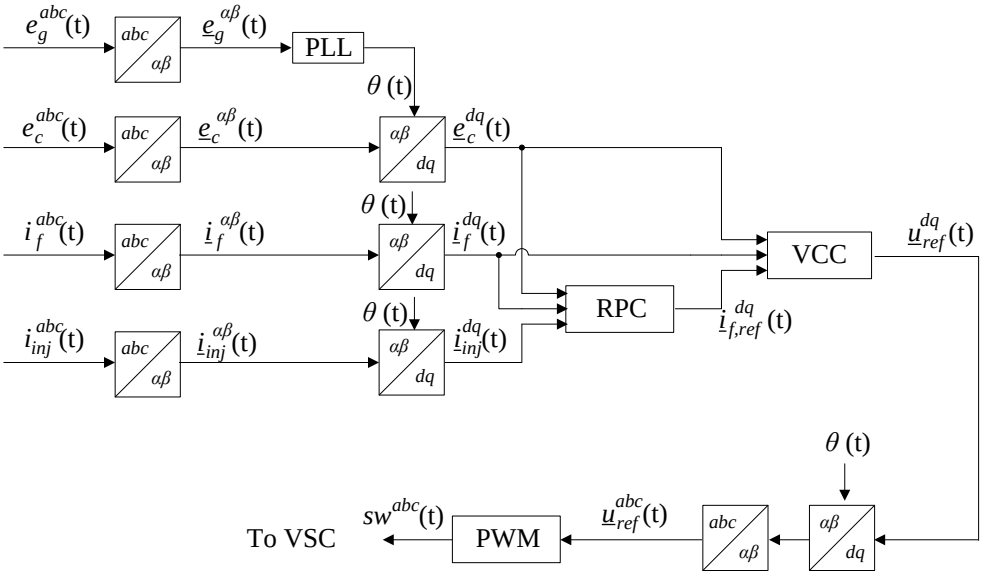

Figure 4.7: Block diagram of the D-STATCOM.

If no additional energy storage is attached to the DC-side of the VSC, or if the DC-capacitor is not sufficiently large, the VSC can only produce or consume reactive power. Hence, one degree of freedom is lost and the D-STATCOM can either control the phase of the voltage or, which is most common, only the magnitude of the voltage. This can be done in a number of ways but the method used in this work controls the energy stored in the filter capacitor, a methodology commonly used to control the DC-voltage across DC-capacitors, for example in [18].

The objective is that the D-STATCOM should control the PCC voltage. However, with a LCL-filter, the voltage across the capacitor could be chosen as the desired parameter to control. Thus, the PCC voltage can be used only for synchronization in the PLL. This means that simpler and less expensive voltage measurement equipment can be used at the PCC [6]. Since the impedance between the PCC and the filter capacitor, i.e. the leakage inductance of the injection transformer, is small, there is just a slight difference between the two voltages, in both magnitude and phase. This difference can, in steady state, be compensated for by feed-forwarding a voltage equal to the voltage drop over the injection transformer, or it can be neglected. In this work, the later is chosen.

Hence, the capacitor voltage $\underline{e}_c$ is chosen as the controlled voltage in the VSC.

4.3.1 Electric System

The current-voltage relation in the filter capacitors in the $\alpha\beta$-frame is written as

$$\underline{i}_c^{\alpha\beta}(t) = C_f \frac{d\underline{e}_c^{\alpha\beta}(t)}{dt} \tag{4.22}$$

which in the dq-frame is written as

$$\underline{i}_c^{dq}(t) = C_f \frac{d\underline{e}_c^{dq}(t)}{dt} + j\omega C_f \underline{e}_c^{dq}(t) \tag{4.23}$$

The power exchange in the capacitors is obtained by multiplying the voltage across the capacitors, $\underline{e}_c^{dq}$, with the capacitor current in (4.23). Hence, the power consumed or produced in the capacitors are written as

$$S_c(t) = P_c(t) + jQ_c(t) = \underline{e}_c^{dq}(t)\underline{i}_c^{dq}(t)^* = C_f \underline{e}_c^{dq}(t)\frac{d\underline{e}_c^{dq}(t)}{dt} - j\omega C_f \underline{e}_c^{dq}(t)^2 \tag{4.24}$$

where * denotes the complex conjugate. If it is assumed that the alignment with the PLL is correct, i.e. $e_c^q = 0$, and that the capacitors are ideal, i.e. $P_c = 0$ and $i_c^d = 0$, (4.24) can be simplified as

$$\begin{aligned} S_c(t) &\approx jQ_c(t) && (4.25)\\ &\approx jC_f e_c^d(t)\frac{de_c^q(t)}{dt} - j\omega C_f e_c^d(t)^2 \\ &\approx jC_f e_c^d(t)\frac{de_c^d(t)}{dt} - j\omega C_f e_c^d(t)^2 \\ &= j\frac{C_f}{2}\frac{de_c^d(t)^2}{dt} - j\omega C_f e_c^d(t)^2 \\ &\approx j\frac{C_f}{2}\frac{d|\underline{e}_c^{dq}(t)|^2}{dt} - j\omega C_f |\underline{e}_c^{dq}(t)|^2 && (4.26) \end{aligned}$$

where it is further assumed that the change in the q-component is equal to the change in the d-component and that the magnitude of the voltage vector is the same as the magnitude of the d-component.

Using the notation and the direction of the corresponding currents given in Figure 4.3, the reactive power flowing into the capacitor can be written as

$$Q_c(t) = Q_f(t) - Q_{inj}(t) \tag{4.27}$$

where Q_f denotes the reactive power flowing through the filter reactor and Q_{inj} denotes the reactive power flowing into the PCC through the injection transformer.

4.3.2 Controller Design

Transforming (4.26) into the Laplace domain, using (4.27) and reorganizing gives

$$|\underline{e}_c^{dq}(s)|^2 = \frac{1}{s\frac{C_f}{2} - \omega C_f}\left(Q_f(s) - Q_{inj}(s)\right) \tag{4.28}$$

which describes how the magnitude of the square of the capacitor voltage is related to the controllable parameter Q_f.

The magnitude of $\underline{e}_c^{dq}(s)$ is measured and squared, and compared to its reference value (set to the pre-fault value). This gives an error vector which is sent to the PI-regulator in the RPC. There is only one controller in the RPC since the active power is not controlled, but simply set to

zero. The output from the RPC should be the filter current vector reference that is sent to the VCC. Since the VCC is much faster than the RPC [17], it is approximated that the reference value $\underline{i}_{f,ref}^{dq}$ is instantaneously transformed into the actual filter current $\underline{i}_f^{dq}$. For this approximation to be valid it is commonly said that the inner loop should be at least ten times faster than the outer loop [19].

Since the controllable parameter in (4.28) is a reactive power, while the output from the RPC should be a reference current vector, it is necessary to rewrite (4.28) as a function of the corresponding currents. This causes a problem since only the magnitude of the capacitor voltage is controlled, not the individual dq-components. In steady state, the dq-components of both currents and voltages are know but when injecting reactive power in transient operation, due to the slowness in the PLL, the actual angle θ might change and therefore also the d- and q-components. However, if it assumed that the d- and q-components do not deviate too much from the steady state values, they still can be used to derive the control law.

With the d-axis aligned with the voltage vector, the reactive power flowing in the system can be expressed as

$$Q_f = -e_c^d i_f^q + e_c^q i_f^d \approx -e_c^d i_f^q \tag{4.29}$$

$$Q_{inj} = -e_c^d i_{inj}^q + e_c^q i_{inj}^d \approx -e_c^d i_{inj}^q \tag{4.30}$$

With (4.29) and (4.30) can (4.28) be rewritten as

$$|\underline{e}_c^{dq}(s)|^2 = \frac{-e_c^d(s)}{s\dfrac{C_f}{2} - \omega C_f}\left(i_f^q(s) - i_{inj}^q(s)\right) \tag{4.31}$$

Hence, from (4.31), the process from the q-component of the filter current i_f^q to the square of the capacitor voltage, $|\underline{e}_c^{dq}|^2$, can be obtained as

$$G_r = \frac{|\underline{e}_c^{dq}(s)|^2}{i_f^q(s)} = \frac{-e_c^d(s)}{s\dfrac{C_f}{2} - \omega C_f} \tag{4.32}$$

It can be noticed is (4.31) that i_{inj}^q has an impact on the voltage square. Thus, i_{inj}^q is feed-forwarded in the RPC. In (4.32), ωC_f does not create any cross-coupling but it does act as a disturbance to the system. Hence, it should be feed-forwarded in the RPC. However, it can not be directly feed-forwarded with the square of the voltage since this would give a reactive power and not a current. Instead, to obtain a q-component of the current, $-\omega C_f/e_{c,LP}$ is feed-forwarded where $e_{c,LP}$ is the low-pass-filtered magnitude of the capacitor voltage, expressed as

$$e_{c,LP} = \frac{\omega_{cc}}{s + \omega_{cc}}|\underline{e}_c^{dq}| \tag{4.33}$$

where it is assumed that the bandwidth of the low-pass filter is the same as the bandwidth of the VCC.

Including the feed-forward of $-\omega C_f/e_{c,LP}$, the process can be simplified as

$$G_r' = \frac{G_r}{1 + G_r\dfrac{\omega C_f}{-e_{c,LP}}} = \frac{\dfrac{-e_c^d(s)}{s\dfrac{C_f}{2} - \omega C_f}}{1 + \dfrac{-e_c^d(s)}{s\dfrac{C_f}{2} - \omega C_f}\dfrac{\omega C_f}{-e_{c,LP}}} \approx -\frac{2e_c^d}{sC_f} \tag{4.34}$$

if it once again is assumed that the magnitude of the voltage is the same as the magnitude of the d-component.

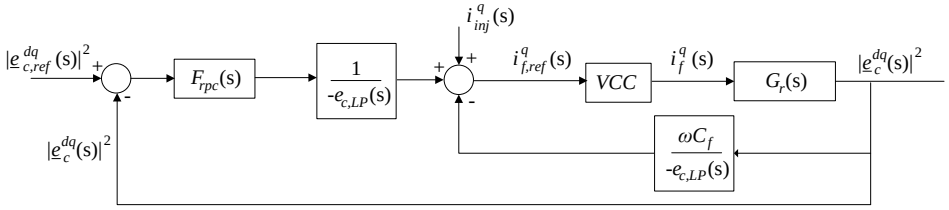

Figure 4.8: Block diagram of the RPC and the process.

Also the output from the PI-regulator has to be transformed into a current quantity. Therefore, the output of the PI-regulator is divided by $-e_{c,LP}$ as well. The complete block digram of the controller and the process is shown in Figure 4.8.

As in the VCC, $F_{rpc}(s)$ is the PI-regulator in the RPC which is described by

$$F_{rpc}(s) = k_{p,rpc} + \frac{k_{i,rpc}}{s} = \frac{k_{p,rpc}s + k_{i,rpc}}{s} \tag{4.35}$$

where $k_{p,rpc}$ is the proportional gain and $k_{i,rpc}$ is the integral gain which can be calculated using the closed-loop transfer function from $|\underline{e}_{c,ref}^{dq}|^2$ to $|\underline{e}_c^{dq}|^2$, shown in Figure 4.8.

The closed-loop transfer function, i.e. the reactive power control loop, is then written as

$$G_{rpc} = \frac{\frac{F_{rpc}}{-e_{c,LP}}G_r'}{1 + \frac{F_{rpc}}{-e_{c,LP}}G_r'} = \frac{-\frac{k_{p,rpc}s + k_{i,rpc}}{se_{c,LP}}\left(-\frac{2e_c^d}{sC_f}\right)}{1 - \frac{k_{p,rpc}s + k_{i,rpc}}{se_{c,LP}}\left(-\frac{2e_c^d}{sC_f}\right)} \approx \frac{k_{p,rpc}s + k_{i,rpc}}{s^2\frac{C_f}{2} + k_{p,vc}s + k_{i,vc}} \tag{4.36}$$

if it is assumed that $e_{c,LP} \approx e_c^d$.

Since the resistances of the capacitors have not been included in the used model, there is no need for adding a damping term as in the VCC since the process already is in the form of a low-pass filter. However, if the capacitor resistances would have been included, a damping term could have been added in a similar way as in the VCC. Now, a satisfying performance of the controller can be obtained by simply selecting $k_{i,rpc} = 0$, and (4.36) can thus be simplified to

$$G_{rpc} = \frac{k_{p,rpc}}{s\frac{C_f}{2} + k_{p,rpc}} \tag{4.37}$$

The desired step response from the reactive power controller should, just as in the VCC, have the form of a low-pass filter, giving

$$G_{rpc} = \frac{\omega_{rpc}}{s + \omega_{rpc}} \tag{4.38}$$

where ω_{rpc} is the desired bandwidth of the RPC. Comparing (4.37) and (4.38) makes it easy to select the controller gains as

$$k_{p,rpc} = \omega_{rpc}\frac{C_f}{2} \tag{4.39}$$

$$k_{i,rpc} = 0 \tag{4.40}$$

To simplify the following notation, the division by two is extracted from the proportional gain in (4.39), and implemented as a part of the low-pass filtered block as shown in Figure 4.9. Hence, (as it will be shown later) the controller gains in the RPC and in the VC will be identical. From now and on, the proportional and the integral gain in the RPC are selected and denoted as

$$k_{p,vc} = \omega_{vc} C_f \tag{4.41}$$

$$k_{i,vc} = 0 \tag{4.42}$$

with the block diagram of the controller updated and shown in Figure 4.9. Note that also the bandwidth of the RPC is now denoted ω_{vc}.

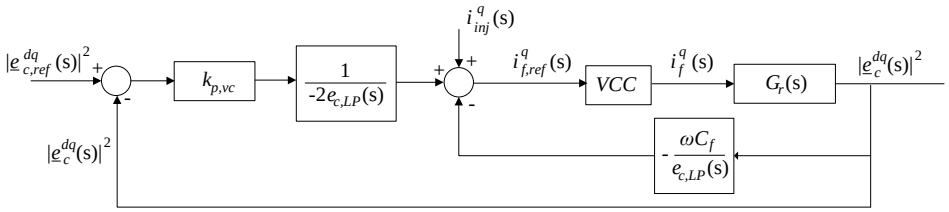

Figure 4.9: Updated block diagram of the RPC and the process.

Hence, according to Figure 4.9, with the reference active current (power) exchange set to zero and the controller parameters selected as in (4.41) and (4.42), the control law can in the time domain be written as

$$\begin{aligned} i^d_{f,ref}(t) &= 0 \\ i^q_{f,ref}(t) &= i^q_{inj}(t) + \omega C_f \frac{|\underline{e}^{dq}_c(t)|^2}{e_{c,LP}(t)} - \frac{k_{p,vc}}{2e_{c,LP}(t)} \left(|\underline{e}^{dq}_{c,ref}(t)|^2 - |\underline{e}^{dq}_c(t)|^2 \right) \end{aligned} \tag{4.43}$$

with $e_{c,LP}$ defined according to (4.33).

4.4 Voltage Controller - VSC with Energy Storage

If a sufficiently large energy storage is attached to the DC-side of the VSC, not only reactive power can be exchanged with the grid, but also active power. Hence, for an E-STATCOM, the outer loop can be set to control both the magnitude and the phase of the voltage, corresponding to both the d- and q-component of the filter current.

The cascade control structure for the E-STATCOM is the same as for the D-STATCOM, shown in Figure 4.10, with the only difference that the RPC-block is exchanged with the VC.

4.4.1 Electric System

Applying Kirchhoff's current law (KCL) on the nodes of the capacitors in Figure 4.3 gives the following differential equations

$$i_{f,a}(t) = i_{inj,a}(t) + C_f \frac{de_{c,a}(t)}{dt} \tag{4.44}$$

$$i_{f,b}(t) = i_{inj,b}(t) + C_f \frac{de_{c,b}(t)}{dt} \tag{4.45}$$

$$i_{f,c}(t) = i_{inj,c}(t) + C_f \frac{de_{c,c}(t)}{dt} \tag{4.46}$$

With the same method as for the VCC can (4.44)-(4.46) be transformed first to the $\alpha\beta$-frame and then to the dq-frame and written as

$$\underline{i}^{dq}_f(t) = \underline{i}^{dq}_{inj}(t) + C_f \frac{d\underline{e}^{dq}_c(t)}{dt} + j\omega C_f \underline{e}^{dq}_c(t) \tag{4.47}$$

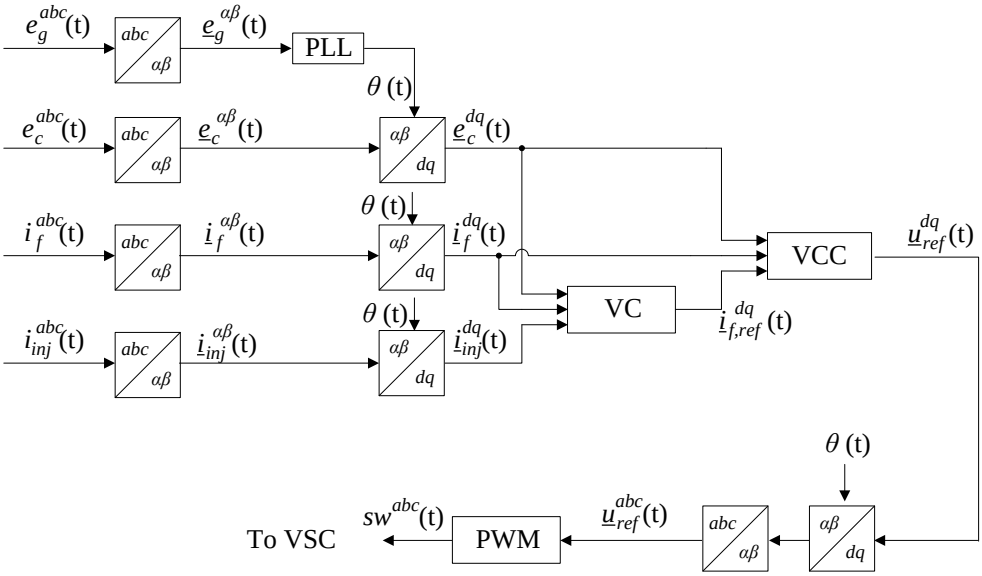

Figure 4.10: Block diagram of the E-STATCOM.

4.4.2 Controller Design

Transforming (4.47) into the Laplace domain and reorganizing gives

$$\underline{e}_c^{dq}(s) = \frac{1}{sC_f + j\omega C_f}\left(\underline{i}_f^{dq}(s) - \underline{i}_{inj}^{dq}(s)\right) \tag{4.48}$$

which describes how the voltage across the capacitor is related to the currents, and in particular to the controllable parameter $\underline{i}_f^{dq}$.

The capacitor voltage vector is measured and compared to its reference value (set to the pre-fault value). The obtained error acts as an input to the PI-regulator in the VC. Similar to the VCC, there are two parallel controllers, one for the real and one for the imaginary part of the voltage vector. The output from the VC is the filter current vector reference which is sent to the VCC. As in the RPC, it is approximated that the reference value $\underline{i}_{f,ref}^{dq}$ instantaneously is transformed into the actual filter current $\underline{i}_f^{dq}$ since the VCC is much faster than the VC [17].

Hence, using (4.48), the process of the system from the controllable filter current $\underline{i}_f^{dq}$ to the capacitor voltage, $\underline{e}_c^{dq}$, can be written as

$$G_v = \frac{\underline{e}_c^{dq}}{\underline{i}_f^{dq}} = \frac{1}{sC_f + j\omega C_f} \tag{4.49}$$

Here, the cross-coupling term is $j\omega C_f$ and it is feed-forwarded in the controller giving the new process

$$G_v' = \frac{G_v}{1 - G_v j\omega C_f} = \frac{1}{sC_f} \tag{4.50}$$

From (4.48) it can be noticed that also $\underline{i}_{inj}^{dq}$ have an impact on the capacitor voltage, hence it is also feed-forwarded into the VC. Figure 4.11 shows the complete block diagram of the voltage control system with the VC, feed-forward terms, the VCC and the process.

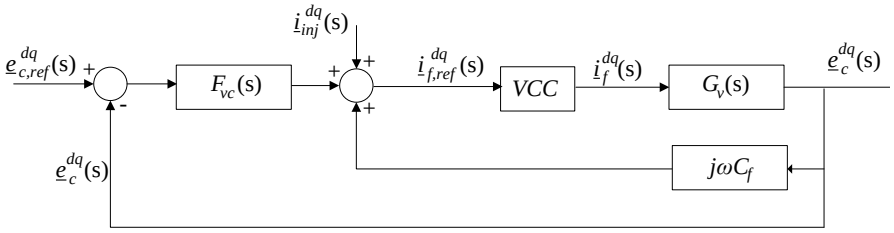

Figure 4.11: Block diagram of the VC and the process.

As in the previous controllers, $F_{vc}(s)$ is the PI-regulator in the VC which is described by

$$F_{vc}(s) = k_{p,vc} + \frac{k_{i,vc}}{s} = \frac{k_{p,vc}s + k_{i,vc}}{s} \tag{4.51}$$

where $k_{p,vc}$ is the proportional gain and $k_{i,vc}$ is the integral gain. The values can be calculated using the closed-loop transfer function from $\underline{e}_{c,ref}^{dq}$ to $\underline{e}_{c}^{dq}$, shown in Figure 4.11.

The closed-loop transfer function, i.e. the voltage control loop, can then be written as

$$\begin{aligned} G_{vc} &= \frac{F_{vc}G'_v}{1 + F_{vc}G'_v} = \frac{\dfrac{k_{p,vc}s + k_{i,vc}}{s}\dfrac{1}{sC_f}}{1 + \dfrac{k_{p,vc}s + k_{i,vc}}{s}\dfrac{1}{sC_f}} \\ &= \frac{k_{p,vc}s + k_{i,vc}}{s^2C_f + k_{p,vc}s + k_{i,vc}} \end{aligned} \tag{4.52}$$

The resistances in the capacitors have, as in the design of the RPC, not been included in the model. Hence, it is not needed to add a damping term. However, if the capacitor resistances would have been included, a damping term could have been added in a similar way as in the VCC. By simply selecting $k_{i,vc} = 0$ a satisfying performance of the controller can be obtained. Hence, (4.36) can be simplified to

$$G_{vc} = \frac{k_{p,vc}}{sC_f + k_{p,vc}} \tag{4.53}$$

Just as in the VCC and the RPC should the desired step response in the VC have the form of a low-pass filter, giving

$$G_{vc} = \frac{\omega_{vc}}{s + \omega_{vc}} \tag{4.54}$$

where ω_{vc} is the desired bandwidth of the VC. Comparing (4.53) and (4.54) makes it possible to select the controller gains as

$$k_{p,vc} = \omega_{vc}C_f \tag{4.55}$$

$$k_{i,vc} = 0 \tag{4.56}$$

Hence, according to Figure 4.11 and the controller gains in (4.55) and (4.56), the control law for the VC can in the time domain be written as

$$\underline{i}_{f,ref}^{dq}(t) = \underline{i}_{inj}^{dq}(t) + j\omega C_f \underline{e}_{c}^{dq}(t) + k_{p,vc}\left(\underline{e}_{c,ref}^{dq}(t) - \underline{e}_{c}^{dq}(t)\right) \tag{4.57}$$

4.5 Synchronization System - PLL

The synchronization system is used to align the d-axis in the dq-frame with the voltage vector by determining the angle θ. θ is then used in the transformation between the fixed $\alpha\beta$-frame and the rotating dq-frame, see Figure 4.4. One method to determine the angle would be by detecting the zero-crossing of the voltage. But due to the presence of noise and harmonics, it would be hard to determining the "correct" zero-crossing. Only measuring on one phase would mean that the other two phases would have to be calculated from the measured phase, or measured as well.

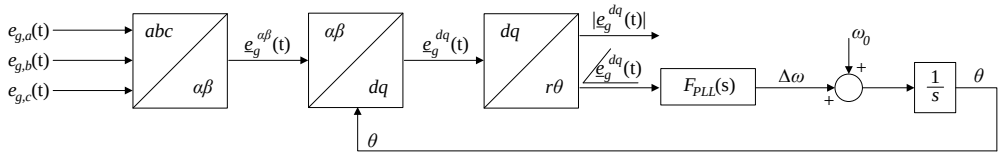

Figure 4.12: Block diagram of the PLL.

Instead, the most common method to set up the synchronization system is to use a PLL. The algorithm in the PLL can vary but the method used in this thesis is shown as a block diagram in Figure 4.12. The three-phase voltage used for synchronization is measured, transformed to a voltage vector in the $\alpha\beta$-frame and, using a previously determined or a guessed value of θ, transforming into the dq-frame. The angle between the voltage vector and the d-axis is then calculated and sent to a PI-regulator which gives an error that is added to the nominal frequency. Integrating the sum gives an updated θ which is used to correct the next transformation between the $\alpha\beta$- and the dq-frame.

The bandwidth of the PLL should be low, and are normally set to around $2\pi 5$ rad/s in order to provide a sufficient damping to harmonics and transients.

4.6 Simplifications in the Used System

A few parts of the control systems have been neglected in these derivation. The reason for this is that the focus of this work is not on designing a real system, but to understand the phenomenon behind the observed performance in Chapter *6 Impact of Load Dynamics on System Performance*. All assumptions have therefore been done with the aim to simplify the system as much as possible, in order to make the analysis easier. This section will highlight the parts of the controller that have been approximated or neglected in this work but would be different in a real shunt-connected VSC.

4.6.1 Continuous System

The used controller is in this work modelled to be continuous but in a real system, the signals would be sampled and sent to a discrete controller. With a continuous controller, there is no limit in the bandwidth of the VCC since the sampling frequency is infinitely high. In a discrete controller this can posses a problem and the VCC bandwidth can never be higher than the sampling frequency. Since this work focus on the system performance, a continuous controller can be used. A similar discrete controller is, for example, explained in [7].

In a discrete system it is important to consider the delays in the control system since the time between each sample is so large that it can not be neglected. Some methods have been developed which provide a compensation of this delay. One common method is to use a Smith predictor. Using that, the output of the VCC is estimated by the Smith predictor and feed-forward to the input of the VCC, hence compensating for the impact of the delays. More extensive information about the Smith predictor can be found in [35].

4.6.2 Balanced System and Faults

Only balanced systems and faults have been studied in this work, while, in reality, a majority of the faults are unbalanced [5]. The reason for only considering balanced system is that one of the aims have been to find applications for energy storage equipped STATCOMs. Including unbalanced systems in the model would not increase the number of applications. Secondly, simplifying the system as much as possible, i.e. only studying balanced systems, makes it easier to analyse the system dynamic performance without considering other effects.

While a balanced system only contains positive sequence components, i.e. voltage or current vectors rotating with +50 Hz, an unbalanced systems also consists of negative sequence components, i.e. vectors rotating with −50 Hz. If the D-STATCOM or the E-STATCOM would be used in an unbalanced system, the presented controllers would have to be changed. In that case, two separate cascade controllers would have to be used, one for the positive sequence component and one for the negative sequence components, see for example [7]. The PLL would in that case also be equipped with a sequence separation algorithm that could find and separate the positive and the negative sequence components of the voltage and the corresponding angles.

4.6.3 Unlimited Converter Rating

If the terminal voltage reference in the VCC would exceed the rating of the converter, the VSC would be unable to perform the requested operation. This can be understood since the converter cannot output a voltage that would exceed a certain fraction of the DC-voltage. Therefore, when reaching saturation, the terminal voltage reference $\underline{u}_{ref}$ has to be limited and integrator anti-windup applied in the VCC. [25] gives a more extended description of the possible solutions to the saturation problem.

However, it has in this thesis been assumed that saturation never is reached, i.e. it is assumed that the converter voltage and current rating is large enough to perform all actions requested. The reason for this, as been mentioned before, is that the focus of the work is to investigate the performance in a system that is as simple as possible. Hence, all parts that would cause nonlinear effects in the compensator operation, e.g. saturation, are neglected.

4.6.4 Sinusoidal Three-Phase VSC

As mentioned when deriving the VCC in Section *4.2 Vector Current Controller*, the VSC has in this work been modelled as a continuous sinusoidal three-phase voltage. Hence, all switching harmonics are neglected. Once again, the reason for doing this is that the performance of the system is in focus and not the exact operation.

4.6.5 Fixed DC-voltage

It has been assumed that the DC-voltage across the DC-capacitor is fixed, i.e. the VSC can produce the desired terminal voltage without considering changes in the DC-voltage. In a real VSC, the DC-voltage will change depending on the switching and the instantaneous power exchange. Therefore, the active power exchange is used to controlled the DC-voltage in both the D-STATCOM and the E-STATCOM. Neglecting this simplifies both the controller structure and the analysis of the results.

Furthermore, if some additional energy storage where connected to the DC-side, there might be a need of a DC/DC converter. This DC/DC converter is used to control the DC voltages and the power exchange between the VSC and the energy storage, e.g. a battery. More extensive information about the DC/DC converter can be found in [32].

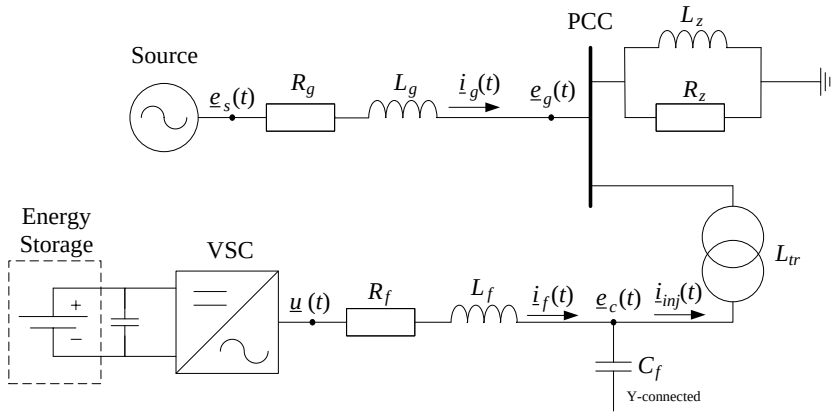

Figure 4.13: Grid model with supply, grid impedance, loads and a shunt-connected VSC connected through a LCL-filter.

4.7 System Performance During Voltage Dips

Testing the cascade control system for both the D-STATCOM and the E-STATCOM gives an understanding of the impact different settings have on the performance. The compensators are tested during a voltage dip and examined by varying the bandwidth of the VCC and the bandwidth of the voltage/reactive power controller. The impact of the capacitor size in the LCL-filter is also examined.

The simulations are done in PSCAD/EMTDC by Manitoba and the single line diagram of the grid model is shown in Figure 4.13. In PSCAD/EMTDC, a voltage dip from 1 pu to 0.75 pu is introduced in the source voltage. Figure 4.14 shows the voltage dip in both three-phase components and in dq-components (synchronized with the source voltage). The values for the grid and filter parameters are shown in table 4.1b.

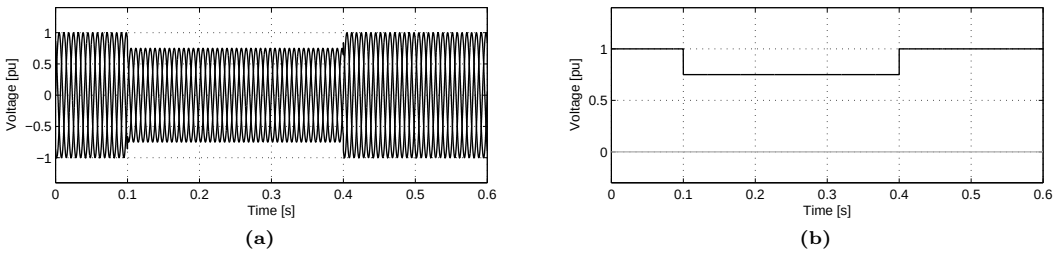

Figure 4.14: Modelled voltage dip in the source voltage. Plot (a): three-phase components, plot (b): dq-components, if the synchronization would have been done with respect to the source voltage.

The settings shown in table 4.1a are the default values that, if nothing else is said, will be used as the normal settings for the D-STATCOM and E-STATCOM in the rest of the thesis. Notice especially that the default VCC bandwidth is $\omega_{cc} = 2\pi 1500$ rad/s and the default bandwidth for the voltage/reactive power controller is $\omega_{vc} = 2\pi 100$ rad/s.

Table 4.1: System parameters. Table (a): Default settings for D-STATCOM and E-STATCOM, plot (b): fixed grid parameters.

(a)

Voltage and reactive power controller		
Bandwidth	ω_{vc}	$2\pi100$ rad/s
Proportional gain	$k_{p,vc}$	$\pm\omega_{vc}C_f$
Integral gain	$k_{i,vc}$	0
Current controller		
Bandwidth	ω_{cc}	$2\pi1500$ rad/s
Proportional gain	$k_{p,cc}$	$\omega_{cc}L_f$
Integral gain	$k_{i,cc}$	0
Active damping	R_{acc}	$\omega_{cc}L_f - R_f$
PLL		
Bandwidth	ω_{PLL}	$2\pi5$ rad/s

(b)

Grid parameters			
Base power	S_b	100 MVA	1 pu
Source voltage	e_s	21 kV	1 pu
Grid frequency	f	50 Hz	1 pu
Grid inductance	L_g	9 mH	0.641 pu
Grid resistance	R_g	100 mΩ	0.023 pu
Load resistance	R_z	10.16 Ω	2.3 pu
Load inductance	L_z	0.116 H	8.26 pu
Load power factor		0.96	
Grid short circuit ratio	SCR	3.5	
Filter parameters			
Filter inductance	L_f	10.5 mH	0.748 pu
Filter resistance	R_f	330.8 mΩ	0.075 pu
Filter capacitance	C_f	39 μF	0.054 pu
Transformer inductance	L_{tr}	0.3509 mH	0.025 pu

4.7.1 D-STATCOM

The dq-components of the PCC voltage are shown in Figure 4.15 together with one plot showing the three-phase components with the default bandwidths. The bandwidth of the VCC is then changed from the default value $\omega_{cc} = 2\pi1500$ rad/s to $2\pi500$ rad/s and $2\pi2000$ rad/s, while keeping $\omega_{vc} = 2\pi100$ rad/s. It can be noticed that the system gets better damped when the bandwidth is decreased and less well-damped when increasing it.

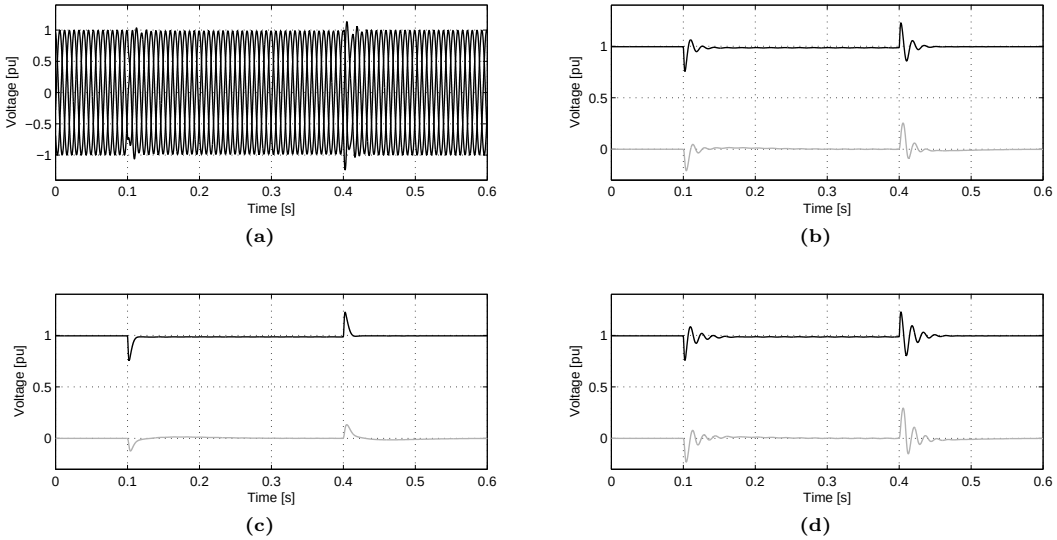

Figure 4.15: PCC voltage during a voltage dip using an D-STATCOM with different bandwidths in the VCC. Plot (a): three-phase components with $\omega_{cc} = 2\pi1500$ rad/s, plot (b): dq-components with $\omega_{cc} = 2\pi1500$ rad/s, plot (c): dq-components with $\omega_{cc} = 2\pi500$ rad/s, plot (d): dq-components with $\omega_{cc} = 2\pi2000$ rad/s.

When varying the bandwidth of the reactive power controller, while keeping $\omega_{cc} = 2\pi1500$ rad/s, the same behaviour can be noticed. The system performance is shown in Figure 4.16 where the bandwidth is changed from the default value $\omega_{vc} = 2\pi100$ rad/s to $\omega_{vc} = 2\pi50$ rad/s and $\omega_{vc} = 2\pi150$ rad/s. Here, it can be noticed that a smaller bandwidth gives a better damping but

a slower response to the voltage dip, and vice versa. As when changing ω_{cc}, it is clear that the bandwidth have a significant impact on the damping on the system when a D-STATCOM is used. The bandwidths $\omega_{cc} = 2\pi 1500$ rad/s and $\omega_{vc} = 2\pi 100$ rad/s gives a good compromise between speed and damping and are therefore chosen as the standard values.

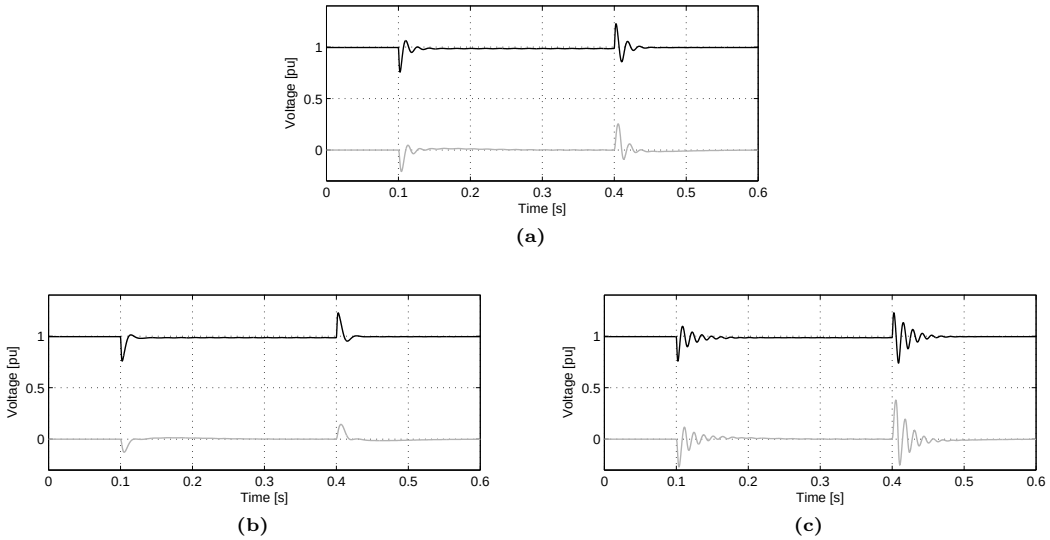

Figure 4.16: PCC voltage during a voltage dip using an D-STATCOM with different bandwidths in the RPC. Plot (a): $\omega_{vc} = 2\pi 100$ rad/s, plot (b): $\omega_{vc} = 2\pi 50$ rad/s, plot (c): $\omega_{vc} = 2\pi 150$ rad/s.

Keeping $\omega_{cc} = 2\pi 1500$ rad/s and $\omega_{vc} = 2\pi 100$ rad/s, the impact of the capacitor size in the LCL-filter can be examined. The filter is in a real system used to smooth out the harmonics related to the switching of the VSC. The size of the filter, or rather the cut-off frequency, depends on the used converter switching frequency which often is in the range of 1-2 kHz. The cut-off frequency is calculated as

$$f_{co} = \frac{1}{2\pi\sqrt{L_f C_f}} \tag{4.58}$$

and with the default values $L_f = 105$ mH and $C_f = 39$ μF, the cut-off frequency is $f_{co} = 249$ Hz.

If a low switching frequency is used, a low cut-off frequency might be needed. If a higher switching frequency is used, the cut-off frequency of the filter could be higher, hence giving a cheaper and less bulky filter. It should be mentioned that a higher switching frequency causes higher losses in a converter.

To show the impact of the capacitor size, the size of the filter capacitor is changed to $C_f = 9.65$ μF which gives a cut-off frequency of $f_{co} = 500$ Hz. The system performance for the two cases are shown in Figure 4.17 and it can be noticed that a smaller capacitor increases the system damping. The reason is that it is easier to change and control the voltage across a smaller capacitor than a large. In other words, with a larger capacitor the VSC needs to force more current through the filter reactor in order to control the capacitor voltage, this makes it harder and worsen the damping.

It should be mentioned that there are other design criterion than might impact the size of the filter capacitors. The capacitors might, in steady state, be used to provide reactive power to the system and this can also demand a particular rating of the capacitors.

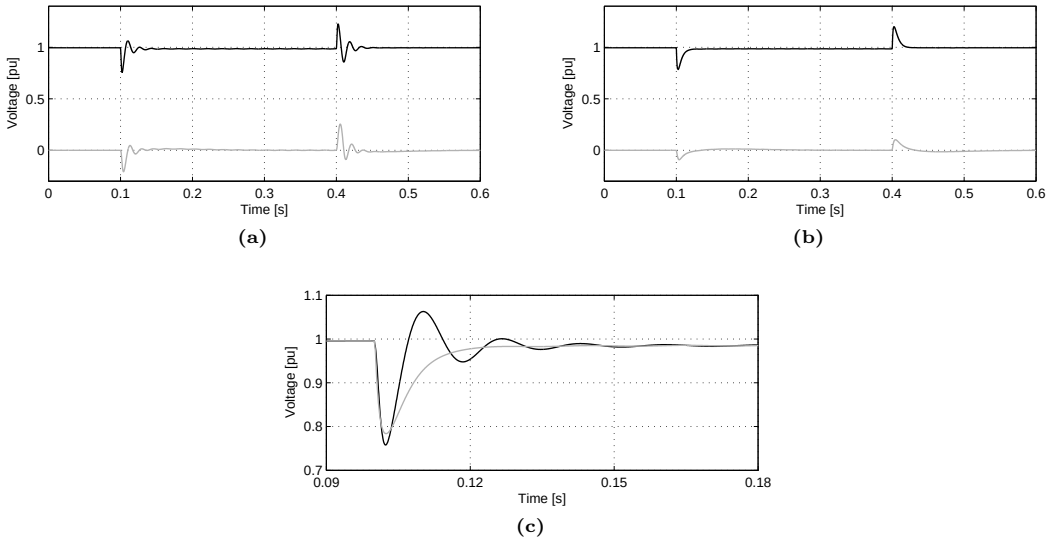

Figure 4.17: PCC voltage during a voltage dip using an D-STATCOM with different capacitor sizes in the LCL-filter. Plot (a): $C_f = 39$ μF, plot (b): $C_f = 9.65$ μF, plot (c): comparison where black curve denotes $C_f = 39$ μF and grey curve $C_f = 9.65$ μF.

4.7.2 E-STATCOM

The same tests are done with the E-STATCOM. Figure 4.18 shows variations of ω_{cc} and Figure 4.19 variations of ω_{vc}. It is clear that the impact of the bandwidth on the damping of the system is much smaller. Furthermore, it can be noticed that a smaller bandwidth gives a slower response, just as for the D-STATCOM.

As in the D-STATCOM, the bandwidths $\omega_{cc} = 2\pi 1500$ rad/s and $\omega_{vc} = 2\pi 100$ rad/s gives a good compromise between speed and damping and are therefore chosen as the standard values.

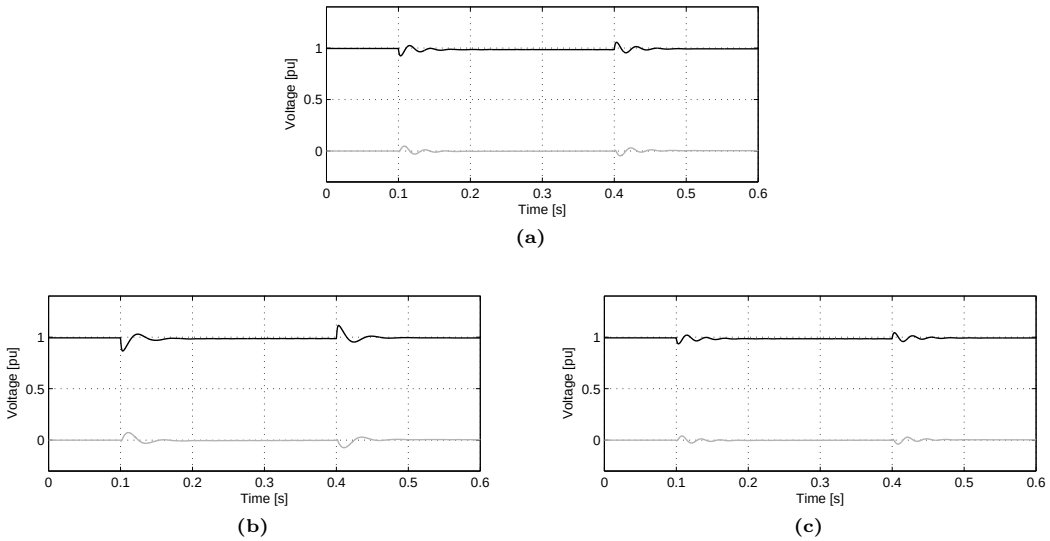

Figure 4.18: PCC voltage during a voltage dip using an E-STATCOM with different bandwidths in the VCC. Plot (a): $\omega_{cc} = 2\pi 1500$ rad/s, plot (b): $\omega_{cc} = 2\pi 500$ rad/s, plot (c): $\omega_{cc} = 2\pi 2000$ rad/s.

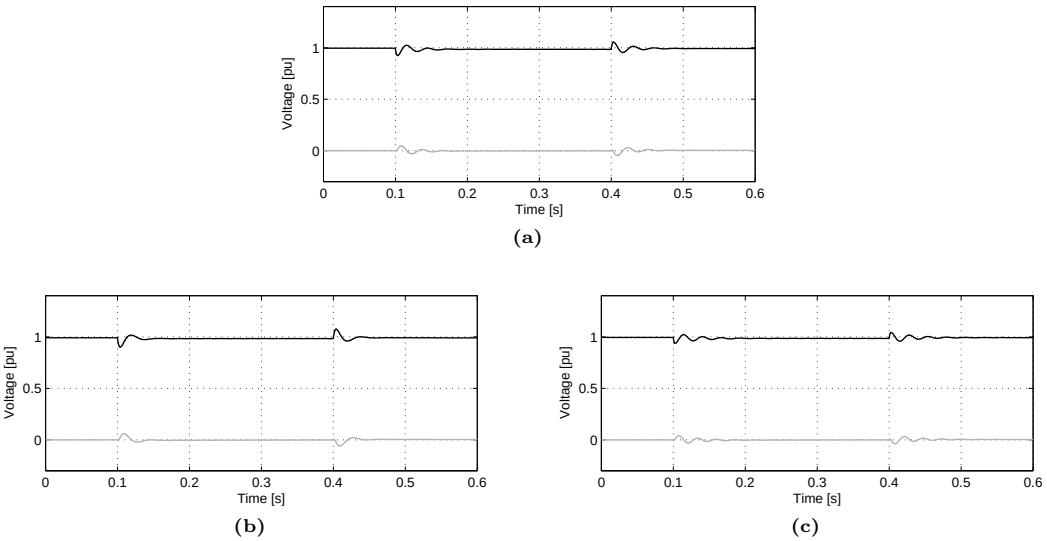

Figure 4.19: PCC voltage during a voltage dip using an E-STATCOM with different bandwidths in the VC. Plot (a): $\omega_{vc} = 2\pi 100$ rad/s, plot (b): $\omega_{vc} = 2\pi 50$ rad/s, plot (c): $\omega_{vc} = 2\pi 150$ rad/s.

4.8 Conclusion

In this chapter has the structure of the control system for both a D-STATCOM and an E-STATCOM been presented. The inner vector current control loop and the outer voltage/reactive power control loop, respectively, have been derived. Furthermore, the structure of the PLL and the simplifications done in the derivation of the controllers have been treated. Finally, the system performance during a voltage dip has been studied with different controller settings.

Chapter 5

Energy Storage Applications for Power Quality Improvements

This chapter treats power quality applications for energy storage equipped VSCs. Furthermore, only those applications that are enabled by the use of energy storage are explained.

5.1 Introduction

As mentioned in Chapter *3 Energy Storage at Distribution Level*, applications for energy storage systems can be classified depending on the needed response time. This chapter presents power quality applications which demand short response times and where the energy storage in the E-STATCOM is necessary. For clarity, note that only power system applications which demand dynamic performance, and applications where the energy storage is critical for the function, are considered. Hence, mitigation of harmonics and other uses which can be performed with only reactive power are not included in this work. Neither are specific uses, like railway applications, since these are not considered as a part of the normal power system.

In the first section, it is explained how energy storage systems enable complete mitigation of voltage dips, i.e. by controlling both the magnitude and the phase of the voltage. The focus of this part is on phase jumps and not the drop in voltage magnitude. The reason for this is that mitigation of the magnitude drop can be done with only reactive power, while both active and reactive power are needed to compensate for both the magnitude drop and phase jump.

In the second section, it is described how energy storage systems can be used to enable islanding by balancing the loads at the moment when the system is disconnected from the main grid.

5.2 Voltage Dips and Phase Jumps

Voltage dips are reductions in voltage with short durations which are known to cause problems to generators, loads and other equipments in the power system. A single voltage dip can, by making equipment trip, cause large economic losses in process or manufacturing industries. There are different definitions of what a voltage dip is, but it is usually classified as an event in which the voltage is between 90% and 1 or 10% for a duration less than 1-3 minutes and longer than half a cycle [5]. Voltage dips are often caused by short circuits, overloads, starting of large motors or energizing of transformers.

The experienced magnitude of the dip is very dependent on the location of the event that caused the dip. For example, a short circuit on a feeder close to the point of common-coupling (PCC) would cause a bigger drop in voltage than if the event would occur further out on the

feeder. Severe events close to, or on transmission level, will cause the voltage on the transmission level to decrease, hence affect all connected distribution grids. However, a majority of the dips are caused by reasons in the distribution systems which only have a minor impact on transmission systems [5].

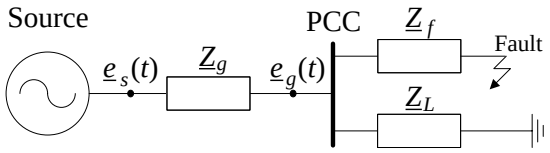

Figure 5.1: Fault on a feeder causes a voltage dip at the PCC.

Voltage dips are often associated with phase jumps. A voltage dip is basically caused by a reconfiguration in the grid, e.g. a short-circuit, which causes the voltage magnitude to drop and, in some conditions, a a change in the voltage angle. This sudden change of the angle, from its pre-event value to its post-event value, is called a phase jump.

The drop in the voltage magnitude and the corresponding phase jump can, for simple radial grids, be calculated using voltage division. Depending on the cause of the dip, different approximations can be done. If the dip is caused by a short circuit in a feeder connected to the PCC, as shown in Figure 5.1, the load impedance can be neglected since it usually is very large in comparison to the fault impedance. Therefore, according to [5], the voltage at the PCC during the fault can be calculated as

$$\underline{E}_{g,f} = \frac{\underline{Z}_f}{\underline{Z}_f + \underline{Z}_g}\underline{E}_s \tag{5.1}$$

where $\underline{Z}_g = R_g + jX_g$ is the grid impedance and $\underline{Z}_f = R_f + jX_f$ is the impedance between the PCC and the fault. The difference between the argument of the PCC voltage before and during the fault is the phase jump. From (5.1) is the argument during the event, denoted $\theta + \Delta\theta$, calculated as

$$\theta + \Delta\theta = \arg \underline{E}_{g,f} = \arctan \frac{X_f}{R_f} - \arctan \frac{X_f + X_g}{R_f + R_g} \tag{5.2}$$

The normal (pre-fault) voltage at the PCC is calculated as

$$\underline{E}_{g,n} = \frac{\underline{Z}_L}{\underline{Z}_L + \underline{Z}_g}\underline{E}_s \tag{5.3}$$

with the argument

$$\theta = \arg \underline{E}_{g,n} = \arctan \frac{X_L}{R_L} - \arctan \frac{X_L + X_g}{R_L + R_g} \tag{5.4}$$

and the phase jump can thus be determined to

$$\begin{aligned} \Delta\theta &= \arg \underline{E}_{g,f} - \arg \underline{E}_{g,n} \\ &= \arctan \frac{X_f}{R_f} - \arctan \frac{X_f + X_g}{R_f + R_g} - \left(\arctan \frac{X_L}{R_L} - \arctan \frac{X_L + X_g}{R_L + R_g} \right) \end{aligned} \tag{5.5}$$

Another cause of voltage dips are sudden connections of big loads, for example starting of large motors, showed in Figure 5.2. In this case, the PCC voltage after the connection can be determined to

$$\underline{E}_{g,a} = \frac{\underline{Z}_{tot}}{\underline{Z}_{tot} + \underline{Z}_g}\underline{E}_s \tag{5.6}$$

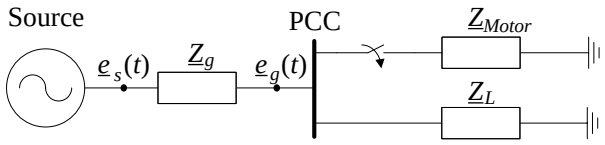

Figure 5.2: An large load is switched on at the PCC and causes a voltage dip.

where $\underline{Z}_{tot} = R_{tot} + jX_{tot}$ is the impedance of the total load. The phase angle after the connection is

$$\theta + \Delta\theta = \arg \underline{E}_{g,a} = \arctan \frac{X_L}{R_L} - \arctan \frac{X_L + X_g}{R_L + R_g} \tag{5.7}$$

and the phase jump can thus be written, using (5.4) and (5.7), as

$$\begin{aligned} \Delta\theta &= \arg \underline{E}_{g,a} - \arg \underline{E}_{g,n} \\ &= \arctan \frac{X_{tot}}{R_{tot}} - \arctan \frac{X_{tot} + X_g}{R_{tot} + R_g} - \left(\arctan \frac{X_L}{R_L} - \arctan \frac{X_L + X_g}{R_L + R_g} \right) \end{aligned} \tag{5.8}$$

As seen in (5.5) and (5.8), the phase jump depends on parameters in the grid, the type of fault and other loads. A phase jump can be both positive and negative.

5.2.1 Problems Related to Phase Jumps

To most equipment, phase jumps are not a big concern [5]. However, for a thyristor based load, a phase jump of a few degrees per second can be enough to make it trip.

Thyristor rectifiers are used in many types of power electronic based equipments such as HVDC systems, FACTS, AC adjustable speed drives and DC-motor rectifiers [27]. In high power applications are thyristor based rectifiers always used due to their lower losses, compared to more controllable switches. However, in the low to medium power range, the thyristor is loosing market shares to the IGBT which offers greater controllability and less switching harmonics.

Compared to diode rectifiers, thyristor rectifiers offer more control of the DC-voltage since the firing instant can be delayed. This delay is normally called the firing angle. There are different methods to obtain and calculate the firing angle but crucial to all methods is a correct synchronization with the grid voltage. Using a PLL is one of the most common methods, however, this makes the rectifier very sensitive to phase jumps [5]. The reason is the slowness in the PLL which means that it can take several cycles to react on a phase jump. When the thyristor is fired, it starts to conduct and the grid voltage is put on the DC-side. If the grid voltage is different from what the controller thinks, e.g. during a phase jump, the device will output a voltage different from the desired. This could potentially lead to tripping of the rectifier due to large variations in the DC-voltage, or, in worst case, commutation failures. However, this depends on the direction of the phase jump. A negative phase jump decreases the risk of commutation failure while a positive phase jump increases the risk.

Phase jumps can also cause problems to directly fed induction machines by increasing the risk of torque oscillations [5].

5.2.2 Phase Jump Mitigation

As mentioned in Chapter *2 Power Electronics in Power Systems* can many devices be used to mitigate voltage dips. Among them are the D-STATCOM and the E-STATCOM. However, as explained before, to completely mitigate a voltage dip, also the phase jump needs to be considered. Only if both the voltage magnitude drop and the phase jump are mitigated, it can be assured that a load is unaffected by the event.

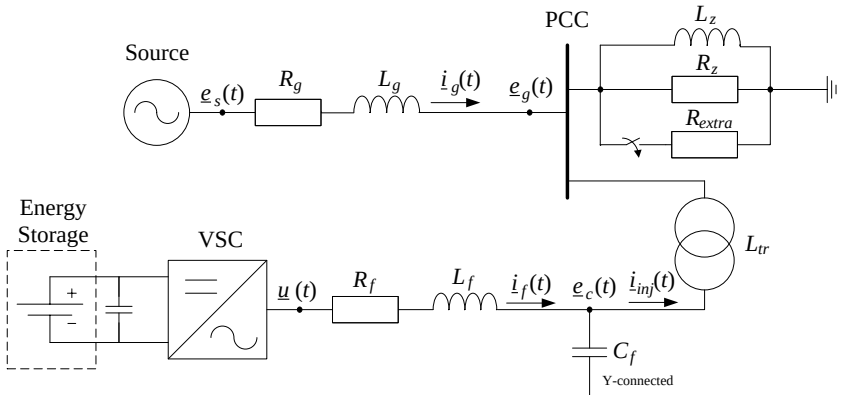

Figure 5.3: Grid model with supply, grid impedance, a shunt-connected VSC connected through a LCL-filter and loads. A large load is suddenly connected to the PCC to create a phase jump.

The performance of a D-STATCOM and an E-STATCOM, respectively, during a voltage dip with a phase jump has been simulated in PSCAD/EMTDC on a grid model shown in Figure 5.3. A voltage dip with a phase jump is obtained by connecting an extra resistive load to the PCC. Figure 5.4 shows the PCC voltage and the phase difference between the source and the PCC during the voltage dip. It can be seen that the D-STATCOM mitigates the magnitude of the voltage drop but it is unable to mitigate the associated phase angle jump, showed in Figure 5.4b. The E-STATCOM, on the other hand, not only reduces the voltage magnitude drop more efficiently, it also slows down the phase angle jump. Hence, a sensitive load connected to the PCC would notice a change in the angle, but probably in such a speed that the PLL is able to follow the change and avoid tripping.

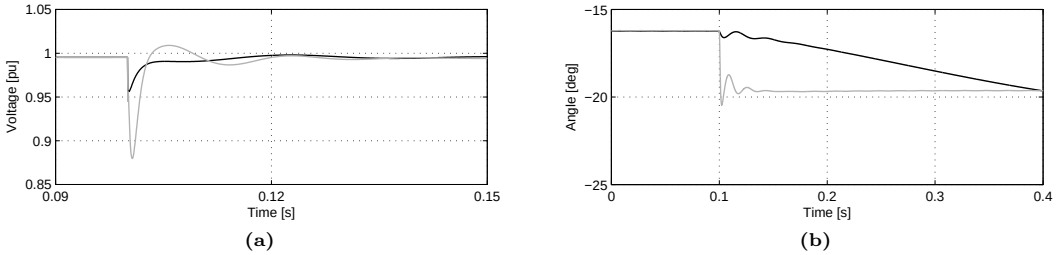

(a) **(b)**

Figure 5.4: Voltage dip and corresponding phase jump when a resistive load is switched on using an E-STATCOM (black curve) or a D-STATCOM (grey curve). Plot (a): PCC voltage, plot (b): phase difference between source and PCC.

The active power flow in the grid during the event, described by Figure 5.4, is shown in Figure 5.5. With the D-STATCOM, the source instantaneously has to supply the extra load with power. With the E-STATCOM, the compensator initially supplies the extra load itself. By doing so, the phase angle at the PCC is initially unchanged and the rapid phase jump is avoided.

5.2.3 Understanding the Phase Jump Mitigation

From the simulations in Figure 5.4 and 5.5 it is shown that combined active and reactive power compensation completely can mitigate a voltage dip. With only reactive compensation this is not

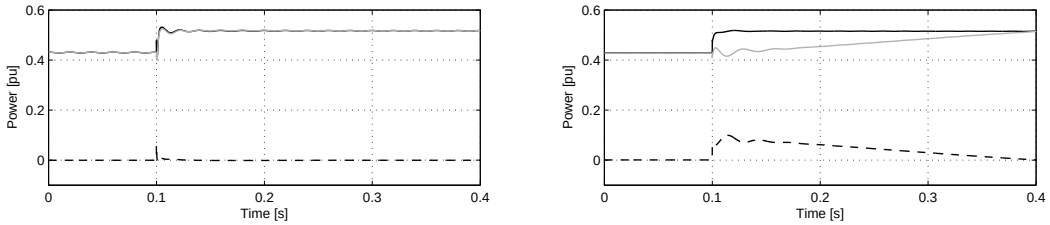

Figure 5.5: Active power flow during the event described by Figure 5.4. Black curves denote active power taken by the loads, grey curves denote active power supplied from the grid and dashed lines indicate active power from the compensator. Plot (a): D-STATCOM, plot (b): E-STATCOM.

possible. This can be explained in a simplified way by studying a simple equivalent single-phase grid model, shown in Figure 5.6, and the corresponding phasors shown in Figure 5.7. The source voltage is denoted as E_s, the PCC voltage as E_g, the steady state phase angle θ, the grid reactance jX_g, the load current i_L and the current injected by the compensator as i_c. For simplicity, it is approximated that the grid impedance only constitutes by a reactor and that the load only draws active power. The analysis is further done in steady state, hence neglecting the derivative term of the grid inductance and the transient response of the compensators.

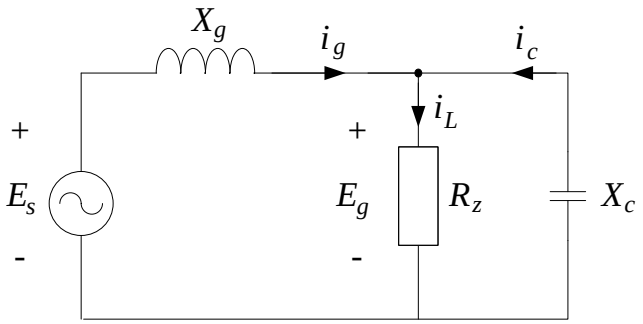

Figure 5.6: Simplified grid model for understanding phase jump mitigation.

Each of the phasor plots in Figure 5.7 show one operation condition, with or without compensator. The reference case without a compensator is showed in Figure 5.7a. Here, the source voltage $\underline{E}_s$ is 1 pu, indicated by the dotted arc. Due to the voltage drop $jX_g i_L$ over the grid impedance, there is a difference in both magnitude and phase between $\underline{E}_s$ and $\underline{E}_g$. Since the load is resistive, the load current is aligned with $\underline{E}_g$ and the voltage drop is hence shifted 90° with respect to $\underline{E}_g$.

Both the size of the voltage drop and the steady state phase shift θ depend on the load current i_L. If the load increases, i_L grows and the voltage drop increases together with the phase angle. The difference between the steady state phase shift and the new phase shift, with a bigger load, is denoted $\Delta\theta$. Figure 5.7b shows the phasors if the load is increased. The solid arrows denote the reference case and the dashed arrows indicate two cases with a bigger load. It is clear that the magnitude of $\underline{E}_g$ decreases while the phase difference increases. Hence, if the load suddenly would increase, it would result in a voltage dip with a phase jump of $\Delta\theta$.

Figure 5.7c shows the reference case when a compensator is used to boost $\underline{E}_g$ to 1 pu. It is done by injecting a reactive current i_c into the PCC which creates an inverse voltage drop $jX_g i_c$ over the grid impedance. Doing this, the steady state phase difference has to increase slightly,

compared to the case without a compensator (still denoted θ). Even if the load is increased, the compensator is able to keep $\underline{E}_g$ at 1 pu by increasing the injected reactive current as showed in Figure 5.7d. However, it can be noticed that the phase difference $\Delta\theta$ has to increase further. Similar to the case before, the solid arrows indicate the reference case with a compensator while the dashed arrows show two cases with a bigger load. Hence, with a sudden load increase, a compensator with only reactive power compensation, i.e. a D-STATCOM, can only mitigate the voltage drop but not the phase jump.

However, when combining active and reactive power the compensator is capable of keeping both the voltage magnitude and the phase difference as showed in Figure 5.7e. Here, i_c^q indicates the reactive current and i_c^d the active compensator current. Even if i_L increases, the compensator can mitigate the increased voltage drop over the grid impedance by providing extra active power itself, showed as a phasor with opposite direction compared to $jX_g i_L$. With both reactive and active power, an E-STATCOM can span the whole plane and thus resist any impact of a load change and therefore mitigate both voltage drops and phase jumps.

Even though only steady state behaviour is considered in this analysis, the same explanation is valid when considering transients. Also, the same method can be used when considering voltage dips with corresponding phase jumps that are due to events affecting the source voltage. The important conclusion is that an E-STATCOM with both active and reactive power can span the whole plane. Hence, if the rating of the converter, and the size of the energy storage, is large enough with an infinitely fast response time, the voltage dip can always be completely mitigated. A D-STATCOM with only reactive power compensation can either control the phase angle or the voltage magnitude, never both at the same time. It should be mentioned that a D-STATCOM sometimes will be able to keep both the magnitude and the phase after a voltage dip. However, this is only possible if the voltage dip and the phase jump happens to be of a certain combination, which can not be considered when designing a compensator.

5.3 Rapid Balancing of Loads

Another application in which the power quality can be improved with the use of a energy storage is rapid balancing of loads during faults, hence preventing interruptions. It is possible that future grid codes will allow islanding, i.e. independent operation of a small area of a grid without being connected to the main grid. This could happen if the regional grid or main grid experiences a blackout while a distribution grid have enough distributed generation to stay balanced. However, the most likely case of islanding occurs if a line connecting one area to the main grid is lost. Today, the grid codes demand that the area should be interrupted even if there are enough generation within the area. Allowing islanding would, however, led to a few issues of which some potentially could be solved by using E-STATCOMs.

One of the problems are due to the power imbalance that might occur when the line to the main system is lost, shown in an example in Figure 5.8. Unless the area happens to be completely self supplied, and no more power than necessary is generated, there will be a power flow in the feeder when it disconnects. At the disconnection moment will the area either have a lack of, or have an excess of, power. Hence, very fast power balancing is needed in order to not let the voltage nor the frequency deviate too much. As seen in Figure 5.5b, can an E-STATCOM use its energy storage to compensate for fast load changes. In the same way can an E-STATCOM be used to stabilize a grid during an event such as tripping of a line.

By consuming or producing active power, the E-STATCOM can keep the power balance in the area until slower control systems bring the area into stability. These slower systems could potentially control the local generators to either increase or decrease the production. It could also involve disconnection of certain predetermined loads, in case the power consumption is higher than the available production, to save the rest of the area. However, these systems cannot react with the speed needed to keep the system in balance. Hence, an E-STATCOM could be useful. More extensive information regarding this application can be found in [24].

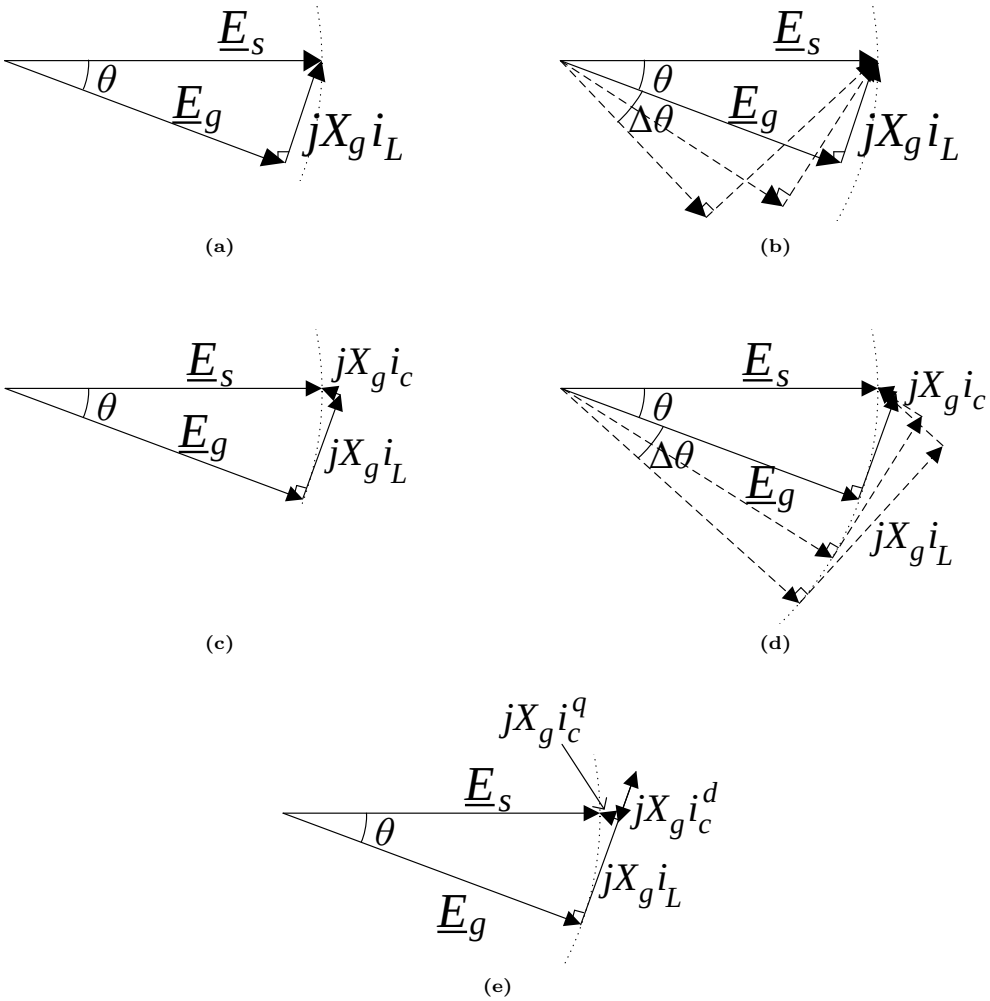

Figure 5.7: Voltage phasors explaining how combined active and reactive power compensation can mitigate phase jumps.

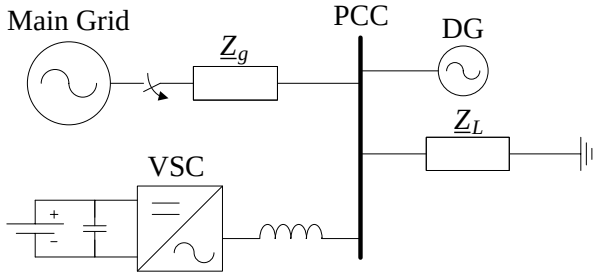

Figure 5.8: An area in which the only line connected to the main grid is lost.

5.4 Conclusion

In this chapter has power quality applications, in which energy storage equipped STATCOMs are needed, been explained. It has been showed that an E-STATCOM can completely mitigated voltage dips and in particular the phase jumps associated with the dips. However, this only holds

if the rating of the converter and the energy storage are large enough. Furthermore, it has been described how E-STATCOMs can be used to balance loads during line tripping, hence, enable entering of islanding operation.

Chapter 6

Impact of Load Dynamics on System Performance

This chapter presents a dynamic load model and a derivation of state space models for a grid with a D-STATCOM, an E-STATCOM or none of them. Furthermore, by examining the pole placement are the damping and stability of the systems investigated, and especially the impact of load dynamics .

6.1 Introduction

According to [11] did power electronics control more than 40% of the total electrical energy consumed in 2008, and it is expected that this share will increase up to 80% in 2015. One reason for this is the increasing usage of motor drive systems which give an increased controllability and higher efficiency. More power is also consumed by loads directly connected to power electronic rectifiers, e.g. chargers for electric vehicles and computers.

This might put an increased stress on distribution systems since these types of loads have different dynamical properties compared to traditional loads. It will be shown later that dynamic loads even can make systems turn unstable.

As mentioned in Chapter *2 Power Electronics in Power Systems*, a shunt-connected VSC can be used to provide an increased control of the voltage and improve the power quality in distribution grids. It might also be used to improve the system performance when loads with dynamic properties are connected. However, there is a risk that the damping and stability of the system can get worsen when STATCOMs without energy storage are used together with dynamic loads, a phenomena which will be shown later. Although this behaviour has not been observed in any grid today, it is not impossible that this interaction can cause future problem since more and more equipment uses fast power electronic converters. It is therefore important to study the impact of load dynamics on the damping and stability of a system and this can be done by investigating the pole placement.

In this chapter is first the concept and modelling of dynamic loads explained, followed by a derivation of state space systems which expresses the dynamic performance of the examined systems. Two compensators are studied, a shunt-connected VSC without significant energy storage, a D-STATCOM, and a compensator with significant energy storage, an E-STATCOM. The last part in this chapter examines the damping and stability of a grid when the compensators are used, one at a time.

6.2 Dynamic Loads

In power system analysis, load behaviour has not attained the same attention from researchers as generation and transmission studies. However, there are cases when unexpected load properties are known to have caused large problems, for example in the Swedish blackout in December 1983 where the loads made the system unstable. In the simulation following the blackout, the first calculations showed that the system should have stayed stable but it was later understood that after the initial drop in power demand, due to the voltage drop, the loads recovered due to the voltage restoration by the on-load tap changers in transformers [16].

Many studies have highlighted this behaviour, among them [9], which performed measurements in the power system and tried to determine the parameters of the load recovery in the range of minutes. Among the first to study the dynamic performance of systems with a time scale of less than a second were [15]. However, the dynamic properties and the time scale in focus in this thesis are determined by power electronic based loads which can react to changes in the range of milliseconds. The power electronics considered is mainly self-commutated semiconductor switches like the IGBT.

In distributed DC systems, often used on ships or aircraft, power electronic based loads with fast dynamics is a well studied topic, known to cause operation problems [34], [1]. With the increasing number of power electronic loads in AC systems, caution has to be taken to ensure satisfying safety margins also in AC distribution and transmission systems [21]. So far, stability criteria studies similar to those for DC systems have not been common for AC systems [2].

In AC systems, the impact of load dynamics on system performance in systems with or without voltage compensators is gaining increasing attention from researchers, although the dynamic loads mostly considered are induction machines as in [3], [29]. Power electronic based loads have different dynamic properties than induction machines and it is therefore important to investigate the impact from these types of loads.

This section describes the behaviour of one type of dynamic load, a constant power load, and how this load can be modelled.

6.2.1 Understanding Constant Power Loads

When classifying a load, it is common to split the load into three parts with different characteristics; constant impedance Z, constant current I and constant power P [26]. This is mainly a definition of the steady state power consumption after a voltage disturbance, but it has also an impact on the dynamic properties. A constant impedance load does not show any load recovery, since the impedance is fixed and does not depend on the voltage, while both the constant current and constant power have this recovery in different extent. Power system loads are often modelled as a mixture of these parts, called a ZIP-model, where each characteristic describe a certain portion of the total load. The behaviour of the active and reactive part of the load are often different and should therefore be modelled separately [9].

To simplify the analysis, it has in this thesis been assumed that the loads show either constant impedance or constant power load characteristics. As it is shown later, the active power part have a bigger impact on the system performance than the reactive power part. Thus, the constant power loads studied in these work, except in one case, are only consuming active power while the reactive power is consumed by constant impedance loads. This is in most cases a reasonable assumption since most power electronic loads are used to control active power. For example, motor drives or chargers for electric vehicles have a rectifier which controls the DC voltage and, hence, the active power. If the voltage in the AC system drops, the rectifier tries to retain the power consumption to the pre-event value since the load still needs the same amount of power. With a lower AC voltage, the rectifier has to draw a bigger current if the power use should be the same as before the voltage drop. Due to this, a constant power load can, around an operation point, be considered as an incremental negative resistance, i.e. a lower voltage would cause the resistance in the load to decrease and hence increase the current.

6.2.2 Modelling of Constant Power Loads

The traditional way of modelling loads only consider the steady state equations, hence, these models do not show any transient behaviour and are not good enough when studying fast dynamics. The constant power load model in PSCAD/EMTDC is one example of this. The PSCAD/EMTDC model is tested during a voltage dip and the consumed power are supposed to return to the pre-fault value. However, as can be seen in Figure 6.1, where the power consumption is showed, the constant power load model is unable to do so. Furthermore, the notches in the curve are not realistic and are probably due to changes in operating point of the model, hinting that the model in fact is using steady state equations. Instead, a load model which includes the time dependency has to be used when studying dynamic systems.

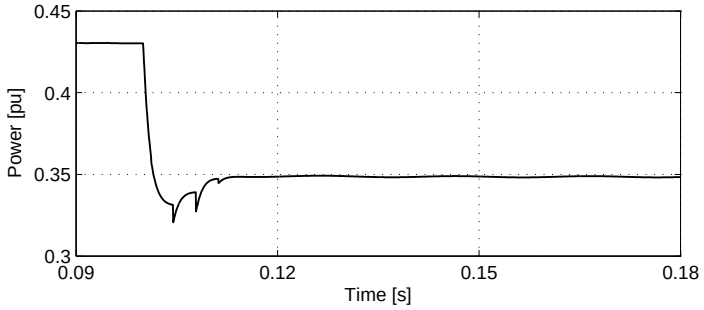

Figure 6.1: Power consumed by the constant power load model in PSCAD during a voltage dip.

A load model used in [31] has been shown to correspond well with measured load characteristics. The load model expresses the power consumed by a load with a generic model, written as

$$\begin{aligned} \dot{x}(t) &= -\frac{x(t)}{T_p} + P_0 \left[\frac{V_L(t)}{V_0}\right]^{N_{ps}} - P_0 \left[\frac{V_L(t)}{V_0}\right]^{N_{pt}} \\ P_L(t) &= \frac{x(t)}{T_p} + P_0 \left[\frac{V_L(t)}{V_0}\right]^{N_{pt}} \end{aligned} \tag{6.1}$$

$$\begin{aligned} \dot{z}(t) &= -\frac{z(t)}{T_q} + Q_0 \left[\frac{V_L(t)}{V_0}\right]^{N_{qs}} - Q_0 \left[\frac{V_L(t)}{V_0}\right]^{N_{qt}} \\ Q_L(t) &= \frac{z(t)}{T_q} + Q_0 \left[\frac{V_L(t)}{V_0}\right]^{N_{qt}} \end{aligned} \tag{6.2}$$

where $P_L(t)$ and $Q_L(t)$ are the active and reactive power consumed by the load, respectively. T_p and T_q, respectively, denote the time constants of the state space variables $x(t)$ and $z(t)$. N_{ps}, N_{pt}, N_{qs} and N_{qt} denote the voltage indices of the steady state and transient response. Here, and in the rest of the thesis, the frequency dependency of the load is neglected. This is a done since it is assumed that the loads are connected to a infinite grid behind a grid impedance which would keep the frequency fixed. It also simplifies the analysis of the result.

Depending on the chooses for N_{ps}, N_{pt}, N_{qs} and N_{qt}, different load characteristics are obtained. For example, setting $N_{ps} = 2$ gives a constant impedance (resistance) load, $N_{ps} = 1$ gives a constant (active) current load and $N_{ps} = 0$ gives a constant (active) power load, all in steady state and with similar results for reactive power. The transient response, N_{pt}, provides similar characteristics but with the difference that its dependency is decaying. After a time corresponding to the time constants T_p, its dependency is practically eliminated and the steady state response

is dominating. Hence, setting $N_{ps} = 0$ and $N_{pt} = 2$ gives a constant active power load in steady state but where the power consumption initially drops as in a constant impedance load.

Although (6.1) and (6.2) express a generic and accurate model of load characteristics, neither of them have been used in this thesis. Instead, another constant power load model has been derived in which the load resistance is expressed as a function of the load voltage, the power reference and the load time constant in the Laplace domain. The reason is that this allows a more simple implementation of the load model in a simulation tool, in this case PSCAD/EMTDC.

The idea behind this derived model is that the load resistance changes according to the low-pass filtered square of the load voltage amplitude, expressed as

$$R_p = \frac{1}{(T_L\, s + 1)} \frac{|\underline{V}_L|^2}{P_{ref}} \tag{6.3}$$

where $\underline{V}_L$ is the load voltage, P_{ref} is the load power reference and T_L is the time constant of the load. Introducing a new variable V_{2L} as the low-passed filtered load voltage in square, written as

$$\underline{V}_{2L} = \frac{1}{T_L\, s + 1} \underline{V}_L^2 \tag{6.4}$$

gives, together with (6.3), a more simple expression of the equivalent load resistance as

$$R_p = \frac{|\underline{V}_{2L}|}{P_{ref}} \tag{6.5}$$

with the instantaneous power consumed by the load given by

$$P_L = \frac{|\underline{V}_L|^2}{R_p} \tag{6.6}$$

A comparison is done between the derived model in (6.3)-(6.6) and the generic model given in (6.1). Only active power is considered, with a load time constant $T_p = T_L = 20$ ms and $N_{ps} = 0$ and $N_{pt} = 2$. The reference power is set to $P_0 = P_{ref} = .5$ pu with a steady state voltage $V_0 = 1$ pu. A voltage dip is introduced with a drop in $V_L(t)$ from 1 pu to 0.75 pu and the output power is studied and showed in Figure 6.2. There is a small difference between the two models where the generic model show a faster load recovery compared to the derived model. However, the differences are neglectable and both models give a response such that the power is back to the reference value after 20 ms. It is therefore assumed that the derived load model has a dynamic performance that is accurate enough and it will hence be used in the rest of the thesis.

The drawback of the derived model is that the load characteristics with (6.3)-(6.6) cannot be determined in a simple and accurate way as in (6.1). Here, as explained before, changing N_{ps}, N_{pt}, N_{qs} and N_{qt} gives loads with different characteristics. Similar characteristics can, in some extent, be obtained with the derived model by adding a parallel resistance. However, it is still more complicated to determine the aggregated load characteristics.

It should be mentioned that in a real rectifier, the capacitors on the DC-sides would, to some extent, resist the constant power load behaviour since the DC voltage stored in the capacitors might be higher than the AC voltage during a dip. Initially, this causes the power consumption to drop until the DC voltage have reached a level where the rectifier can operate again. It is in this thesis assumed that the capacitor size is such that it corresponds to the time constant of the load recovery.

6.3 State Space Models

In this section will the state space models be derived which are used to examine the impact of load dynamics on the damping and stability of distribution systems. First it is shown how a state space system is modelled, and the last part in this section shows how such systems can be linearized.

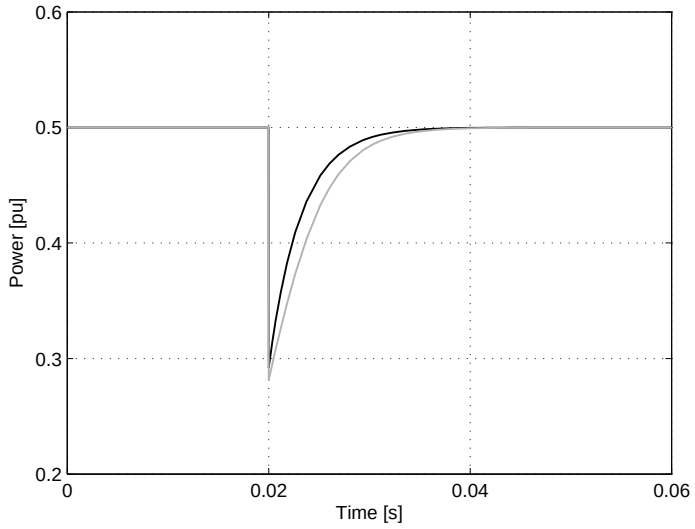

Figure 6.2: Power consumed by a load during a voltage dip for two different load models, in black the generic model and in grey the derived model which is used in the rest of the thesis.

The model derivation, however, starts with the simplest grid without compensators and with only constant impedance loads (CZL) for both active and reactive power. The resistive part of the load is later changed to a load with dynamic properties, modelled as a constant active power load (CPL). In the next step is a D-STATCOM connected to the system, which gives control over the reactive power flowing in the grid, and later an energy storage is attached to the compensator, i.e. an E-STATCOM, which can control both active and reactive power.

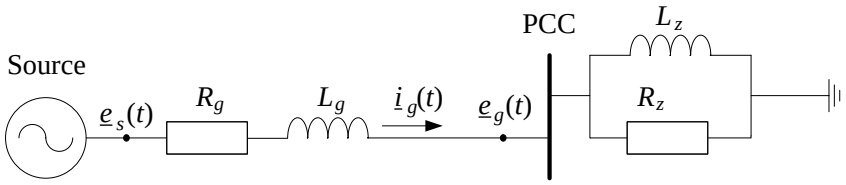

Figure 6.3: A simplified grid model with supply, line impedance and constant impedance loads.

6.3.1 State Space Systems

Representing a system in state space form is useful when the system consists of multiple inputs and/or multiple outputs [19]. A linear continuous system is written in state space form as

$$\begin{aligned} s\,\boldsymbol{x} &= A\boldsymbol{x} + B\boldsymbol{u} \\ \boldsymbol{y} &= C\boldsymbol{x} + D\boldsymbol{u} \end{aligned} \tag{6.7}$$

where $\boldsymbol{x}$ denotes the state space variables, $\boldsymbol{u}$ denotes the inputs and $\boldsymbol{y}$ denotes the outputs. A, B, C and D are matrices representing the system dynamics. The Laplace variable s should be

interpreted as the time derivative operator $s = d/dt$ from now and on. A state space system is formed by expressing the time derivative of each state space variables by using the other variables and inputs. If the equations are nonlinear, but still continuous, the system model is written as

$$\begin{aligned} s\,\boldsymbol{x} &= \boldsymbol{f}\left(\boldsymbol{x}, \boldsymbol{u}\right) \\ \boldsymbol{y} &= \boldsymbol{g}\left(\boldsymbol{x}, \boldsymbol{u}\right) \end{aligned} \tag{6.8}$$

which has to be linearized before it can be analysed. The linearization will be explained later in Section *6.3.5 Linearization Method*.

The notation used are such that a boldface quantify , e.g. $\boldsymbol{x} = [x_1, x_2, ..., x_n]'$ denotes a vector quantity used to describe state space systems. $'$ denoted the transpose symbol. A quantity with an underline denotes complex space vectors, e.g. $\underline{e}^{dq} = e^d + je^q$ or $\underline{i}^{\alpha\beta} = i^\alpha + ji^\beta$, with the same notation for voltages, currents or other quantities.

6.3.2 Without Compensator

Constant Impedance Loads

The system is modelled according to Figure 6.3. An infinite bus is assumed to supply the system with a source voltage $\underline{e}_s$ with constant frequency w through a grid impedance L_g and R_g. The voltage at the PCC is denoted $\underline{e}_g$ and this is the node where the loads are connected. The loads are modelled as parallel connected loads since this makes it more simple to separate the load into an active and a reactive part. Having the load modelled as series connected would have made this harder. The constant inductive load is denoted L_z and the constant resistive load R_z. The current flowing through the grid is denoted $\underline{i}_g$ and in this case, when there is no compensator, the grid current is the same as the total load current.

Applying KVL between the source voltage and the PCC voltage in Figure 6.3, and using the same method as when deriving the control equations in *4.2 Vector Current Controller*, the following equation is obtained in the fixed two-phase $\alpha\beta$-frame

$$\underline{e}_s^{\alpha\beta} - \underline{e}_g^{\alpha\beta} = R_g \underline{i}_g^{\alpha\beta} + sL_g \underline{i}_g^{\alpha\beta} \tag{6.9}$$

Transforming (6.9) into the (positive) synchronous rotating reference frame, i.e. the dq-frame, gives

$$\underline{e}_s^{dq} - \underline{e}_g^{dq} = R_g \underline{i}_g^{dq} + sL_g \underline{i}_g^{dq} + j\omega L_g \underline{i}_g^{dq} \tag{6.10}$$

where the time derivative of the state space variable $\underline{i}_g^{dq}$ is extracted as

$$s\,\underline{i}_g^{dq} = -\left(\frac{R_g}{L_g} + j\omega\right)\underline{i}_g^{dq} + \frac{1}{L_g}\left(\underline{e}_s^{dq} - \underline{e}_g^{dq}\right) \tag{6.11}$$

The PCC voltage can be expressed as

$$\underline{e}_g^{\alpha\beta} = \underline{Z}_L \cdot \underline{i}_g^{\alpha\beta} \tag{6.12}$$

where Z_L is the equivalent impedance of the loads and can be written as

$$\begin{aligned} Z_L &= \frac{sL_zR_z}{sL_z + R_z} \\ &= R_z\left(1 - \frac{R_z/L_z}{s + R_z/L_z}\right) \end{aligned} \tag{6.13}$$

The reason for writing Z_L in this form is that it later makes it easier to express $\underline{e}_g$ in state space form. Combining (6.12) and (6.13) gives

$$\begin{aligned}\underline{e}_g^{\alpha\beta} &= R_z\left(\underline{i}_g^{\alpha\beta} - \frac{R_z/L_z}{s+R_z/L_z}\underline{i}_g^{\alpha\beta}\right)\\ &= R_z\left(\underline{i}_g^{\alpha\beta} - \frac{R_z}{L_z}\underline{V}_t^{\alpha\beta}\right)\end{aligned} \tag{6.14}$$

where $\underline{V}_t^{\alpha\beta}$ is introduced as a state space variable

$$\underline{V}_t^{\alpha\beta} = \frac{1}{s+R_z/L_z}\underline{i}_g^{\alpha\beta} \tag{6.15}$$

From (6.15) can the time derivative of $\underline{V}_t$, in the synchronous rotating reference frame, be extracted as

$$s\,\underline{V}_t^{dq} = -\left(\frac{R_z}{L_z} + j\omega\right)\underline{V}_t^{dq} + \underline{i}_g^{dq} \tag{6.16}$$

with the PCC voltage written as

$$\underline{e}_g^{dq} = R_z\underline{i}_g^{dq} - \frac{R_z^2}{L_z}\underline{V}_t^{dq} \tag{6.17}$$

Splitting (6.11) and (6.16) into real and imaginary parts gives the following state space system which represents the grid in Figure 6.3.

$$\begin{aligned}s\,i_g^d &= -\frac{R_g}{L_g}i_g^d + \omega i_g^q + \frac{1}{L_g}\left(e_s^d - e_g^d\right)\\ s\,i_g^q &= -\frac{R_g}{L_g}i_g^q - \omega i_g^d + \frac{1}{L_g}\left(e_s^q - e_g^q\right)\\ s\,V_t^d &= -\frac{R_z}{L_z}V_t^d + \omega V_t^q + i_g^d\\ s\,V_t^q &= -\frac{R_z}{L_z}V_t^q - \omega V_t^d + i_g^q\end{aligned} \tag{6.18}$$

Observe that the system is linear. The state space vector is $\boldsymbol{x} = \left[i_g^d, i_g^q, V_t^d, V_t^q\right]'$, with the inputs $\boldsymbol{u} = \left[e_s^d, e_s^q\right]'$ and outputs $\boldsymbol{u} = \left[e_g^d, e_g^q\right]'$ given by

$$e_g^d = R_z i_g^d - \frac{R_z^2}{L_z}V_t^d \tag{6.19}$$

$$e_g^q = R_z i_g^q - \frac{R_z^2}{L_z}V_t^q \tag{6.20}$$

Constant Power Load

Now, let the constant resistance R_z change into a constant active power load R_p, shown in Figure 6.4, where R_p is expressed using the derived model in Section *6.2.2 Modelling of Constant Power Loads* with

$$R_p = \frac{|\underline{V}_{2g}^{dq}|}{P_{ref}} \tag{6.21}$$

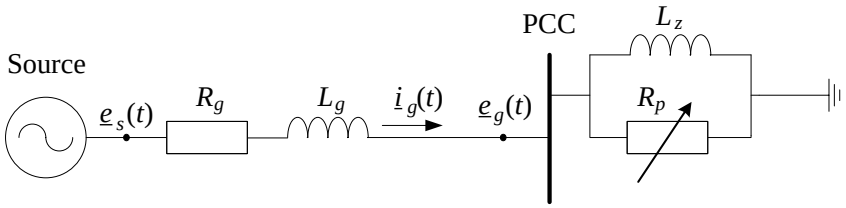

Figure 6.4: A simplified grid model with supply, line impedance and constant active power load.

where P_{ref} is the power demand and the low-pass filtered square of the PCC voltage (assumed to be the same as the load voltage) is expressed with the state space variable

$$\underline{V}_{2g}^{dq} = \frac{1}{T_L s + 1} \underline{e}_2^{dq\,2} \tag{6.22}$$

with T_L being the load time constant, i.e. the time before the power has recovered to the reference value. From (6.22) is the time derivative of $\underline{V}_{2g}^{dq}$ extracted as

$$s\,\underline{V}_{2g}^{dq} = -\frac{1}{T_L}\underline{V}_{2g}^{dq} + \frac{1}{T_L}\underline{e}_g^{dq\,2} \tag{6.23}$$

Splitting (6.23) into real and imaginary part and adding them to (6.18) gives a state space system representing the grid in Figure 6.4.

$$\begin{aligned}
s\,i_g^d &= -\frac{R_g}{L_g} i_g^d + \omega i_g^q + \frac{1}{L_g}\left(e_s^d - e_g^d\right) \\
s\,i_g^q &= -\frac{R_g}{L_g} i_g^q - \omega i_g^d + \frac{1}{L_g}\left(e_s^q - e_g^q\right) \\
s\,V_t^d &= -\frac{R_p}{L_z} V_t^d + \omega V_t^q + i_g^d \\
s\,V_t^q &= -\frac{R_p}{L_z} V_t^q - \omega V_t^d + i_g^q \\
s\,V_{2g}^d &= -\frac{1}{T_L} V_{2g}^d + \frac{1}{T_L}\left(e_g^{d\,2} - e_g^{q\,2}\right) \\
s\,V_{2g}^q &= -\frac{1}{T_L} V_{2g}^q + \frac{1}{T_L} 2 e_g^d e_g^q
\end{aligned} \tag{6.24}$$

with R_p expressed according to (6.21) and e_g^d and e_g^q by (6.25) and (6.26), respectively. Observe that the system no longer is linear and has to be linearized. The state space vector is $\boldsymbol{x} = \left[i_g^d, i_g^q, V_t^d, V_t^q, V_{2g}^d, V_{2g}^q\right]'$, with the inputs $\boldsymbol{u} = \left[e_s^d, e_s^q, P_{ref}\right]'$ and outputs $\boldsymbol{y} = \left[e_g^d, e_g^q\right]'$.

$$e_g^d = R_p i_g^d - \frac{R_p^2}{L_z} V_t^d \tag{6.25}$$

$$e_g^q = R_p i_g^q - \frac{R_p^2}{L_z} V_t^q \tag{6.26}$$

6.3.3 With D-STATCOM

Connecting a D-STATCOM to the PCC through a LCL-filter gives a grid model which can be seen in Figure 6.5. This grid model is very simplified compared to a real grid. In addition to all the simplifications of the compensator, mentioned in Section *4.6 Simplifications in the Used*

System, is the grid source modelled as a infinite grid behind an impedance. Furthermore, both the load and the compensator are connected right at the PCC which means that there is nothing that can decouple the controllers. In fact, this is the worst condition since there are nothing to slow down the changes, hence the risk for interaction is increased.

The converter-side filter inductance is denoted L_f, the filter capacitance is denoted C_f while the grid-side filter inductance, constituted by the leakage inductance of the injection transformer, is denoted L_{tr}. Voltages and currents are denoted and directed according to Figure 6.5, i.e. a positive current (power) is hence obtained when injected into the PCC.

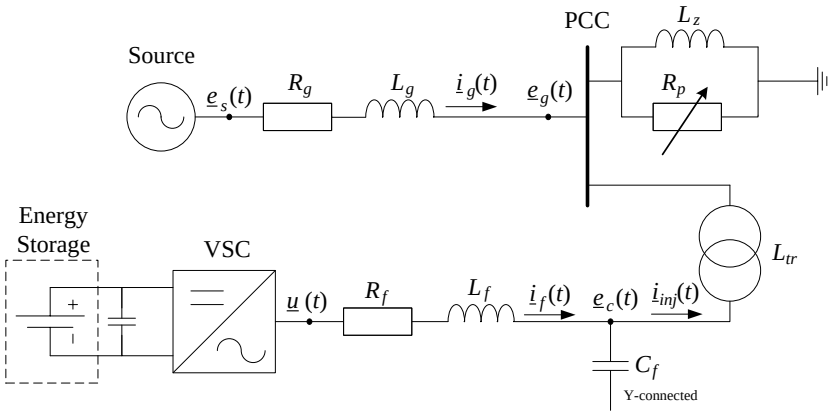

Figure 6.5: Grid model with supply, line impedance, constant power load and D-STATCOM connected through a LCL-filter.

KVL between the PCC voltage $\underline{e}_g^{dq}$ and the capacitor voltage $\underline{e}_c^{dq}$ gives, with the same method as when calculating the grid current in (6.11), a time derivative of the current injected into the PCC, $\underline{i}_{inj}^{dq}$, as

$$s\,\underline{i}_{inj}^{dq} = -j\omega \underline{i}_{inj}^{dq} + \frac{1}{L_{tr}}\left(\underline{e}_c^{dq} - \underline{e}_g^{dq}\right) \tag{6.27}$$

Using KCL for the node connecting the capacitor gives, in the synchronous rotating reference frame,

$$\underline{i}_f^{dq} = \underline{i}_{inj}^{dq} + \underline{i}_c^{dq} = \underline{i}_{inj}^{dq} + sC_f\underline{e}_c^{dq} + j\omega C_f \underline{e}_c^{dq} \tag{6.28}$$

where $\underline{i}_f^{dq}$ is the current through the filter reactor and $\underline{i}_c^{dq}$ is the current going into the filter capacitor. The time derivative of $\underline{e}_c^{dq}$ can thus be extract from (6.28) as

$$s\,\underline{e}_c^{dq} = -\omega \underline{e}_c^{dq} + \frac{1}{C_f}\left(\underline{i}_f^{dq} - \underline{i}_{inj}^{dq}\right) \tag{6.29}$$

As explained in Section *4.3 Reactive Power Controller - VSC without significant Energy Storage*, is the reactive power controller in the D-STATCOM used to control the voltage magnitude over the filter capacitor by injecting or absorbing reactive power. The reactive power controller is set to inject a current according to (4.43), rewritten here as,

$$i_{f,ref}^q = i_{inj}^q + \frac{\omega C_f}{e_{c,LP}}\left|\underline{e}_c^{dq}\right|^2 - \frac{k_{p,vc}}{2e_{c,LP}}\left(\left|\underline{e}_{c,ref}^{dq}\right|^2 - \left|\underline{e}_c^{dq}\right|^2\right) \tag{6.30}$$

where $e_{c,LP}$ is the low-pass filtered amplitude of the capacitor voltage, expressed as

$$e_{c,LP} = \frac{\omega_{cc}}{s+\omega_{cc}}\left|\underline{e}_c^{dq}\right| \tag{6.31}$$

However, (6.30) is only useful when the voltage over the capacitor is aligned in the dq-system such that the q-component is zero and the d-component equals the magnitude of the voltage. In a real system or when simulated in PSCAD/EMTDC, a PLL makes sure that this is true (in steady-state), see Section *4.5 Synchronization System - PLL*. It is possible to implement a PLL in the state space system to make sure that the alignment is correct, however, this has not been done in this thesis. Instead, another method has been used where the d- and q-component of the currents have been decoupled from active and reactive power, respectively, such that the d-component no longer corresponds to active power and the q-component to reactive power.

Hence, (6.30) has to be rewritten to make sure that the correct amount of reactive power is injected and no active power is produced or consumed. The power expressions in the dq-frame

$$P = e^d i^d + e^q i^q \tag{6.32}$$

$$Q = -e^d i^q + e^q i^d \tag{6.33}$$

can, when the voltage vector is aligned with the d-axis, be simplified to $P \approx e^d i^d$ and $Q \approx -e^d i^q$. Thus, the reactive power reference in (6.30) can be written as

$$Q_{f,ref} = -e_c^d i_{f,ref}^q \approx -|\underline{e}_c^{dq}| i_{f,ref}^q \tag{6.34}$$

Equation (6.34) shows that the reference filter current should be multiplied by the voltage amplitude in order to achieve the wanted reactive power reference. This is true for the amplitude dependent terms in (6.30), i.e. $\omega C_f |\underline{e}_c^{dq}|^2 / e_{c,LP}$ and $k_{p,vc} \left(|e_{c,ref}^d|^2 - |\underline{e}_c^{dq}|^2 \right) / (2e_{c,LP})$. However, for the feed-forward term i_{inj}^q, multiplying it by the voltage amplitude is not correct since the d-component of the voltage and the voltage amplitude are not the same without a PLL. Hence, the feed-forward component has to be expressed as

$$Q_{inj} = -e_c^d i_{inj}^q + e_c^d i_{inj}^d \tag{6.35}$$

In all, the reactive power reference for the D-STATCOM is written as

$$Q_{f,ref} = Q_{inj} + \frac{\omega C_f}{e_{c,LP}} |\underline{e}_c^{dq}|^3 - \frac{k_{p,vc}}{2e_{c,LP}} |\underline{e}_c^{dq}| \left(|\underline{e}_{c,ref}^{dq}|^2 - |\underline{e}_c^{dq}|^2 \right) \tag{6.36}$$

and, using (6.33), the q-component of the filter current reference is given by

$$i_{f,ref}^q = -\frac{Q_{f,ref} - e_c^q i_f^d}{e_c^d} \tag{6.37}$$

Since the active power exchange of the D-STATCOM should be equal to zero, i.e. $P_f = e_c^d i_f^d + e_c^q i_f^q = 0$, the d-component of the filter current reference is set to

$$i_{f,ref}^d = -\frac{e_c^q i_{f,ref}^q}{e_c^d} \tag{6.38}$$

The d- and q-component of the filter current are assumed to follow the references as if they were low-pass filtered. This is a valid approximation as long as the bandwidth of the inner current controller is fast enough, normally said to be at least 10 times faster than the outer reactive power controller [19]. Thus, it is assumed that the VSC and the LC-part of the filter can be modelled as a CSC, showed in Figure 6.6. In reality there is also a cross-coupling between the d- and q-component due to the filter reactor but this effect is neglected here since the current controller, i.e the CSC, is assumed be fast enough to mitigate such effects. The filter current is hence written as

$$\underline{i}_f^{dq} = \frac{\omega_{cc}}{s + \omega_{cc}} \underline{i}_{f,ref}^{dq} \tag{6.39}$$

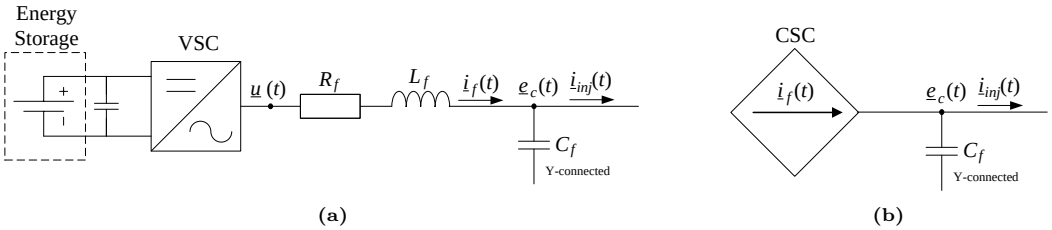

Figure 6.6: The VSC with the LC-filter that is modelled as a CSC. Plot (a): VSC, plot (b): CSC.

where ω_{cc} is the bandwidth of the current controller. Hence, the time derivative is expressed as

$$s\,\underline{i}_f^{dq} = -\omega_{cc}\underline{i}_f^{dq} + \omega_{cc}\underline{i}_{f,ref}^{dq} \tag{6.40}$$

The time derivative of the low-passed filtered capacitor voltage is extracted from (6.31) and written as

$$s\,e_{c,LP} = -\omega_{cc}e_{c,LP} + \omega_{cc}|\underline{e}_c^{dq}| \tag{6.41}$$

where it is assumed the bandwidth of the low-pass filter is the same as the bandwidth of the current controller.

In all, the space system for the D-STATCOM is formed from (6.11), (6.16), (6.23), (6.27), (6.29), (6.40) and (6.41). Splitting the equations into real and imaginary parts gives the following state space system for the grid with the D-STATCOM

$$\begin{aligned}
s\,i_g^d &= -\frac{R_g}{L_g}i_g^d + \omega i_g^q + \frac{1}{L_g}\left(e_s^d - e_g^d\right)\\
s\,i_g^q &= -\frac{R_g}{L_g}i_g^q - \omega i_g^d + \frac{1}{L_g}\left(e_s^q - e_g^q\right)\\
s\,V_t^d &= -\frac{R_p}{L_z}V_t^d + \omega V_t^q + i_g^d\\
s\,V_t^q &= -\frac{R_p}{L_z}V_t^q - \omega V_t^d + i_g^q\\
s\,V_{2g}^d &= -\frac{1}{T_L}V_{2g}^d + \frac{1}{T_L}\left(e_g^{d\,2} - e_g^{q\,2}\right)\\
s\,V_{2g}^q &= -\frac{1}{T_L}V_{2g}^q + \frac{1}{T_L}2e_g^d e_g^q\\
s\,i_{inj}^d &= \omega i_{inj}^q + \frac{1}{L_{tr}}\left(e_c^d - e_g^d\right)\\
s\,i_{inj}^q &= -\omega i_{inj}^d + \frac{1}{L_{tr}}\left(e_c^q - e_g^q\right)\\
s\,e_c^d &= \omega e_c^q + \frac{1}{C_f}\left(i_f^d - i_{inj}^d\right)\\
s\,e_c^q &= -\omega e_c^d + \frac{1}{C_f}\left(i_f^q - i_{inj}^q\right)\\
s\,i_f^d &= -\omega_{cc}i_f^d + \omega_{cc}i_{f,ref}^d\\
s\,i_f^q &= -\omega_{cc}i_f^q + \omega_{cc}i_{f,ref}^q\\
s\,e_{c,LP} &= -\omega_{cc}e_{c,LP} + \omega_{cc}\sqrt{e_c^{d\,2} + e_c^{q\,2}}
\end{aligned} \tag{6.42}$$

where R_p is expressed according to (6.21), e_g^d by (6.25), e_g^q by (6.26), $i_{f,ref}^d$ by (6.38) and $i_{f,ref}^q$ by (6.37). Observe that the system is nonlinear and has to be linearized to obtain a state space model

that can be analysed. The state space vector is $\boldsymbol{x} = \left[i_g^d, i_g^q, V_t^d, V_t^q, V_{2g}^d, V_{2g}^q, i_{inj}^d, i_{inj}^q, e_c^d, e_c^q, i_f^d, i_f^q, e_{c,LP}\right]'$, with the inputs $\boldsymbol{u} = \left[e_s^d, e_s^q, P_{ref}, e_{c,ref}^d, e_{c,ref}^q\right]'$ and outputs $\boldsymbol{y} = \left[e_g^d, e_g^q\right]'$.

6.3.4 With E-STATCOM

Using an energy storage on the DC-side of the VSC, in other words an E-STATCOM, gives the advantage to control not only the magnitude, but also the phase of the voltage at the PCC (still done by controlling the voltage over the filter capacitor). The modelled system is the same as for the D-STATCOM, shown in Figure 6.5, with the exception that the energy storage now is used, enabling an active power exchange. This means that the voltage across the filter capacitor can be controlled with an extra degree of freedom, i.e. a reference for both the d- and q-component of the filter current. As shown in Section *4.4 Voltage Controller - VSC with Energy Storage*, the voltage controller is set to inject currents according to (4.57), rewritten here as

$$\underline{i}_{f,ref}^{dq} = \underline{i}_{inj}^{dq} + j\omega C_f \underline{e}_c^{dq} + k_{p,vc}\left(\underline{e}_{c,ref}^{dq} - \underline{e}_c^{dq}\right) \tag{6.43}$$

Except that (6.37) and (6.38) are replaced with (6.43), and that the low-passed filtered capacitor voltage no longer is used, there are no other difference between the D-STATCOM system and the E-STATCOM. Hence, the spate space system for the E-STATCOM is written as

$$\begin{aligned}
s\, i_g^d &= -\frac{R_g}{L_g} i_g^d + \omega i_g^q + \frac{1}{L_g}\left(e_s^d - e_g^d\right) \\
s\, i_g^q &= -\frac{R_g}{L_g} i_g^q - \omega i_g^d + \frac{1}{L_g}\left(e_s^q - e_g^q\right) \\
s\, V_t^d &= -\frac{R_p}{L_z} V_t^d + \omega V_t^q + i_g^d \\
s\, V_t^q &= -\frac{R_p}{L_z} V_t^q - \omega V_t^d + i_g^q \\
s\, V_{2g}^d &= -\frac{1}{T_L} V_{2g}^d + \frac{1}{T_L}\left(e_g^{d\,2} - e_g^{q\,2}\right) \\
s\, V_{2g}^q &= -\frac{1}{T_L} V_{2g}^q + \frac{1}{T_L} 2 e_g^d e_g^q \\
s\, i_{inj}^d &= \omega i_{inj}^q + \frac{1}{L_{tr}}\left(e_c^d - e_g^d\right) \\
s\, i_{inj}^q &= -\omega i_{inj}^d + \frac{1}{L_{tr}}\left(e_c^q - e_g^q\right) \\
s\, e_c^d &= \omega e_c^q + \frac{1}{C_f}\left(i_f^d - i_{inj}^d\right) \\
s\, e_c^q &= -\omega e_c^d + \frac{1}{C_f}\left(i_f^q - i_{inj}^q\right) \\
s\, i_f^d &= -\omega_{cc} i_f^d + \omega_{cc} i_{f,ref}^d \\
s\, i_f^q &= -\omega_{cc} i_f^q + \omega_{cc} i_{f,ref}^q
\end{aligned} \tag{6.44}$$

with R_p expressed according to (6.21), e_g^d by (6.25), e_g^q by (6.26) and $i_{f,ref}^{dq}$ by (6.43). Also this system is nonlinear and has to be linearized around an operation point to obtain the state space model. The state space vector is $\boldsymbol{x} = \left[i_g^d, i_g^q, V_t^d, V_t^q, V_{2g}^d, V_{2g}^q, i_{inj}^d, i_{inj}^q, e_c^d, e_c^q, i_f^d, i_f^q\right]'$, with the inputs $\boldsymbol{u} = \left[e_s^d, e_s^q, P_{ref}, e_{c,ref}^d, e_{c,ref}^q\right]'$ and outputs $\boldsymbol{y} = \left[e_g^d, e_g^q\right]'$.

6.3.5 Linearization Method

The above state space systems are nonlinear and have to be linearized around an operation point $\boldsymbol{x}_0, \boldsymbol{u}_0, \boldsymbol{y}_0$ to be analysed with a simple method. The parameter values at the operation points can be obtained using simulations in PSCAD/EMTDC and by solving the following equation system

$$\begin{aligned} 0 &= \boldsymbol{f}\left(\boldsymbol{x}_0, \boldsymbol{u}_0\right) \\ \boldsymbol{y}_0 &= \boldsymbol{g}\left(\boldsymbol{x}_0, \boldsymbol{u}_0\right) \end{aligned} \tag{6.45}$$

where the time derivative of the state space variables are set to zero since it is assumed that the system is in steady state at the operation point.

The system matrices can be obtained as

$$A = \frac{\partial \boldsymbol{f}}{\partial \boldsymbol{x}}\Big|_{(\boldsymbol{x}_0, \boldsymbol{u}_0)} \quad B = \frac{\partial \boldsymbol{f}}{\partial \boldsymbol{u}}\Big|_{(\boldsymbol{x}_0, \boldsymbol{u}_0)} \quad C = \frac{\partial \boldsymbol{g}}{\partial \boldsymbol{x}}\Big|_{(\boldsymbol{x}_0, \boldsymbol{u}_0)} \quad D = \frac{\partial \boldsymbol{g}}{\partial \boldsymbol{u}}\Big|_{(\boldsymbol{x}_0, \boldsymbol{u}_0)} \tag{6.46}$$

where $\boldsymbol{f}$ is a state space system from either (6.18), (6.24), (6.42) or (6.44) with the corresponding state space variables, inputs and outputs. If the load active power is taken by a CZL then $\boldsymbol{g}$ is given by (6.19) and (6.20), and if the active power is taken by a CPL, $\boldsymbol{g}$ is given by (6.25) and (6.26).

With the deviation from the operation points expressed as

$$\Delta\boldsymbol{x}(t) = \boldsymbol{x}(t) - \boldsymbol{x}_0(t) \quad \Delta\boldsymbol{u}(t) = \boldsymbol{u}(t) - \boldsymbol{u}_0(t) \quad \Delta\boldsymbol{y}(t) = \boldsymbol{y}(t) - \boldsymbol{y}_0(t) \tag{6.47}$$

the linearized system can be written as

$$\begin{aligned} s\,\Delta\boldsymbol{x} &= A\Delta\boldsymbol{x} + B\Delta\boldsymbol{u} \\ \Delta\boldsymbol{y} &= C\Delta\boldsymbol{x} + D\Delta\boldsymbol{u} \end{aligned} \tag{6.48}$$

The linearization gives a valid approximation of the dynamic properties of the nonlinear system if the deviations are not too far from the operation point.

6.3.6 Operation Points and System Parameters

Using the previously derived state space systems which are linearized according to the method explained by (6.46) and (6.48), a grid model is used to study the system performance. Grid and VSC parameters that are fixed in the following studies, except if else is stated, are given in table 6.1.

The exact operation point of the systems depends on the case that is studied. Without a compensator, the PCC voltage is lower than with a D-STATCOM or an E-STATCOM due to the voltage drop over the grid impedance. This could also cause the CZL and the CPL to have different operation points since the CPL will reduce its impedance until the reference power is obtained, thus, affecting the PCC voltage. By tuning the power reference of the CPL it can be done such that the operation point is the same as with a CZL. With a compensator, there is no need for tuning since the compensator keeps the voltage fixed even if the power demand increases slightly. The operation point for the case when no compensator is used is given in table 6.2.

It is further assumed that the E-STATCOM does not inject any active power at the operation point since this corresponds to an unrealistic steady state operation condition. The D-STATCOM and the E-STATCOM is on the other hand assumed to inject a certain amount of reactive power into the grid to raise the PCC voltage. This is also a bit from the truth, since a constant reactive power injection would cause high losses in the converters. In practise is often a capacitor bank used to provide reactive power in steady state operation while the VSC handles fast changes and

Table 6.1: Fixed system parameters, (a) grid parameters and (b) VSC parameters (same for D-STATCOM and E-STATCOM).

(a)

System parameters			
Base power	S_b	100 MVA	1 pu
Source voltage	e_s	21 kV	1 pu
Grid frequency	f	50 Hz	1 pu
Grid inductance	L_g	9 mH	0.641 pu
Grid resistance	R_g	100 mΩ	0.023 pu
Filter inductance	L_f	10.5 mH	0.748 pu
Filter resistance	R_f	330.8 mΩ	0.075 pu
Filter capacitance	C_f	39 μF	0.054 pu
Transformer inductance	L_{tr}	0.3509 mH	0.025 pu

(b)

Voltage or reactive power controller		
Bandwidth	ω_{vc}	$2\pi100$ rad/s
Proportional gain	$k_{p,vc}$	$\omega_{vc}C_f$
Integral gain	$k_{i,vc}$	0
Current controller		
Bandwidth	ω_{cc}	$2\pi1500$ rad/s
Proportional gain	$k_{p,cc}$	$\omega_{cc}L_f$
Integral gain	$k_{i,cc}$	$\omega_{cc}\left(R_{acc}+R_f\right)$
Damping term	R_{acc}	$\omega_{cc}L_f - R_f$
PLL		
Bandwidth	ω_{PLL}	$2\pi5$ rad/s

Table 6.2: Operation point for the system without compensator.

State space variables			
Grid current	$i_{g0}^d + ji_{g0}^q$	$1.84 + j0.514$ kA	$0.387 + j0.108$ pu
Temporary state	$V_{t0}^d + jV_{t0}^q$	$0 - j5.86$ As	$0 - j0.387$ pu
PCC voltage square	${e_{g0}^d}^2 + j{e_{g0}^q}^2$	$350 + j0$ MV^2	$0.795 - j0$ pu
Inputs and outputs			
Source voltage	$e_{s0}^d + je_{s0}^q$	$20.36 - j5.16$ kV	$0.969 - j0.246$ pu
Load power reference	P_{ref0}	34.5 MW	0.345 pu
PCC voltage	$e_{g0}^d + je_{g0}^q$	$18.72 + j0$ kV	$0.891 + j0$ pu
Miscellaneous parameters			
Load reactive power	Q_{L0}	9.6 MVar	0.096 pu
Load resistance	R_{p0}	10.16 Ω	2.3 pu
Load inductance	L_z	0.116 H	8.26 pu
Phase difference	θ	$-14.2°$	
Load power factor		0.96	
Short circuit ratio	SCR	4.55	

transients. The operation points of the D-STATCOM and the E-STATCOM are hence assumed to be identical and the parameter values are given in table 6.3.

Using the operation points given in either table 6.2 or 6.3, together with the grid parameters given in table 6.1, the matrices A, B, C and D are obtained according to (6.46).

6.4 Damping and Stability

The damping and stability of the derived systems can be studied using the state space matrices. The location of the poles corresponds to the dynamic properties of the system and from the system A-matrix, the poles are calculated as the eigenvalues of the matrix, given by

$$\det\left(A - I\boldsymbol{\lambda}\right) = 0 \tag{6.49}$$

where $\boldsymbol{\lambda}$ denotes the system poles (eigenvalues) and I is the identity matrix. The pole, or pole-pair, that dominates the dynamic properties is the one(s) that is closest to the imaginary axis. A pole located on the real axis corresponds to a first-order system with dynamical properties similar to a low-pass filter, with a faster response time the further away from the imaginary axis the pole is. A pole-pair with one pole on the opposite side of the real axis, expressed as

$$\frac{1}{s^2 + 2\zeta\omega_0 s + \omega_0^2} \tag{6.50}$$

gives a second-order system with properties depending on the damping ζ and the natural frequency ω_0. A damping close to zero, i.e poles close to the imaginary axis, gives a badly damped system

Table 6.3: Operation point for the system with either D-STATCOM or E-STATCOM.

State space variables			
Grid current	$i_{g0}^d + ji_{g0}^q$	$2.06 - j0.334$ kA	$0.423 - j0.070$ pu
Temporary state	$V_{t0}^d + jV_{t0}^q$	$0 - j6.55$ As	$0 - j0.432$ pu
PCC voltage square	${e_{g0}^d}^2 + j{e_{g0}^q}^2$	$437 + j0$ MV^2	$0.990 + j0$ pu
Injected current	$i_{inj0}^d + ji_{inj0}^q$	$0 + j0.907$ kA	$0 + j0.190$ pu
Capacitor voltage	$e_{c0}^d + je_{c0}^g$	$21 + j0$ kV	$1 + j0$ pu
Filter current	$i_{f0}^d + ji_{f0}^q$	$0 + j0.65$ kA	$0 + j0.136$ pu
Low-pass filtered voltage	$e_{c,LP0}$	21 kV	1 pu
Inputs and outputs			
Source voltage	$e_{s0}^d + je_{s0}^q$	$20.18 - j5.82$ kV	$0.961 - j0.277$ pu
Load power reference	P_{ref0}	43 MW	0.43 pu
Capacitor voltage references	$e_{c,ref0}^d + je_{c,ref0}^g$	$21 + j0$ kV	$1 + j0$ pu
PCC voltage	$e_{g0}^d + je_{g0}^g$	$20.9 + j0$ kV	$0.995 + j0$ pu
Miscellaneous parameters			
Load reactive power	Q_{L0}	12 MVar	0.12 pu
Load resistance	R_{p0}	10.16 Ω	2.3 pu
Load inductance	L_z	0.116 H	8.26 pu
Phase difference	θ	$-16.1°$	
Load power factor		0.96	
Short circuit ratio	SCR	3.5	

where the oscillations attenuate very slowly. On the other hand, if ζ approaches one, i.e. poles move closer to the real axis, the system will be more and more damped until the dynamic properties are close to the properties of a fist-order system [19]. A pole located on the positive side of the real axis would cause the whole system to be unstable. In general, the poles should be located within the grey area in Figure 6.7 to ensure stability and a good damping in the continuous time domain.

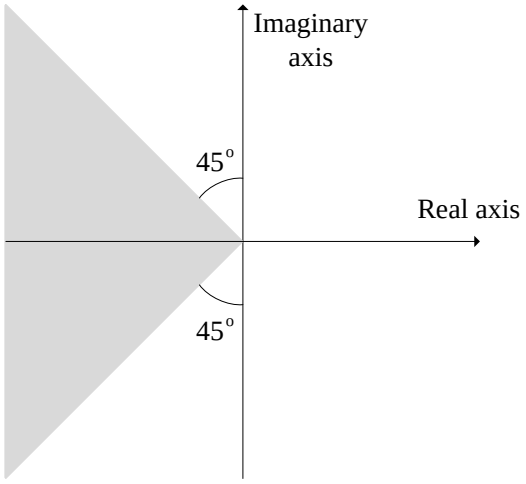

Figure 6.7: Desired pole placement.

The dynamic performance of the systems is examined by the pole placement and validated by simulations on a similar grid model in PSCAD/EMTDC. In PSCAD/EMTDC, a voltage dip from 1 pu to 0.75 pu is introduced in the source voltage as a disturbance to the system and the dq-components of the PCC voltage are studied. Due to the action from the D-STATCOM and the E-STATCOM, a voltage dip will not cause big deviations from the operation points, hence,

the linearized system models are valid.

It should be noticed that the interest of this work is not to determine the exact location of the poles and the corresponding damping. The focus is instead on the movements of the poles when one parameter is varied, for example the load time constant. Thus, making it possible to study that parameter's impact on the system performance. It should also be pointed out that the plots showing the pole placement of the D-STATCOM should not be directly compared to the E-STATCOM and vice versa. The reason is that different types of controllers are used when modelling the two compensators. However, plots showing the D-STATCOM, or the E-STATCOM, can be compared individually. Also, it is possible to compare how much the poles move. If the pole movements are small with one compensator when varying a parameter, but large with the other compensator, it can be said that the system performance with the first compensator is much less dependent on the studied parameter than with the second compensator.

6.4.1 Without Compensator

Using the same structure as when deriving the state space systems, the system performance of the grid without a compensator will first be shown with only CZL and later with the CPL.

Constant Impedance Load

The location of the poles are shown in Figure 6.8a. It is clear that the pole-pair closest to imaginary axis is very badly damped with a resonant frequency of 50 Hz (1 pu). However, this pole-pair does not affect the system in any significant way. There is indeed a frequency component of 50 Hz, shown in Figure 6.8b, but the amplitude of the oscillations is very small, approximately 0.00005 pu. It will later be shown that this pole-pair appears in all systems, with or without compensator and with CZL or CPL. Since this pole-pair appears in this simple system, without both compensator and dynamic loads, it is likely that it is caused by some resonances in the grid. The pole-pair is thus neglected in the following analysis. The pole-pair that dominates the system performance in Figure 6.8a is instead the pole-pair to the left.

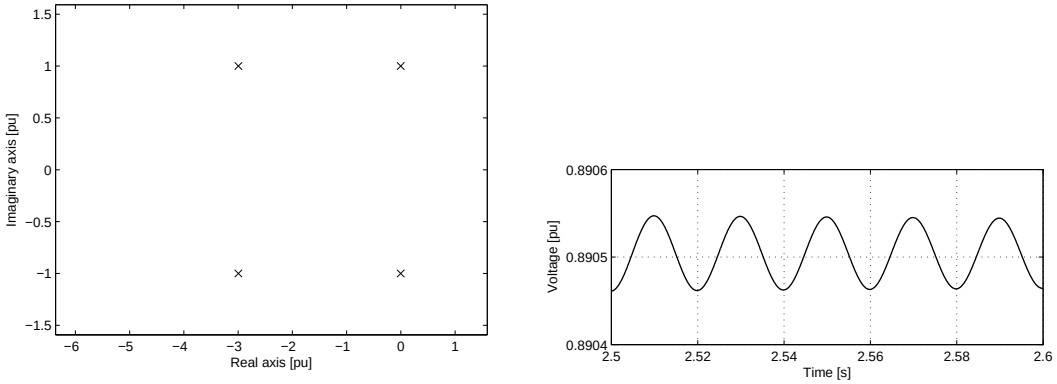

Figure 6.8: System with constant impedance loads and no compensator. Plot (a): location of poles, plot (b): the badly damped 50 Hz component.

Constant Power Load

Introducing a CPL and reducing the load time constant worsen the system damping, as shown in Figure 6.9 where different load time constants are marked. It is clear that decreasing the load time constant do have a large impact on the system performance and, if the bandwidth of the load is too high, the system would get unstable. By comparing 6.8a and 6.9 it is also clear

that when the time constant of the load increases, the location of the poles approaches the pole location of the CZL. In fact, a CPL with a time constant of 60000 ms is, when studying dynamic properties, practically a CZL which this model confirms.

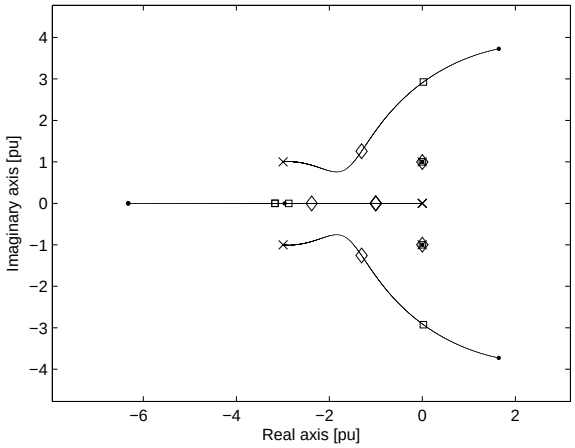

Figure 6.9: Pole placement for a system with CPL and no compensator. "x" denotes a load time constant of 60000 ms, "◊" denotes $T_L = 20$ ms, "□" $T_L = 6$ ms and "•" $T_L = 3$ ms.

Figure 6.10a indicates, neglecting the 50 Hz-pole-pairs, two different load time constants where one is stable and the other is unstable. This accuracy of the derived state space model is confirmed by comparing the pole placement in Figure 6.10a with the simulated response of the d-component of the PCC voltage after a small voltage dip shown in Figure 6.10b. It is clear that the grey curve, indicating a system with a load time constant of 6 ms, is unstable while the black curve, corresponding $T_L = 6.5$ ms, is stable. The disturbance that caused these responses are small voltage dips of .96 pu, which should be small enough not to cause the system to deviate too much from the operating point, i.e. making sure that the linearized state space model is valid.

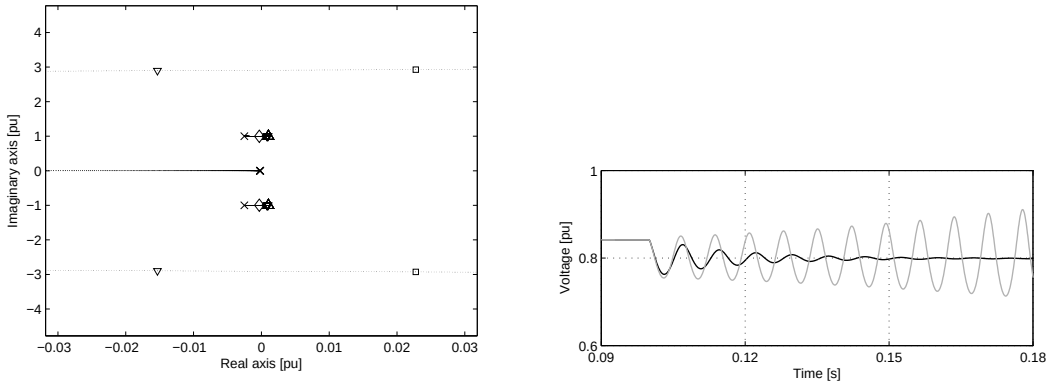

(a) **(b)**

Figure 6.10: System with CPL and no compensator. Plot (a): pole placement zoomed in around the imaginary axis, plot (b): d-component of the PCC voltage after a voltage dip. Marker "▽" in plot (a) denotes a load time constant of 6.5 ms, corresponding to the black curve in plot(b), and marker "□" in plot (a) denotes $T_L = 6$ ms, corresponding to the grey curve in plot (b).

6.4.2 With D-STATCOM

Figure 6.11a shows all the poles of the system with the D-STATCOM connected to the PCC together with a CPL, while Figure 6.11b shows the more dominant poles with specific load time constants marked. The pole-pair corresponding to the 50 Hz component is visible but does not affect the system performance and is neglected. Instead, the second closest pole-pair to the imaginary axis in Figure 6.11b is the one that has the dominating effect on the performance. As for the case without any compensator, it is seen that the system gets unstable by reducing the load time constant of the CPL. Comparing Figure 6.9 and 6.11b it can be noticed that the system turns unstable close to $T_L = 20$ ms with the D-STATCOM while it turns unstable close to $T_L = 6$ ms without the D-STATCOM. In other words, the D-STATCOM has worsen the stability margin. One plausible explanation could be an interaction between the controllers in the CPL and in the D-STATCOM which might occur if the bandwidths of the controllers are of similar speeds. Hence, changes in the load's power consumption might be compensated at the same time by the D-STATCOM, this can then create a resonance effect. This is a phenomena which is a know to cause problems in distributed DC systems [34], [1].

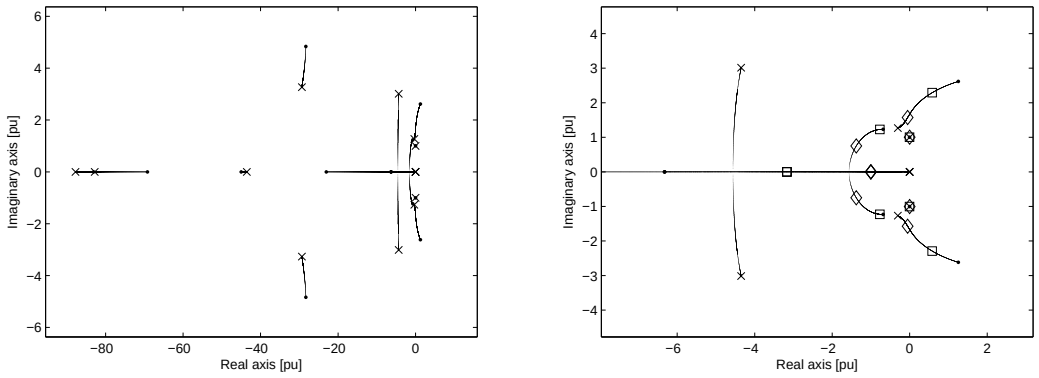

Figure 6.11: Pole placement for the grid with a D-STATCOM and a CPL where marker "x" denotes a load time constant of 60000 ms, marker "◊" denotes $T_L = 20$ ms, marker "□" $T_L = 6$ ms and marker "•" $T_L = 3$ ms. Plot (a): all poles, plot (b): zoomed in around dominating poles.

Figure 6.12 shows the system performance during a voltage dip for different types of loads, this corresponds well with the results obtained from the pole placement in Figure 6.11b. Figure 6.12a shows the dq-components of the PCC voltage during a voltage dip without the D-STATCOM and with a CZL, note that the d-component in steady state is lower than 1 pu due to the absence of a compensator. In Figure 6.12b is the performance with the D-STATCOM and a CZL load shown, and in Figure 6.12c and 6.12d are the PCC voltages shown for a CPL with a load time constant of $T_L = 20$ ms and $T_L = 7.5$ ms, respectively. It can be noticed that the system is unstable for $T_L = 7.5$ ms even without any disturbance. In all, it is clear that load time constant has a big impact on the system performance.

Varying the bandwidth of the reactive power controller, ω_{vc}, shows how the system performance is affected by the outer control loop of the D-STATCOM. In Figure 6.13, which shows the dominating pole-pairs, ω_{vc} is set to six different values, $2\pi \cdot [30, 50, 70, 100, 150, 200]$ rad/s. The arrows indicate the main trends of the pole movements when ω_{vc} is increased. The load time constant is then varied from 60000 ms to 3 ms as in the previous studies. From this, it is clear that an increased ω_{vc} worsen the system damping and eventually makes the system unstable. Even though this is just a discrete examination of the impact of the reactive power controller, i.e. not all controller values have been tested in a continues way, it is still clear the bandwidth of the

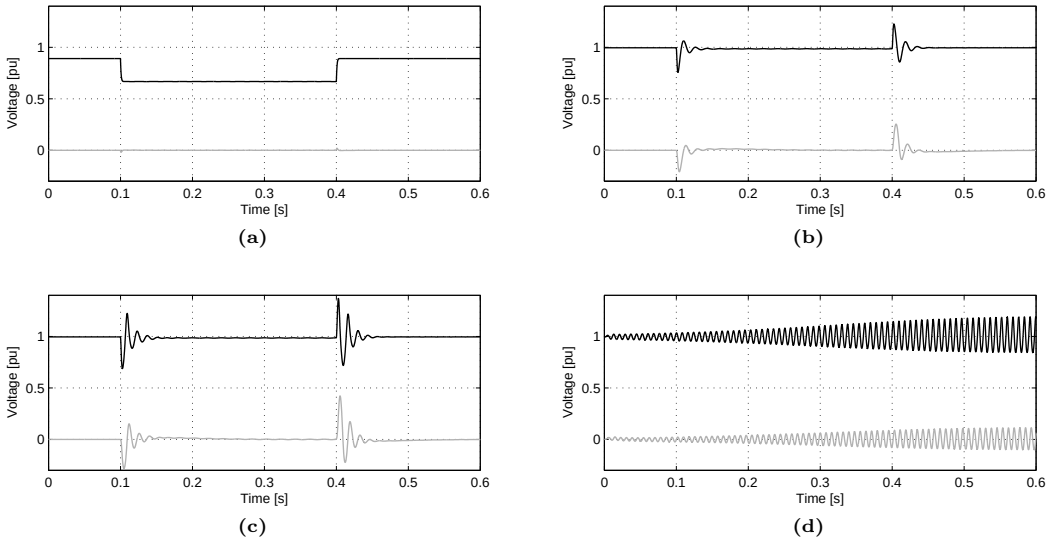

Figure 6.12: PCC voltages during a voltage dip with D-STATCOM for three different loads and a reference case without the D-STATCOM and with a CZL. Plot (a): CZL without D-STATCOM, plot(b): CZL with D-STATCOM, plot(c): CPL with D-STATCOM and $T_L = 20$ ms, plot (c): CPL with D-STATCOM and $T_L = 7.5$ ms

reactive power controller does have a large impact on the system performance.

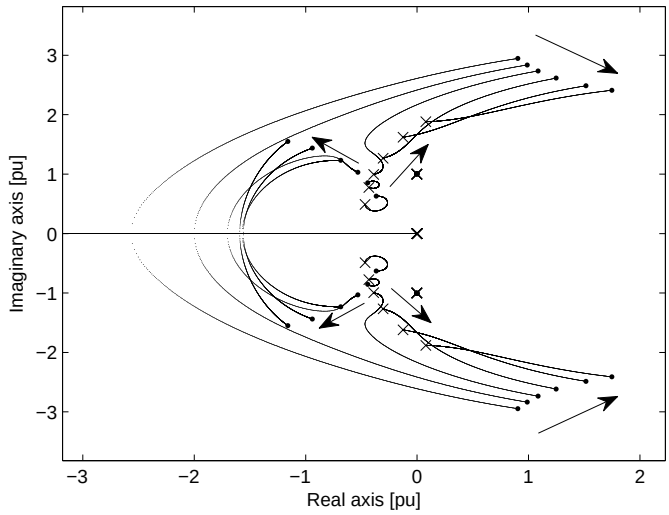

Figure 6.13: Pole placement with the D-STATCOM when ω_{vc} is set to $2\pi \cdot [30, 50, 70, 100, 150, 200]$ rad/s. The arrows indicate the main trends of the pole movements when ω_{vc} increases. Marker "x" denotes $T_L = 60000$ ms and marker "•" corresponds to $T_L = 3$ ms.

To examine the impact of the grid strength on the system performance, the power consumed by the load is varied to achieve different short circuit ratios (SCR). Hence, by keeping the grid impedance constant and varying the constant active power load reference, P_{ref0}, and the constant

reactance load, L_z, with the same tuning variable, the system performance can be studied without changing other parameters in table 6.1 and 6.3. By decreasing P_{ref0} and increasing L_z a stronger grid is obtained with a higher SCR and vice verse.

Investigating the SCR in the range from 2.9 to 8.7 in nine steps of equal size gives an understanding of how the SCR impacts the performance. Figure 6.14 shows the pole placement of the dominating pole-pairs and their movements, SCR= 2.9 and SCR= 8.7 are pointed out with arrows while larger arrows show the main trend of the pole movements when the SCR increases, i.e. when the grid strength increases. It can be noticed that a stronger grid gives a better damping since the markers, and especially "□", shows that the system is moved in the direction of getting more stable (even though it still is unstable) when the grid strength is increased. In all, it is clear the SCR does have a significant impact on the system performance when a D-STATCOM is used.

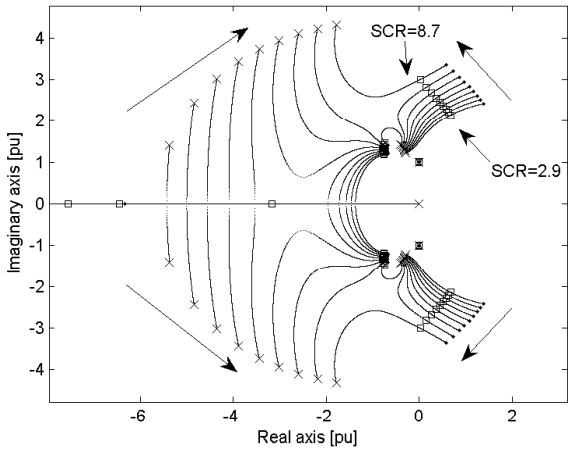

Figure 6.14: Pole placement with the D-STATCOM when the SCR is varied. Marker "x" denotes $T_L = 60000$ ms, "□" $T_L = 6$ ms and "•" $T_L = 3$ ms. The larger arrows show the main trends of the pole movements when the SCR is increased.

6.4.3 With E-STATCOM

The system pole placement with the E-STATCOM is shown in Figure 6.15a, in which all poles are shown, and in Figure 6.15b, in which only the dominating pole-pairs are shown. Comparing Figure 6.11b and 6.15b clearly shows how the E-STATCOM improves the system performance and makes it much less affected by the load dynamics. With the E-STATCOM connected to the PCC, the system is well damped disregarding of the load time constants, i.e. the system shows an almost identical performance with a CZL as with a CPL. This is confirmed by Figure 6.16 which shows the PCC voltage with a CZL, a CPL with a load time constant of $T_L = 20$ ms and a third case with a CPL with $T_L = 7.5$ ms. As shown in Figure 6.12, this is not the case for the D-STATCOM.

Just as with the D-STATCOM, is the bandwidth ω_{vc} of the voltage controller in the E-STATCOM varied to examine how the system performance changes. In Figure 6.17a, which only shows the dominating pole-pairs, is ω_{vc} set to six different values, $2\pi \cdot [30, 50, 70, 100, 150, 200]$ rad/s. The arrows indicate the main trends of the pole movements when ω_{vc} is increased. As before, the load time constant is varied from 60000 ms to 3 ms. Figure 6.17b is zoomed in around the most important movements. From this, it is clear that a faster ω_{vc} worsen the system damping but unlike the case with the D-STATCOM, showed in Figure 6.13, it is still stable for all examined bandwidths. In all, the system with the E-STATCOM is much less dependent on

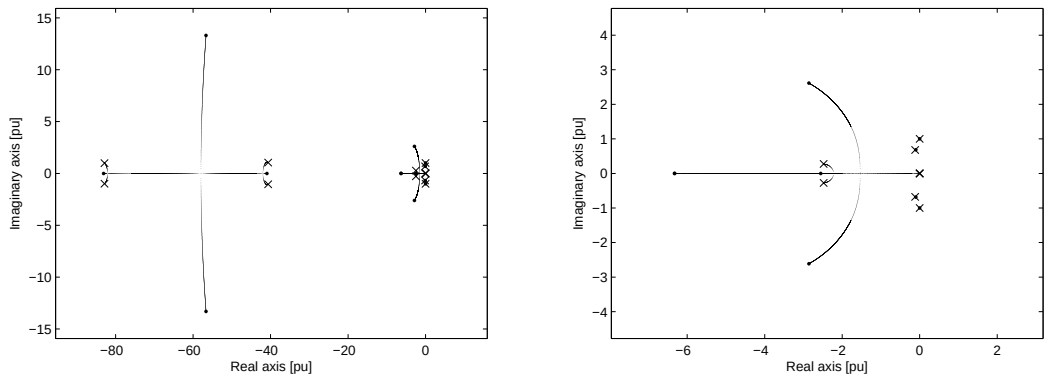

(a) **(b)**

Figure 6.15: Pole placement for the grid with a E-STATCOM and a CPL where marker "x" denotes a load time constant of 60000 ms and marker "•" corresponds to $T_L = 3$ ms. Plot (a): all poles, plot (b): zoomed in around dominating poles.

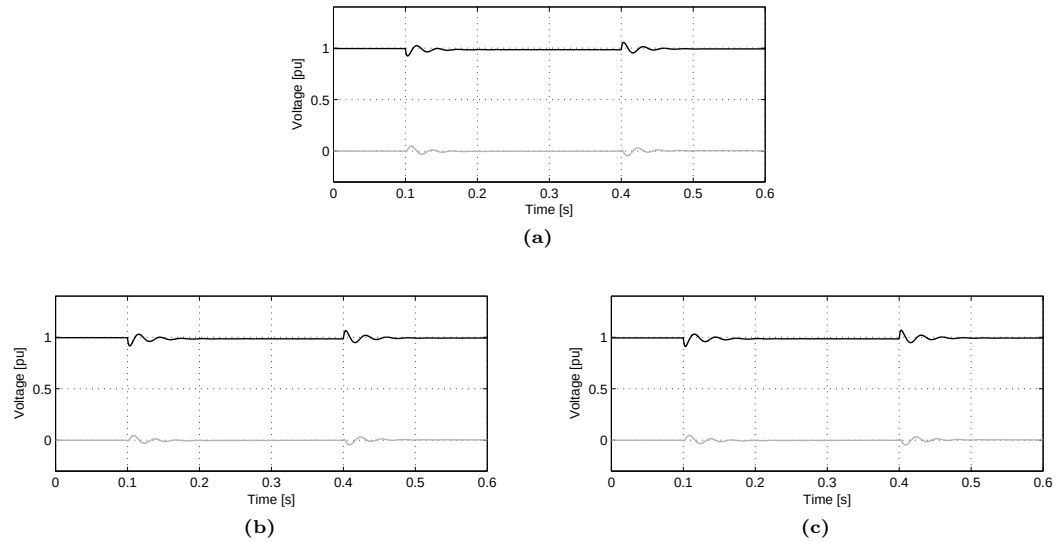

(a)

(b) **(c)**

Figure 6.16: PCC voltages during a voltage dip with E-STATCOM for three different loads. Plot (a): CZL, plot(b): CPL with $T_L = 20$ ms, plot (c): CPL with $T_L = 7.5$ ms.

the tuning of the outer control loop than with the D-STATCOM.

In a similar way as with the D-STATCOM, has the SCR been varied to examine how the system performance is affected by the grid strength when the E-STATCOM is used. Also here the grid impedance is kept constant and the CPL reference, P_{ref0}, and the constant reactance load, L_z, are tuned without changing other parameters in table 6.1 and 6.3. Figure 6.18 shows the dominating pole-pairs and their movements. $SCR = 2.9$ and $SCR = 8.7$ are pointed out with arrows and larger arrows indicate the main trend of the pole movements when the SCR increases. It is clear that the SCR does not have any significant impact of the system dynamic performance when an E-STATCOM is used.

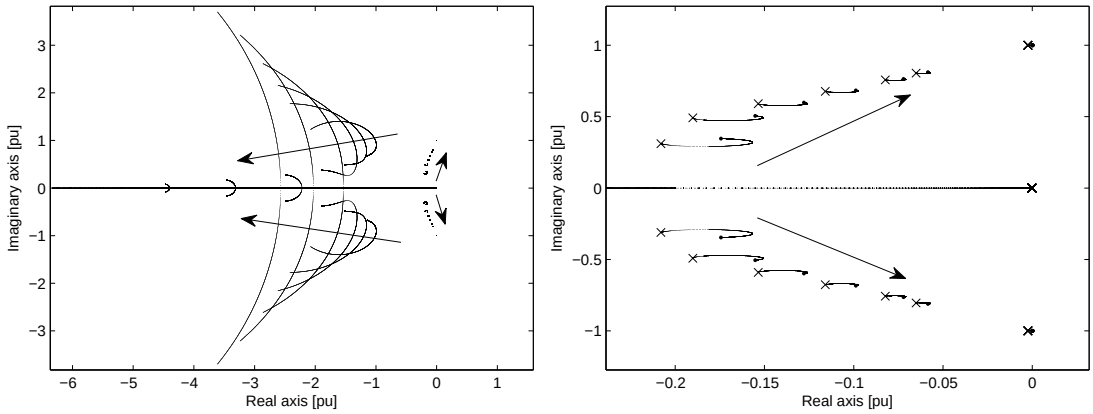

(a) (b)

Figure 6.17: Pole placement with the E-STATCOM when ω_{vc} is set to $2\pi \cdot [30, 50, 70, 100, 150, 200]$ rad/s. The arrows indicate the main trends of the pole movements when ω_{vc} increases. Marker "x" denotes $T_L = 60000$ ms and marker "•" corresponds to $T_L = 3$ ms. Plot (a): dominating pole-pairs, plot (b): zoomed on the most dominant pole-pairs.

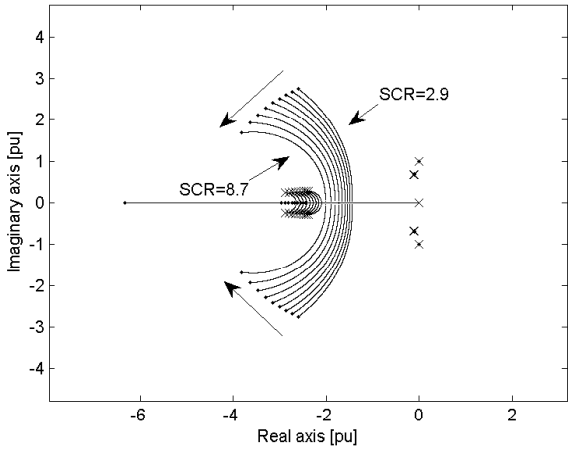

Figure 6.18: Pole placement with the E-STATCOM when the SCR is varied. Marker "x" denotes $T_L = 60000$ ms, "□" $T_L = 6$ ms and "•" $T_L = 3$ ms. The arrows show the main trends of the pole movements when the SCR is increased.

6.5 Mixed Load Characteristic

In the following section are the characteristics of the loads varied in order to give a better understanding of the load influence on the system performance. First the load has been modelled as a combined constant active and reactive power load and later it has been assumed that the load consuming active power consists of both one constant resistance part and one constant active power part.

6.5.1 Constant Active and Reactive Power Load

It has, in the previous analysis, been assumed that the constant power load only consists of an active power controller, i.e. the reactive power taken by the load behaves as a CZL. This is in most cases a good approximation since, for example, chargers for electric vehicles consume active power and does not have a big reactive consumption. It is also a valid approximation for a motor drive system since the active power consumed by the rectifier controls the DC-voltage and hence the power taken by the motor. However, it is interesting to examine the impact of a combined constant active and reactive power load on the system performance.

The constant reactive power load (CQL) is modelled to have the same load time constant as the CPL. Thus, in the state space models for the D-STATCOM and the E-STATCOM, the CZL L_z is replaced with the CQL L_q, expressed as

$$L_q = \frac{|\underline{V}_{2g}^{dq}|}{\omega Q_{ref}} \tag{6.51}$$

where Q_{ref} is the reactive power reference. To simplify the analysis L_q is only modelled with the steady state term and does not include the time derivative term since it would make it more complicated to model. Hence, L_q does in steady state consume a constant amount of reactive power but the load recovery after a disturbance might not be accurately modelled since the time derivative is neglected. In other words, it is assumed that the load is a constant power reactance $X = \omega L$ instead of an inductance dL/dt.

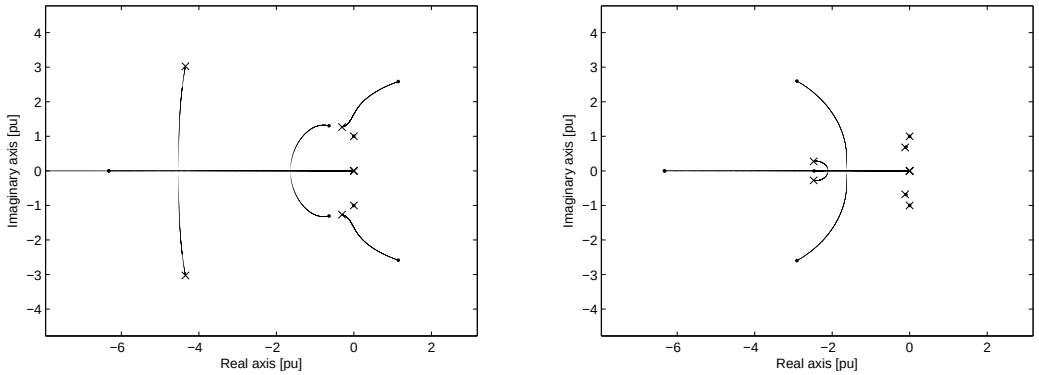

(a) **(b)**

Figure 6.19: Pole placement and movements with a combined constant active and reactive power load. Marker "x" denotes a load time constant of 60000 ms and "•" corresponds to $T_L = 3$ ms. (a) D-STATCOM, (b) E-STATCOM.

Figure 6.19a and 6.19b shows the poles placement and movements for the D-STATCOM and the E-STATCOM, respectively, when the load is modelled as a combined active and reactive power load. Comparing with Figure 6.11b and 6.15b it can be noticed that the pole placement has not changed significantly. Figure 6.20a and 6.20b confirm this by showing a comparison of the d-component of the PCC voltage for the D-STATCOM and the E-STATCOM, respectively, with a CPL or with both a CPL and CQL. It is clear, for both the D-STATCOM and the E-STATCOM, that the differences are neglectable. Hence, it is proven that modelling only the active power as a constant power load can be done without altering the system performance significantly.

6.5.2 Mixed Constant Impedance and Constant Power Loads

When the impact on the system dynamic performance of a pure CPL is identified, it is interesting to study more complex load characteristics. Considering that a distribution system in reality

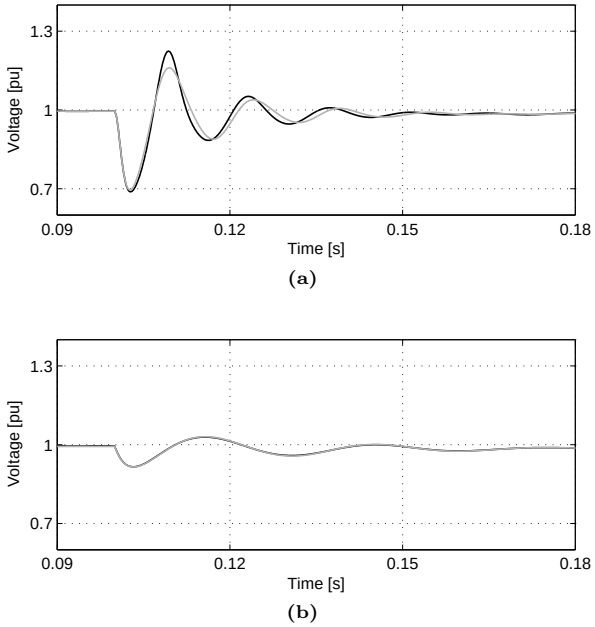

Figure 6.20: D-component of the PCC voltage where the black curves denote a CZL L_z and the grey curves correspond to a CQL L_q, in both cases is the active power consumed by a CPL. Plot (a): D-STATCOM, plot (b): E-STATCOM.

consists of a mixture of loads makes it interesting to study a combination of constant impedance and constant (active) power loads. In [30] is it shown how a large-scale integration of electric vehicles would affect the distribution grid in Gothenburg. It is shown that the charging could cause distribution grids in residential areas to be overloaded during night time. Assuming that the charging would be controlled so that the loading does not exceed rated power of the grid, charging vehicles could contribute to 40% of the total power consumed. Hence, it is reasonable to examine a case where 40% of the active power is consumed by a CPL and 60% is consumed by a CZL (assuming that all other load than electric vehicle-chargers behave as constant impedance loads, which is not true since they have mixed characteristics too).

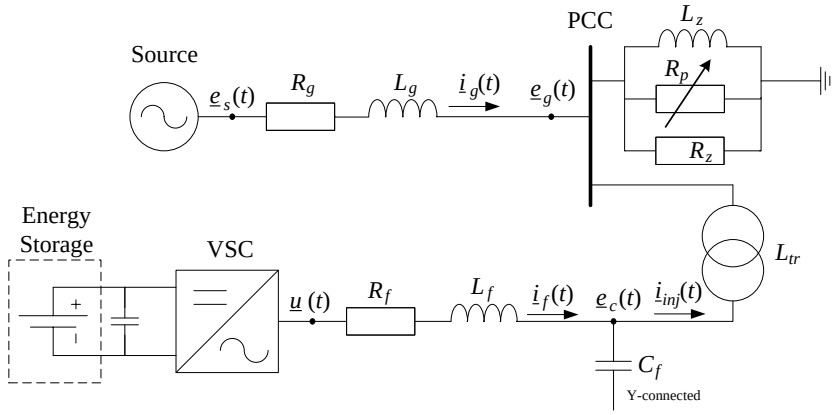

Figure 6.21: Grid model with supply, line impedance, loads and compensator connected through a LCL-filter.

Figure 6.21 shows the grid model where the load consists of both constant impedance and constant power parts. The additional load is connected in parallel which makes it necessary to rewrite some parts of the state space systems for both the D-STATCOM and the E-STATCOM. The equivalent impedance Z_L of the loads is rewritten as

$$\begin{aligned} Z_L &= \frac{sL_zR_zR_p}{sL_z\left(R_z+R_p\right)+R_zR_p} \\ &= \frac{s\xi}{s\gamma+\eta} \\ &= \frac{\xi}{\gamma}\left(1-\frac{\eta/\gamma}{s+\eta/\gamma}\right) \end{aligned} \tag{6.52}$$

where, $\xi = L_zR_zR_p$, $\gamma = R_zR_p$ and $\eta = L_z\left(R_z+R_p\right)$. Using the same method as when originally deriving the state space systems, the time derivative of the temporary state can be written as

$$s\,\underline{V}_t^{dq} = -\left(\frac{\eta}{\gamma}+j\omega\right)\underline{V}_t^{dq} + \underline{i}_g^{dq} \tag{6.53}$$

and the PCC voltage as

$$\underline{e}_g^{dq} = \frac{\xi}{\gamma}\left(\underline{i}_g^{dq}+\underline{i}_{inj}^{dq}\right) - \frac{\xi\eta}{\gamma^2}\underline{V}_t^{dq} \tag{6.54}$$

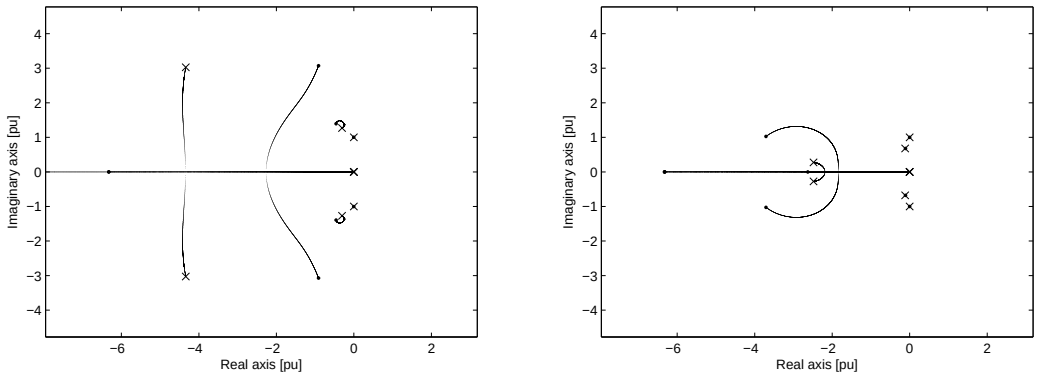

(a) **(b)**

Figure 6.22: Pole locations and movements with 40% of the active power consumed by a constant power load and 60% by a constant impedance load. All reactive power consumed by a constant impedance load. (a) D-STATCOM, (b) E-STATCOM.

Using the same linearization method as in Section *6.3.5 Linearization Method*, new state space systems are obtained for which the dominant pole placement and movements are shown in Figure 6.22a and 6.22b with the D-STATCOM and the E-STATCOM, respectively. Comparing with Figure 6.11b and 6.15b shows that the two systems get better damped and more stable when the CPL share of the total load is smaller. However, the improvement on the system with the E-STATCOM is not very large since the system already was well-damped. The system with the D-STATCOM, on the other hand, shows a significant improvement. The results are confirmed with simulations, shown in Figure 6.23, where it can be seen that the load time constant now can be as small as 3 ms and the systems will still be stable after a voltage dip. This would not have been the case for the D-STATCOM if the constant power load had consumed all the active power.

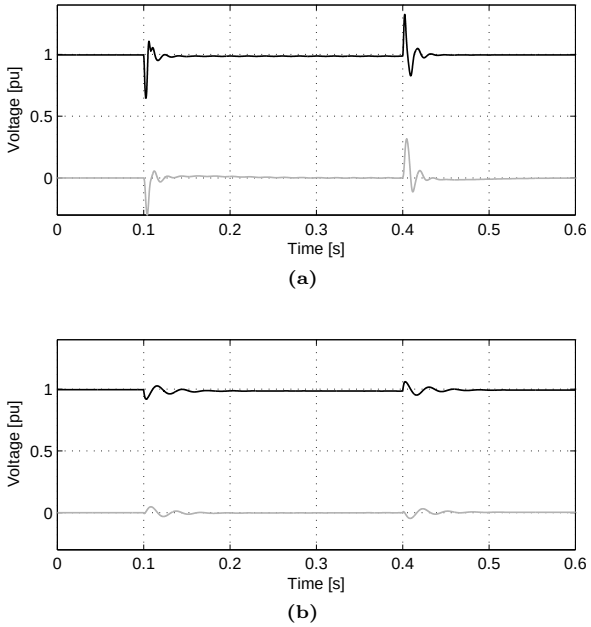

Figure 6.23: PCC voltage with 40% of the active power consumed by a CPL and 60% by a CZL. All reactive power consumed by a CZL. Plot (a): D-STATCOM, plot (b): E-STATCOM.

6.6 Conclusion

In this chapter, a model of a constant power load is presented and state space models, for a grid model with a D-STATCOM and an E-STATCOM, respectively, are derived. Using the linearized state space models, the system dynamic performance is studied by analysing the pole placement when changing the load time constant in a constant power load. Varying the load time constant, the short circuit ratio of the grid and mixing the load characteristics, it is shown that the load dynamics have a much smaller impact on the system performance with an E-STATCOM than with an D-STATCOM. By tuning the bandwidth of the outer control loop in the compensators, it is shown that the system performance with an E-STATCOM is much less dependent on the controller settings than with a D-STATCOM.

Chapter 7

Conclusions and Future Work

This chapter summarizes conclusions and provides some suggestions for further studies.

7.1 Conclusions

The thesis has dealt with energy storage equipped STATCOMs for power quality applications, i.e. applications which demand fast response times. Furthermore, the impact of dynamic loads on system performance has been examined.

Background material regarding uses of power electronics in power systems is provided in Chapter 2. Chapter 3 classifies applications for energy storages and describes some storage mediums suitable for power quality applications.

The control systems in shunt-connected VSCs are derived in Chapter 4. The design includes the inner current control loop and the outer loops, either a voltage controller or a reactive power controller, depending on if an energy storage are connected to the DC-side of the VSC. Furthermore, the performance of the D-STATCOM, without storage, and the E-STATCOM, with storage, are tested and examined by varying parameters in controllers. From this, it can be noticed that a lower controller bandwidth gives a more well-damped system. On the other hand, this prolongs the time before the system has mitigated a disturbance, e.g. a voltage dip. From the analysis, it is clear that the performance of the E-STATCOM is much less dependent on the tuning of the controller parameters than the D-STATCOM.

Applications related to power quality improvements, in which energy storages are necessary, are treated in Chapter 5. The ability of the E-STATCOM to completely mitigate a voltage dip, in both magnitude drop and phase jump, is shown by simulations and through simplified explanations. The E-STATCOM is compared with pure reactive power compensation, i.e. with the D-STATCOM, which only can control either the magnitude or the phase of the voltage. From this, it is clear that if complete voltage dip mitigation is desired, an energy storage equipped STATCOM is needed with a sufficiently large converter rating and energy storage size. Furthermore, it is described how an E-STATCOM can be used to quickly balance loads in areas which experience a loss of a single line, hence, entering islanding operation. By consuming or producing power the E-STATCOM can keep the voltage and frequency within acceptable limits until slower control systems in the islanded system can take action.

The impact of load dynamics on system performances with D-STATCOM and E-STATCOM, respectively, is studied in Chapter 6. A dynamic load model with constant power load characteristics is presented and compared to a generic load model. Using the dynamic load model, state space systems for a grid with a D-STATCOM, an E-STATCOM or without both are derived. By varying the load recovery time in the dynamic load, the load's impact on the system performance is examined. From this, it is noticed that the system turns unstable with a slower load time constant with a D-STATCOM than without any compensator. This might be caused by some

interaction between the controllers in the load and the compensator. Furthermore, it is clear that dynamic properties of loads have a very small impact on the system performance when a E-STATCOM is used. The reason for this is, as explained in Chapter 5, that with combined active and reactive power compensation it is possible to control both the magnitude and the phase of the voltage. On the other hand, the system performance with the D-STATCOM is strongly affected by the load dynamics and the system can even become unstable under certain conditions.

7.2 Future Work

In this thesis, the most interesting studies and results are presented in Chapter 6. It is shown that, with an energy storage attached to the DC-side, it is possible to design a STATCOM which is practically unaffected by load properties. On the contrary, an energy storage greatly increases the cost of the compensator. With energy storage and necessary auxiliary systems, for example protection, the total cost of the compensator could be doubled. Since the active power exchange in the compensator decreases with time after an event, it should be possible to determine a minimum size of the storage that could mitigate a desired type of events and disturbances. Hence, an study that investigates the required size of the energy storage for different events would be useful.

Furthermore, the models used in this work are greatly simplified. To increase the precision of the results, more realistic models should be implemented and analyzed. This includes the load and grid models as well as the configuration of the compensator. For example, a switching converter should be implemented together with a more realistic filter which takes the actual filter requirements into account. Furthermore, the DC-side of the compensator can be made more realistic by adding a DC/DC converter and an actual energy storage. An additional study of different converter topologies can also be done.

It would also be good to determine the exact reason that causes a system with a D-STATCOM to get unstable at lower load bandwidths than a system without compensator. Since the D-STATCOM actually worsen the system performance, it is important to further study this interaction to make sure that it does not happen in a real system. In all, practical studies are needed for validation of the obtained results in Chapter 6.

References

[1] A. B. Jusoh. "The Instability Effect on Constant Power Loads". *Proceeding National Power and Energy Conference* (2004).

[2] A. Emadi. "Modeling of Power Electronic Loads in AC Distribution Systems Using the Generalized State-Space Averaging Method". *IEEE Transactions on Industrial Electronics, vol. 51, no. 5, pp. 992-1000* (2004).

[3] B. Mahyavanshi and G. Radman. "A Study of Interaction between Dynamic Load and STATCOM". *Proceeding of the Thirthy Eighth Southeastern Symposium on System Theory* (2008).

[4] M.H.J. Bollen. *The Smart Grid: Adapting the Power System to New Challenges*. Morgan & Claypool, 2011.

[5] M.H.J. Bollen. *Understanding Power Quality Problems: voltage sags and interruptions*. John Wiley & Sons Inc., 2000.

[6] M. Bongiorno. "Control of Voltage Source Converters for Voltage Dip Mitigation in Shunt and Series Configurations". Licentiate Thesis. Chalmers University of Technology, 2004.

[7] M. Bongiorno. "On Control of Grid-connected Voltage Source Converters: Mitigation of Voltage Dips and Subsynchronous Resonances". Ph.D. dissertation. Chalmers University of Technology, 2007.

[8] J. Casazza and F. Delea. *Understanding Electric Power Systems: An Overview of the Technology and the Marketplace*. Wiley-IEEE Press, 2004.

[9] D. Karlsson and D.J. Hill. "Modelling and identification of nonlinear dynamic loads in power systems ". *IEEE Transactions on Power System, vol. 9, no. 1, pp 157-166* (1994).

[10] E. Twining and D.G Holmes. "Voltage Compensation in Weak Distribution Networks using Multiple Shunt Connected Voltage Source Inverters". *Proc. of IEEE Bologna PowerTech Conference, vol. 4, pp. 619-626* (2003).

[11] ECPE European Center for Power Electronics. *Strategic Research Agenda on Intelligent Power Electronics for Energy Efficiency*. 2008.

[12] J. Eyer and G. Corey. *Energy Storage for the Electricity Grid: Benefits and Market Potential Assessment Guide*. Tech. rep. Sandia National Laboratories, 2010.

[13] F. B. Blanco, M.W. Degner and R.D. Lorenz. "Dynamic Analysis of Current Regulators for AC Motors Using Complex Vectors". *IEEE Transactions on Industry Applications* (1999).

[14] G. Benysek. *Improvement in the Quality of Delivery of Electrical Energy using Power Electronics Systems*. Springer, 2007.

[15] G. Shackshaft, O.C. Symons and J.G. Hadwick. "General-Purpose Model of Power-System Loads". *Proc. of the Institution of Electrical Engineers, vol. 124, no. 8, pp. 715-723* (1977).

[16] M. Gustavsson and N. Krantz. "Voltage Collapse in Power Systems". Licentiate Thesis. Chalmers University of Technology, 2005.

[17] L. Harnefors. *Control of Variable-Speed Drives*. Applied Signal Processing and Control, Dept. of Electronics, Mälardalen University, 2002.

[18] L. Harnefors, M. Bongiorno and S. Lundberg. "Input-Admittance Calculation and Shaping for Controlled Voltage-Source Converters". *IEEE Transactions on Industrial Electronics* (2007).

[19] B. Lennartson. *Reglerteknikens grunder*. Studentlitteratur, 2001.

[20] M. Molinas. "The Role of Power Electronics in Distributed Systems". *The 5th AIST Symposium on Distributed Energy Systems* (2008).

[21] M. Molinas, D. Moltoni, G. Fascendini, J.A. Suul and T. Undeland. "Constant Power Loads in AC Distribution Systems: An investigation of stability Systems". *IEEE International Symposium on Industrial Electronics* (2008).

[22] A. Moreno-Munoz. *Power Quality: Mitigation Technologies in a Distributed Environment*. Springer, 2007.

[23] L. Gyugyi N. G. Hingorani and M. E. El-Hawary. *Understanding FACTS: Concepts and Technology of Flexible AC Transmission Systems*. IEEE Press, 2000.

[24] M. H. Nordlund. "Use of Energy-storage Equipped Shunt Compensator for Frequency Control". M.Sc. Thesis. Chalmers University of Technology, 2010.

[25] R. Ottersten and J. Svensson. "Vector current controlled voltage source converter - deadbeat control and saturation strategies". *IEEE Transactions on Power Electronics* (2002).

[26] N. Balu P. Kundur and M. G. Lauby. *Power System Stability and Control*. McGraw-Hill, 1994.

[27] M. H. Rashid. *Power Electronics Handbook: Devices, Circuits and Applications*. Elsevier Inc., 2007.

[28] D. Rastler. *Electricity Energy Storage Technology Options: A White Paper Primer on Applications, Costs, and Benefits*. Tech. rep. Electric Power Research Institute, 2010.

[29] S. Ammari, Y. Besanger, N. Hadjsaid and D. Georges. "Robust Solutions for the Interaction Phenomena between Dynamic Loads and FACTS Controllers". *IEEE Power Engineering Society Summer Meeting* (2000).

[30] D. Steen. "Impact on the Distribution System due to Plug-In Electric Vehicles and Changes in Electricity Usage". Licentiate Thesis. Chalmers University of Technology, 2012.

[31] V. Knyazkin, C.A. Cañizares and L.H. Söder. "On the Parameter Estimation and Modeling of Aggregate Power System Loads". *IEEE Transactions on Power System, vol. 19, no. 2, pp. 1023-1031* (2004).

[32] H. Xie. "On Power-system Benefits, Main-circuit Design, and Control of StatComs with Energy Storage". Ph.D. dissertation. Royal Institute of Technology, 2009.

[33] A. Yazdani and R. Iravani. *Voltage-Sourced Converters in Power Systems: Modeling, Control, and Applications*. John Wiley & Sons Inc., 2010.

[34] Y.V. Panov and F.C. Lee. "Modeling and Stability Analysis of a DC Power System with Solid State Power Controllers". *Applied Power Electronics Conference and Exposition* (1996).

[35] Z. J. Palmor. *The Control Handbook*. CRC Press, 1996.

Appendix A

Transformations for Three-Phase Systems

A.1 Transformation of Three-Phase Quantities into Vectors

It is possible to transform a three-phase system into a complex vector in a fixed reference frame, usually called the $\alpha\beta$-frame. If v_a, v_b and v_c are components of a positive three-phase system, the transformation can be defined as

$$\underline{v}^{\alpha\beta}(t) = v^{\alpha}(t) + jv^{\beta}(t) = K\left(v_a(t) + v_b(t)e^{j\frac{2\pi}{3}} + v_c(t)e^{j\frac{4\pi}{3}}\right) \tag{A.1}$$

where the factor K is equal to $\sqrt{3/2}$ or $3/2$ to obtain power invariant or voltage invariant transformations between the systems, respectively. Assuming power invariant transformation, (A.1) can be expressed in matrix form as

$$\begin{bmatrix} v^{\alpha} \\ v^{\beta} \end{bmatrix} = \sqrt{\frac{2}{3}} \begin{bmatrix} 1 & -\frac{1}{2} & -\frac{1}{2} \\ 0 & \frac{\sqrt{3}}{2} & -\frac{\sqrt{3}}{2} \end{bmatrix} \begin{bmatrix} v_a \\ v_b \\ v_c \end{bmatrix} \tag{A.2}$$

where the inverse transformation, assuming no zero-component, is written as

$$\begin{bmatrix} v_a \\ v_b \\ v_c \end{bmatrix} = \sqrt{\frac{2}{3}} \begin{bmatrix} 1 & 0 \\ -\frac{1}{2} & \frac{\sqrt{3}}{2} \\ -\frac{1}{2} & -\frac{\sqrt{3}}{2} \end{bmatrix} \begin{bmatrix} v^{\alpha} \\ v^{\beta} \end{bmatrix} \tag{A.3}$$

A.2 Transformation between fixed and rotating coordinate systems

The complex vector $\underline{v}^{\alpha\beta}(t)$ is, in the $\alpha\beta$-frame, rotating with an angular frequency $\omega(t)$. If a coordinate system is introduced which rotates with the same angular frequency $\omega(t)$, the projections of $\underline{v}^{\alpha\beta}(t)$ would appear as constant on the rotating frame. Denoting the rotating coordinate system the dq-frame with alignments according to Figure A.1, the transformation from the fixed $\alpha\beta$-frame to the rotating dq-frame can be written in vector form as

$$\underline{v}^{dq}(t) = \underline{v}^{\alpha\beta}(t)e^{-j\theta(t)} \tag{A.4}$$

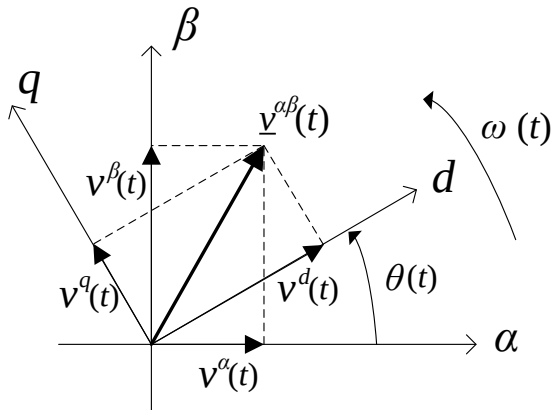

Figure A.1: Relation between $\alpha\beta$-frame and dq-frames.

where the angle $\theta(t)$ is given by

$$\theta(t) = \theta_0 + \int_0^t \omega(\tau) d\tau \tag{A.5}$$

The inverse transformation of (A.4) is defined as

$$\underline{v}^{\alpha\beta}(t) = \underline{v}^{dq}(t) e^{j\theta(t)} \tag{A.6}$$

The vector equation (A.4) can be written in matrix form with the dq-components, as shown in Figure A.1, expressed as

$$\begin{bmatrix} v^d(t) \\ v^q(t) \end{bmatrix} = \begin{bmatrix} \cos(-\theta(t)) & -\sin(-\theta(t)) \\ \sin(-\theta(t)) & \cos(-\theta(t)) \end{bmatrix} \begin{bmatrix} v^\alpha(t) \\ v^\beta(t) \end{bmatrix} \tag{A.7}$$

and similarly can (A.6) be written in matrix form as

$$\begin{bmatrix} v^\alpha(t) \\ v^\beta(t) \end{bmatrix} = \begin{bmatrix} \cos(\theta(t)) & -\sin(\theta(t)) \\ \sin(\theta(t)) & \cos(\theta(t)) \end{bmatrix} \begin{bmatrix} v^d(t) \\ v^q(t) \end{bmatrix} \tag{A.8}$$